

**UCSF**

**UC San Francisco Electronic Theses and Dissertations**

**Title**

The clustered gamma-protocadherins regulate cortical interneuron programmed cell death

**Permalink**

<https://escholarship.org/uc/item/1ms8d52p>

**Author**

Mancia Leon, Walter Rene

**Publication Date**

2022

Peer reviewed|Thesis/dissertation

The clustered gamma-protocadherins regulate cortical interneuron programmed cell death

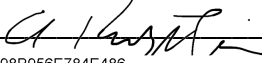
by  
Walter Rene Mancía Leon

DISSERTATION  
Submitted in partial satisfaction of the requirements for degree of  
DOCTOR OF PHILOSOPHY

in  
Biomedical Sciences

in the  
GRADUATE DIVISION  
of the  
UNIVERSITY OF CALIFORNIA, SAN FRANCISCO

Approved:

DocuSigned by:  
  
B98B956E784E486... Arnold Kriegstein  
Chair

DocuSigned by:  
  
Duan Xin

DocuSigned by:  
  
John Rubenstein

DocuSigned by:  
Arturo Alvarez-Buylla  
A98A3A270B5D492... Arturo Alvarez-Buylla

Committee Members

Copyright 2022,  
by Walter R. Mancía Leon

To Alphons Smit and Mirna Lizabeth Leon Linares

## ACKNOWLEDGEMENTS

I am very grateful to Arturo Alvarez-Buylla for the opportunity to undertake my graduate thesis work under his supervision; I began my thesis work with little, or no experience in the field of neurodevelopment, but , and continue to have, extreme curiosity for how this remarkable organ is put together. I am grateful for the financial support I received from Arturo, Michael Stryker, and the Biomedical Science Program. Despite the fact that my legal status in the United States prevented me from accessing key financial resources, I received full financial support which allowed me to commit fully to research, training, and discovery. While in his laboratory, I have enjoyed a great deal of intellectual and experimental freedom to carry out my thesis work. Notwithstanding, Arturo was always available when I needed guidance. He encouraged me to approach seemingly difficult problems with an unbiased mind and develop simple yet elegant solutions to a biological question.

One key lesson I will take with me, and something that Arturo always encouraged all his trainees to follow, is to apply alternative independent methods to answer the same question. In the end, the goal is not only to publish one's scientific discovery, but primarily to be correct.

I am also grateful to Michael Stryker and Andrea Hasenstaub for their mentorship and project collaboration. My work would not have been possible without the many ideas, and discussions that emanated from this collaboration. The long hours discussing ideas, reviewing data, writing manuscripts and grants, leave me with valuable lessons for my future work. I am extremely grateful to Benjamin Rakela who performed all the electrophysiological and neuronal activity work and also who was truly instrumental in obtaining funding for the project. I am grateful to Julien Spatazza, my first mentor in graduate school, who mentored me and taught me valuable skills during the first months in the Alvarez-Buylla lab.

I extend my gratitude to my Ph.D. thesis committee members Dr. Arnold Kriegstein , Dr. John Rubenstein and Dr. Xin Duan for their intellectual contributions and discussion during my time at UCSF. I am also grateful to the various laboratory members for their unconditional support and encouragement throughout my training in the laboratory. I would also like to give special thanks to many of my colleagues, family members and friends who supported me on this crusade. In particular I would like to acknowledge my father Alphons Smit who has been my number one supporter throughout my entire training.

Last but not least, I am extremely grateful to the Biomedical Science Program at the University of California at San Francisco for the training and financial support provided throughout my journey as a Ph.D. student.

## CONTRIBUTIONS

Mancia Leon WR, Spatazza J, Rakela B, Chatterjee A, Pande V, Maniatis T, et al. Clustered gamma-protocadherins regulate cortical interneuron programmed cell death. *Elife*. 2020;9 <https://doi.org/10.7554/eLife.55374>.

**EPIGRAPH** - "A half-read book is a half-finished love affair."

— David Mitchell, *Cloud Atlas*



## ABSTRACT

### **The clustered gamma-protocadherins regulate cortical interneuron programmed cell death**

**Walter Rene Mancía Leon**

In the field of neurodevelopmental biology, what regulates the production of cells and how the final number of cells is determined in the central nervous system (CNS) remains one of the long-standing questions. Indeed, what ultimately determines the brain size and how the final number of neurons is computed in the CNS remains unknown. What makes this question more intriguing is that in the CNS, a supernumerary number of neurons is produced in development. Excess neurons are eliminated postnatally through PCD (PCD). Hence PCD is a developmental feature necessary to establish the final number of neurons in each region of the brain. Yet, how PCD is regulated in the CNS and what molecules are involved in its regulation remains controversial and largely unresolved.

In my thesis, I introduce a set of fifty-eight cell-adhesion molecules named clustered protocadherins (Pcdhs) and show evidence that these molecules are key to establishing the final inhibitory neuronal population in the cerebral cortex through the regulation of PCD. The 58 Pcdh genes are tandemly arranged into three smaller gene clusters: alpha (*Pcdha*), beta (*Pcdhb*) and gamma (*Pcdhy*). Given the genomic complexity of Pcdhs, I first use a series of whole cluster genetic deletions of the Pcdhs gene locus to probe the function of *Pcdha*, *Pcdhb* or *Pcdhy* in the regulation of cIN cell death in mice. Using these cluster deletion mice, we show that *Pcdhy* genes, but not *Pcdha* or *Pcdhb* genes, are required for the survival of approximately 50% of cINs through a BAX-dependent mechanism. I then probe whether cINs compete for survival using PCDhs by employing a co-transplantation assay I developed. My data suggest that indeed *Pcdhy*-deficient and wild-type (WT) cINs of the same age compete for survival in a mechanism that involves

*Pcdhy*. Surprisingly, three-dimensional reconstructions and patch-clamp recordings indicate that the *Pcdhy* mutant cells have similar morphology, excitability and receive similar numbers of inhibitory and excitatory synaptic inputs compared to wild type cINs.

Next, I investigated which *Pcdhy* genes are key to the regulation of cIN survival. The *Pcdhy* gene cluster encodes 22 unique isoforms, which are subclassified as A-type, B-type, or C-type isoforms. Importantly, deletion of the C-type isoforms (*Pcdhyc3*, *Pcdhyc4* and *Pcdhyc5*), but not of the A-type or B-type *Pcdhys*, results in neonatal lethality. Hence, to compare in the same host microenvironment the survival of cINs carrying WT or mutant *Pcdhy* and to bypass neonatal lethality, I developed a co-transplantation assay using two different reporter systems (GFP and RFP). Using this assay and a series of constitutive *Pcdhy* isoform deletions mice, I found that the A- and B-type *Pcdhy* have no significant role in cIN PCD. However, the removal of *Pcdhy* C-type isoforms (*Pcdhyc3*, *Pcdhyc4* and *Pcdhyc5*), and in particular the sole removal of *Pcdhyc4*, resulted in increased cIN cell death. Together these transplantation experiments suggested that survival of cINs largely depends on the expression of *Pcdhyc4*, but not expression of *Pcdhyc3* or *Pcdhyc5*, in cINs.

To complement observations above, I developed lentiviral constructs to overexpress *Pcdhyc4* or *Pcdhyc5* in cIN precursors that lack the entire *Pcdhy* gene set. I found that the expression of *Pcdhyc4*, but not that of *Pcdhyc5*, significantly rescued a fraction of cINs destined to die.

Lastly and in collaboration with Andrea Hasentaub and Michael Striker laboratories, we probed the activity of cINs carrying or lacking a full set of *Pcdhy* genes using two-photon calcium imaging across the period of cell death (data not included)

In summary, my thesis work identifies for the first time a cell-adhesion molecule involved in the regulation of PCD in cINs and shows evidence that among all *Pcdh* genes, *Pcdhyc4* is key for determining the final number of cINs for the cortex.

## TABLE OF CONTENTS

<b>CHAPTER 1: INTRODUCTION</b> .....	1
a. Statement about development.....	1
b. Development of pallial radial glial cells and excitatory neurons.....	2
c. Radial glial cells and inhibitory neurons in the subpallium .....	3
d. Setting up the main question of this thesis work .....	3
e. Introduction to cIN development .....	4
f. Specification and birth of cINs .....	5
g. cIN Migration .....	7
h. Cell death and the neurotrophin hypothesis.....	8
i. Neuronal programmed cell death in the cortex. ....	9
<b>CHAPTER 2: THESIS STRUCTURE</b> .....	12
a. Regulation of programmed cell death through a cell or population mechanism .....	12
b. Thesis hypothesis.....	14
c. The Clustered Protocadherins .....	14
d. Thesis organization: .....	17
<b>CHAPTER 3: RESULTS</b> .....	<b>21</b>
<b>PART I - Expression of clustered Pcdhs in cINs</b> .....	<b>21</b>
Expression of clustered Pcdhs (Pcdh $\alpha$ , Pcdh $\beta$ , and Pcdhy) in the cerebral cortex and Pcdhy isoforms in cINs. ....	21
<b>PART II - The clustered Pcdhs and their role in the regulation of cIN programmed     cell death</b> .....	<b>26</b>

PCDHγ expression is lost in Pcdhy <sup>con3</sup> mice that also express CRE. ....	26
Reduced number of cIN in the cortex of Pcdhy mutants.....	27
Pcdhy function is not required for the proliferation and migration of cIN precursor cells .....	47
Loss of Pcdhy function results in increased cIN programmed cell death. ....	50
Loss of Pcdhy does not affect survival of cINs after the period of PCD. ....	53
Pcdhα or Pcdhβ do not affect cIN survival.....	58
<b>PART III - cINs compete for survival using PCDHγ. ....</b>	<b>61</b>
Heterochronic transplantation recapitulates timing and extent of PCD in cINs. ....	61
cINs compete for survival using Pcdhy.....	67
Morphological and Physiological maturation of cINs lacking Pcdhy.....	76
<b>PART IV - Genomic complexity of Pcdhy and its role in cIN survival .....</b>	<b>82</b>
Genomic complexity of Pcdhy is not required for the regulation of PCD.....	82
Loss of Pcdhy C-type isoforms is sufficient to increase cell death.....	82
Pcdhyc4, but not the A-, B- or other C-type isoforms, plays a key role in the regulation of cIN PCD.....	86
<b>PART V - Pcdhyc4 plays a key role in cIN survival .....</b>	<b>98</b>
Expression of Pcdhyc4 rescues cINs that lack the entire Pcdhy gene cluster. ....	98
<b>Part VI - Future directions .....</b>	<b>110</b>
<b>CHAPTER 4: DISCUSSION .....</b>	<b>111</b>
Appendix I - Methods .....	121

## LIST OF FIGURES

<b>Figure 1.1</b> - Expression of clustered Pcdhs in the mouse cortex and purified cortical GABAergic cells.....	<b>23</b>
<b>Supplement Figure 1.1</b> - GABAergic markers are enriched in GFP positive FACS-sorted cells from Gad1-GFP mice.....	<b>25</b>
<b>Figure 2.1</b> - Reduced number of GABAergic cINs in Pcdhy-deficient mice.....	<b>29</b>
<b>Supplement Figure 2.1</b> - Reduced number of GABAergic cIN subtypes in Pcdhy-deficient mice.....	<b>31</b>
<b>Supplement Figure 3.1</b> - Reduced number of GABAergic cINs across cortical layers in Pcdhy-deficient mice.....	<b>33</b>
<b>Figure 3.1</b> - Loss of Pcdhy genes targeted to Nkx2.1 expressing cells results in selective loss of cIN derived from the MGE.....	<b>37</b>
<b>Supplement Figure 4.1</b> - Reduced number of MGE cIN subtypes after loss of Pcdhy in Nkx2.1-derived cells.....	<b>39</b>
<b>Supplement Figure 5.1</b> - Numbers of Nkx2.1-derived RLN positive cINs are reduced in layers II-VI in Pcdhy-deficient mice. ....	<b>41</b>
.....	<b>43</b>
<b>Supplement Figure 6.1</b> - Cortical layer distribution of Nkx2.1-derived cINs in Pcdhy WT and mutant mice. ....	<b>43</b>
<b>Supplement Figure 7.1</b> - Increased survival of non-Nkx2.1-derived SST and PV cINs in Pcdhy-deficient mice.....	<b>45</b>
<b>Figure 4.1</b> - Proliferation and migration are not affected by the loss of Pcdhy in Nkx2.1 expressing cells. ....	<b>48</b>
<b>Figure 5.1</b> - Increased PCD in Pcdhy mutants is rescued in Pcdhy-Bax null animals. ....	<b>51</b>
<b>Figure 6.1</b> - Pcdhy function is not required for the survival of PV cINs after the period of PCD. ....	<b>54</b>

<b>Supplement Figure 8.1</b> - Late postnatal expression of Parvalbumin in cINs. ....	<b>56</b>
<b>Figure 7.1</b> - Loss of <i>Pcdha</i> , <i>Pcdhb</i> , or <i>Pcdhya1</i> , <i>Pcdhya2</i> , and <i>Pcdhya3</i> genes does not affect the survival of MGE-derived cINs. ....	<b>59</b>
<b>Figure 8.1</b> - <i>Pcdhy</i> are required for cIN survival after transplantation. ....	<b>63</b>
<b>Supplement Figure 9.1</b> - Number of cIN drops for both the <i>Pcdhy</i> WT and <i>Pcdhy</i> mutant transplanted population. ....	<b>65</b>
<b>Figure 9.1</b> - MGE cell transplantation reveals a non-cell autonomous effect of <i>Pcdhy</i> on cIN survival. ....	<b>69</b>
<b>Supplement Figure 10.1</b> - Fluorescent reporter or breeding background does not affect the survival of transplanted MGE-derived cINs.....	<b>71</b>
<b>Figure 10.1</b> - Survival of cINs, WT, or mutant for <i>Pcdhy</i> , was not affected by cell density. ....	<b>74</b>
<b>Figure 11.1</b> - Loss of <i>Pcdhy</i> does not affect the morphological maturation of cIN during the period of PCD. ....	<b>78</b>
<b>Figure 12.1</b> - <i>Pcdhy</i> deletion does not affect the physiological properties of cINs during the period of PCD. ....	<b>80</b>
<b>Figure 13.1</b> - Loss of <i>Pcdhyc3</i> , <i>Pcdhyc4</i> , and <i>Pcdhyc5</i> is sufficient to increase cIN cell death.....	<b>84</b>
<b>Figure 14.1</b> - With the exception of <i>Pcdhyc4</i> , all other <i>Pcdhy</i> isoforms, including <i>Pcdhyc5</i> are largely not required for cIN survival. ....	<b>90</b>
<b>Figure 15.1</b> - Genetic labeling of MGE-derived cIN confirms that the loss of <i>Pcdhyc4</i> increased cIN cell death.....	<b>93</b>
<b>Figure 16.1</b> - Elimination of all <i>Pcdhy</i> , except for <i>Pcdhyc4</i> , results in survival of the majority of cINs. ....	<b>96</b>
<b>Figure 17.1</b> - Lentiviral constructs expressing <i>Pcdhyc4</i> and <i>Pcdhyc5</i> .....	<b>99</b>
<b>Figure 18.1</b> - In vitro validation of lentiviral constructs expressing <i>Pcdhy</i> .....	<b>102</b>

**Figure 19.1** - Infection with lentivirus and expression of GFP does not affect the survival of cINs. ....105

**Figure 20.1** - Lentiviral expression of Pcdhyc4rescues cINs lacking the function of all Pcdhy isoforms. ....108



## LIST OF ABBREVIATIONS

Brain-derived neurotrophic factor (BDNF)

Caudal ganglionic eminence (CGE)

Cleaved-Caspase 3 (cc3)

Clustered protocadherin alpha cluster (*Pcdh $\alpha$* )

Clustered protocadherin beta cluster (*Pcdh $\beta$* )

Clustered protocadherin gamma cluster (*Pcdh $\gamma$* )

Clustered protocadherins(Pcdhs)

Cortical inhibitory neurons (cIN)

Cortical plate (CP)

Days after transplantation (DAT)

Dorsal root ganglion sensory neurons (DRG)

Embryonic day (E)

Excitatory neurons (EN)

Fluorescence Activated Cell Sorting (FACS)

Intermediate zone (IZ)

Intermediate precursor cells (IPCs)

Lateral ganglionic eminence (LGE)

Marginal zone (MZ)

Medial ganglionic eminences (MGE )

Nerve growth factor (NGF)

Neurotrophin-3 (NT3)

Olfactory bulb (OB)

Parvalbumin (PV)

*Pcdh $\gamma$*  conditional allele (*Pcdh $\gamma$ <sup>con3</sup>*)

Phosphohistone H3 (PH3)

Postnatal day (P)

Preoptic area (PoA)

Pro-apoptotic Bcl-2-associated X protein (BAX)

Programmed cell death (PCD)

Radial glial cells (RGC)

Reelin (RLN)

Rostral migratory stream (RMS)

Somatostatin (SST)

Subplate (SP)

Subventricular zone (SVZ)

Vasoactive intestinal peptide (VIP )

Vasoactive intestinal polypeptide (VIP)

Visual cortex (V1)

Wild-type (WT)

## CHAPTER 1: INTRODUCTION

### a. Statement about development

Mammalian development is one of the most beautiful biological phenomena in the realm of biology. The rules that guide cells to proliferate, migrate, die, and assemble into the complex functional tissues and organs remain largely unknown. Remarkably, these elemental processes governing embryonic development are played out in every developing part of the embryo. For example, cell proliferation and cell death, two contrasting developmental features, are necessary for the growth and morphogenesis of all organs including that of the brain.

Among the developmental processes, perhaps the most intriguing and fascinating, is that of the nervous system. In mammals the nervous system is composed of the peripheral and central nervous system, and together they are responsible for perception, controlling activity across the entire body and behavior. The brain and spinal cord are the two components that make up the central nervous system. The brain, and particularly the forebrain has evolved in some mammalian species to arguably become the most complex organ. This intricate network of cells consisting mainly of neurons and glial cells is derived from a simple epithelial sheet, the neuroepithelium, that appears in mice around embryonic day (E) 9.5 (V. S. Chen et al. 2017). This single layer of cells in the neural tube undergoes a remarkable transformation giving rise to specialized formations that will form the various parts of the central nervous system. For example the telencephalon develops in the most anterior part of the neural tube as a pair of bilateral vesicle-like swelling formations. Each swelling develops into one of the two brain hemispheres.

## **b. Development of pallial radial glial cells and excitatory neurons**

The pallium, subpallium and septum are among the first regional distinctions that emerge in the telencephalon. The dorsal region of the telencephalon, which is also called the pallium, becomes the neocortex, and it is also the source of all the excitatory neurons in the cerebral cortex. The pallium develops multiple layers, including the cortical plate, the most superficial layer where most newborn neurons will ultimately reside, the subventricular zone which is rich in intermediate precursor cells (IPCs), and the ventricular-subventricular zone (VZ/SVZ) where the radial glial cells (RGC) exist.

RGCs are derived from the neuroepithelial cells and function as the neural stem cells for the production of most neurons and glial cells in the CNS. RGCs serve as progenitor cells for other RGCs (self-renewals), IPCs, neurons and glia (Stephen C. Noctor et al. 2004; Haubensak et al. 2004; Lui, Hansen, and Kriegstein 2011). A subpopulation of RGCs also transitions into neural stem cells that reside in the walls of the ventricles in the postnatal brain. RGCs also provide a scaffold for newly generated neurons to migrate (S. C. Noctor et al. 2001). Early in development RGCs have an apical process that contacts the ventricle exposing this small apical ending and the primary cilia to the components of the cerebrospinal fluid. Early RGCs also have a basal process that is anchored to the pial surface. In mice as well as in humans, RGCs residing in the ventricular zone are generally referred to as ventricular RGCs (vRGCs). A second type of RGCs is located in the outer subventricular zone, and are referred to as outer RGCs (oRGCs). oRGCs lack an apical contact to the cerebrospinal fluid, maintain a process that contacts the pia or blood vessels, and are enriched in large brain mammals such as humans (Hansen et al. 2010; Smart 2002; Reillo et al. 2011; Fietz et al. 2010). As the cortex grows in size, RGCs lose their pial contact but retain a basal process that can contact blood vessels. Notably, vRGCs are not only distinct from oRGCs in the location of their cell bodies, these two cell types have unique gene expression profiles (Pollen et al. 2015). Importantly, in

humans a large number of oRGCs along with an increased number of IPCs has been associated with protracted development and the expansion of the human cerebral cortex (Hansen et al. 2010; Borrell and Götz 2014). Newly generated neuroblasts migrate along the basal processes of RGCs to populate the developing cortex in an inside out manner; early born neurons populate deeper cortical layers, whereas late born neurons make up the upper layers of the cortex. The majority, if not all of the neurons derived from the pallial VZ and SVZ become excitatory neurons that express the neurotransmitter glutamate.

### **c. Radial glial cells and inhibitory neurons in the subpallium**

The ventral telencephalon or subpallium generates cells to form basal ganglia, such as the striatum and globus pallidus. Interestingly, however, ventral germinal zones are also the source of most, if not all, inhibitory neurons in the neocortex (Tan and Shi 2013). RGCs and IPCs in the subpallium are also responsible for generating a diverse pool of neurons to various parts of the brain including GABAergic projection neurons for globus pallidus (Nóbrega-Pereira et al. 2010) and amygdala (Hirata et al. 2009), cINs for the striatum (Deacon, Pakzaban, and Isacson 1994; Marín, Anderson, and Rubenstein 2000) and olfactory bulb (H. Wichterle et al. 2001) and cholinergic neurons that reside in the basal telencephalon (Marín and Rubenstein 2003).

### **d. Setting up the main question of this thesis work**

From the above, it is clear that the cerebral cortex derives its neurons from two sources that separate in development. In fact, the excitatory neurons are locally derived from the pallium, but the inhibitory neurons need to migrate tangentially a long distance from subpallium to reach the cortex. How the final number of these cell populations is determined remains fundamental to understanding how the proper levels of excitation and inhibition are established during development. An intriguing aspect about the development of cerebral cortex neurons is that both the pallium and subpallium produce a supernumerary number of neurons during

embryonic development. This surplus of neurons is eliminated in mice through programmed cell death (PCD), a process that occurs perinatally for excitatory neurons and postnatally for inhibitory neurons. The overproduction of cortical neurons raises several fundamental questions including why neurons are overproduced, how is the process of elimination regulated and whether these two distinct populations of cells interact to regulate their survival.

#### **e. Introduction to cIN development**

Perhaps most intriguing is how cIN numbers are adjusted after their long tangential migration from the ventral telencephalon. Before explaining this problem in more detail, I will further explain the origin and remarkable migration of these populations of essential inhibitory neurons of the cerebral cortex. In humans, the cerebral cortex is a highly folded structure, consisting of many sulci and gyri to accommodate a greatly expanded (compared to most other mammalian species) surface area and a large number of cells. In mice, for example, the cerebral cortex has a smooth surface and is 1000-fold smaller. At the microscopic level however, the cytoarchitecture of the cerebral cortex is strikingly similar. The cerebral cortex is organized into a six-layered structure that is readily distinguished by the density and types of cells in each layer. While great efforts have been made to uncover the many subtypes of neurons existing in the cortex, neurons are broadly classified as explained above into excitatory (EN) or inhibitory (cIN). In the mouse cortex, GLUTAmatergic ENs amount to roughly seventy to eighty percent of all neurons while GABAergic cINs comprise about twenty to thirty percent of the total neuronal population (Hendry et al. 1987; Markram et al. 2004; Sherwood et al. 2010). In the human cerebral cortex the proportion of cINs is consistently higher than that of mice, with some cortical regions displaying similar proportions of EN and cINs (Fang et al. 2022). While usually smaller in proportion, cINs are essential for gating and modulating activity in the brain. Indeed, dysfunction or changes in the number of cINs is a hallmark of several neurological disorders (Rubenstein and Merzenich 2003; Lewis, Hashimoto, and Volk 2005; Chao et al. 2010; Marín

2012; Verret et al. 2012; Rossignol 2011). Given the pivotal role that cINs play in regulating the level of cortical inhibition, how sufficient numbers of these cells are produced in their sites of birth, and ultimately how their number is adjusted by PCD are key features of cerebral cortex development and essential for proper brain function.

#### **f. Specification and birth of cINs**

As explained above, while ENs are born locally in the developing pallial cortex, cINs are produced in the subpallium. The subpallium is anatomically divided into the caudal, lateral, and medial ganglionic eminences (CGE, LGE and MGE respectively), and preoptic area (PoA). These germinal zones are also defined by unique marker expression, and in the types of neurons they produce. Indeed, the emergence of GABAergic cIN diversification is in part due to the regional and temporal marker expression in these subpallial regions.

For example, the LGE can be readily distinguished by the combinatorial expression of Pax6, Meis2 (Low in MGE) and Gsx2 (low in MGE)(Su et al. 2022; Pei et al. 2011). Expression of NKX2.1 alone demarcates the MGE from the CGE and LGE (Sussel et al. 1999; Corbin et al. 2003). However, the MGE can also be distinctly distinguished by the combinatorial expression of the transcription factors Lhx6, Nkx6.2 and Nkx2.2 (Alifragis, Liapi, and Parnavelas 2004; Sousa et al. 2009; Fogarty et al. 2007; Flames et al. 2007). The CGE is rich in Coup-TFII positive progenitor cells (Kanatani et al. 2008). Lastly, the PoA can be distinguished by the combinatorial expression of Nkx2.1, and Nkx2.5, and Dbx1(Gelman et al. 2009).

While the function of some of the regionally expressed genes within the GEs has been known, the role of many of these genes still remain largely understudied. Many of the above regionally expressed genes exert more than one function during development. For example, the transcription factor Pax6 plays a role in proliferation, laminar fate specification and neuronal

migration(Manuel et al. 2015). *Gsx2* is a transcription factor that is required for LGE specification and key for maintaining LGE progenitors in an undifferentiated state (Pei et al. 2011) while the transcription factor *Meis2* is important for the differentiation of LGE precursor cells (Su et al. 2022). In the MGE, *NKX2.1* and *NKX6.2* are required for the specification of PV+ and SST+ cINs (Sussel et al. 1999; Sousa et al. 2009; Fogarty et al. 2007) while *Lhx6* plays an important role in the migration of MGE-derived cINs to the developing cortex (Alifragis, Liapi, and Parnavelas 2004). *Nkx2.2* plays a role in the specification of oligodendrocyte cells (Cai et al. 2010). In the CGE *COUP-TFII* plays an important role in specifying the unique migratory behavior of CGE cells (Kanatani et al. 2008).

Fate mapping studies have shown that the types, composition, and number of neurons arising from each of the above germinal zones varies significantly. For example, the LGE primarily gives rise to striatal medium spiny neurons and olfactory bulb cINs that include granular cells, periglomerular cells and short-axon cells(sussel 1999 and Wichterle 199). The CGE generates gabaergic projection neurons for the amygdala and is the second largest source of cINs for neocortex and hippocampus (Nery, Fishell, and Corbin 2002). About 30% of all cINs are born in the CGE and express the vasoactive intestinal polypeptide (VIP) or Reelin (RLN) (Miyoshi et al. 2010; Rudy et al. 2011; Lee et al. 2010). The medial ganglionic eminence (MGE) produces GABAergic projection neurons for the globus pallidus, cINs for striatum and cortex, and cholinergic neurons that reside in the basal telencephalon (Sussel et al. 1999; Hynes Wichterle et al. 1999; Zhao et al. 2003). MGE-derived cINs make up roughly 60% of all cINs in cortex and express parvalbumin (PV) or somatostatin (SST) largely in a non-overlapping manner. The remaining 10% of all cINs are derived from the PoA and express PV, SST or RLN (Anastasiades and Butt 2011; Gelman, Marín, and Rubenstein 2012; Hernández-Miranda, Parnavelas, and Chiara 2010; Wonders and Anderson 2006). Together the MGE, CGE and PoA, in mice, generate all cINs that reside in the cerebral cortex. In the more complex primate



brain, it has been suggested that a subpopulation of striatal cINs and cINs, is derived from pallium and LGE (Delgado et al. 2022; Letinic, Zoncu, and Rakic 2002; Petanjek, Berger, and Esclapez 2009). However, the CGE and MGE remain a very important source of cIN in the human cerebral cortex, with expanded proliferation and amplification of IPCs in the MGE (Hansen et al. 2013; Alzu'bi et al. 2017; M. F. Paredes et al. 2022; T. Ma et al. 2013).

Notably, the diversity of cINs in the cortex not only stems from regional differences in gene expression of key transcription factors in the different subpallial germinal zones, but also from changes in the timing of development. Generally cINs are produced between E11.5 and E16.5. In the MGE, early born progenitors have a bias for the production of SST positive cINs while later born progenitors tend to produce more PV cINs (Valcanis and Tan 2003; Butt et al. 2005; Miyoshi et al. 2007; Wonders et al. 2008; Batista-Brito and Fishell 2009). Generation of cINs in the CGE starts later than that in the MGE; hence while neurogenesis peaks around E13.5 in the MGE, the CGE production of neurons peaks around E15.5 (Butt et al. 2005; Nery, Fishell, and Corbin 2002). Accordingly, early born neurons tend to occupy deeper cortical areas while late born neurons settle in more superficial layers of the cortex (Valcanis and Tan 2003; Miyoshi et al. 2007). Indeed, the final layer position of cINs in the cortex is also a reflection of their place and time of birth. MGE-born cINs generally occupy deeper layers, while CGE-derived cINs are more frequently found in the upper cortical layers (Butt et al. 2005).

#### **g. cIN Migration**

Postmitotic cINs exit the MGE and CGE in the subpallium through various routes to reach their final destination: LGE cINs migrate rostrally to the olfactory bulb (OB) along the rostral migratory stream (RMS) a process that is retained postnatally (Hynek Wichterle et al. 1999; Lois and Alvarez-Buylla 1994; Luskin 1993). In contrast, MGE- and CGE- derived cINs migrate tangentially and mostly dorsally to the cortex during a restricted period of embryonic

development (S. Anderson 1999; Parnavelas 2000; Lavdas et al. 1999; Hynek Wichterle et al. 1999; Sussel et al. 1999; H. Wichterle et al. 2001; N. Tamamaki, Fujimori, and Takauji 1997; Tanaka et al. 2003; Tong Ma et al. 2012; Miyoshi et al. 2010). A subpopulation of MGE- and pallial- derived cINs also joins the RMS and migrates into the olfactory bulb to generate specific subtypes of cINs (Delgado et al. 2020). In contrast to newborn cortical projection neurons, cINs must travel far greater distances and change modes of migration to reach their final location. Indeed, cINs first migrate tangentially long distances from their birthplace to reach the cortical plate where they switch to a radial migration mode to reach their final layer position within the cortex. In the developing human brain, cINs must migrate significantly greater distances given the larger brain size and cIN migration is retained for protracted periods that extend into postnatal stages of development (M. F. Paredes et al. 2022) , a testament to the remarkable migratory capacity of young cINs.

#### **h. Cell death and the neurotrophin hypothesis.**

Programmed cell death(PCD) is an essential feature to the development of all organs. Among neurons, PCD has been best characterized in the peripheral nervous system and is explained through the neurotrophic factor hypothesis. In the peripheral nervous system, neurons are overproduced and their survival depends on limited availability of factors secreted by the target tissues (Huang and Reichardt, 2001; Aloe and Chaldakov, 2013; Oppenheim and Carolanne, 2013, Cowan, 2001, Levi-Montalcini, 1987, Oppenheim, 1991, Purves et al., 1988, Raff, 1992). For example, the number of surviving dorsal root ganglion sensory neurons (DRG) expressing the TrkA,TrkB or TrkC receptors is determined by limited availability of trophic factors secreted by the target tissue these neurons innervate such as the skin and muscles (Huang and Reichardt 2001). In this order, TrkA+ DRG neurons are dependent on nerve growth factor (NGF), TrkB+ DRG neurons are dependent on neurotrophin-3 (NT3) and TrkB+ DRG neurons depend on brain-derived neurotrophic factor (BDNF) for survival (Hamburger and Yip 1984),

(Mousavi and Jasmin 2006), (Oakley et al. 1997). Other trophic factors (and their corresponding receptors) that are key to the regulation neuronal PCD include NT4(TrkC), GDNF (Ret) and Neurturin (Ret)(Enomoto et al. 2000; Huang and Reichardt 2001) . Importantly, the trophic factors mentioned above exist in a limited amount in their existing locations. Altogether, the studies above along with many others point to the notion that the limited nature of neurotrophic factors available in each target tissue is only sufficient to support survival of a given number of those projections neurons that innervate the target tissue.

#### **i. Neuronal programmed cell death in the cortex.**

As explained above, during embryonic development, cINs are produced in the ganglionic eminences, migrate to the cortex, and become integrated with local cells including local excitatory neurons and other inhibitory cells. Previous work in the Alvarez-Buylla laboratory(Southwell et al. 2012) identified a period of PCD that results in the elimination of nearly 40% of the population of cINs that had integrated into the cortex. This process of cIN cell death occurs between postnatal day (P) 1 and P15, and peaks around 10 to 15 days after cINs are born. Given the large amount of data supporting the neurotrophic hypothesis and the fact that brain derived neurotrophic factor (BDNF) constitutes the most abundant neurotrophin in the CNS (Huang and Reichardt, 2001; Aloe and Chaldakov, 2013; Oppenheim and Carolanne, 2013), how the final number of cINs that survive is determined could potentially be explained by a limited supply of BDNF in the neocortex (explained below). Data in support and against this hypothesis exists. For example, Alcántara S. et al. reported increased numbers of apoptotic cells in the brains of TrkB knockout mice (Alcántara et al. 1997). Others, however, have found no changes in neuronal number upon the overexpression or removal of the TrkB throughout the CNS(Rauskolb et al. 2010; Silos-Santiago et al. 1997; Nikolettou et al. 2010). Recent work from the Alvarez-Buylla Laboratory strongly suggests that BDNF does not play a role in the regulation of the naturally occurring PCD postnatally in cINs. Indeed, heterochronically

transplanted cIN precursors cells that carry or lack the BDNF receptor TrkB display essentially similar survival (Southwell et al. 2012). Still, it remains unknown if other neurotrophins play a role in the selection of cINs that form part of the mature circuit, and how PCD is regulated remains unclear and controversial - discussed more in detail below (Duan et al. 2020; Wong et al. 2018; Southwell et al. 2012).

Interestingly, Glutamatergic ENs also undergo a period of PCD that occurs between P2 and P5, largely before the peak of cIN cell death in the cortex at P7 (Wong et al. 2018). The significance of the sequential waves of PCD, first for ENs and then among cINs in the cortex remains unknown. What makes the process of cIN cell death in the cortex more intriguing is its timing and location. While most cINs are born between E11.5 and 16.5, their elimination occurs postnatally (10-15 days later) and in the cortex, far from their birthplace. It is also during this period that synchronized patterns of activity have been observed in most regions of the developing CNS including the cerebral cortex (Yuste et al. 1995; Dupont et al. 2006; Allene et al., n.d.; Khazipov and Luhmann 2006; Luhmann et al. 2016; Y. Ben-Ari et al. 1989). During the first week of postnatal cortical development, these spontaneous patterns of activity are driven by gap junction-mediated, glutamate-receptors and/or GABA receptor activation (Heiko J Luhmann 2018).

The emergence of such patterns of activity in the developing cortex correlates with 1) the period when cINs increase their morphological complexity (this thesis), 2) the time when synaptic connectivity increases (Seress, Frotscher, and Ribak 1989; Yang et al. 2012; Connors, Benardo, and Prince 1983; Tyzio et al. 1999; Yehezkel Ben-Ari et al. 2004; Agmon, Hollrigel, and O'Dowd 1996), and 3) with the onset of cIN PCD (Egorov and Draguhn 2013; Blanquie et al. 2017). Indeed, several groups have proposed that cIN PCD in the cortex is regulated through activity-dependent mechanisms (Wong et al., 2018; Denaxa et al., 2018; Duan et al.,

2020; Priya et al., 2018). Perhaps the most compelling evidence comes from Nathalie De Marco Laboratory at Cornell University from a study published in Cell Neuron in 2020 (Duan et al. 2020), where they show that GABA transmission plays an important role in the regulation of network activity in the somatosensory cortex. Indeed, blocking vesicular GABA release in cINs via the  $Lhx6^{Cre};Vgat^{fl/fl}$  mouse line or the loss of function of the GABA receptor from ENs via the  $Emx1Cre;GABA\gamma 2^{fl/fl}$  mouse line, led to a higher participation of cINs and ENs in correlated network activity and concomitantly to a decrease in the levels of normal cell death (Duan et al. 2020). In contrast, decreasing the activity of cINs via expression of Kir2.1 led to decreased participation of cINs in network activity and to a simultaneous increase in apoptosis (Duan et al. 2020).

While the above work suggests that activity is essential for survival of MGE derived cINs during the normal period of cell death, it remains unclear how GABA leads to increased participation of cINs and ENs in network activity. It is also unclear whether increased activity in cINs or ENs plays a role in the selection of cINs that will survive or undergo cell death. It is plausible that increased activity leads to the general activation of survival pathways, and that this process is independent of the process of selecting cINs that are eliminated during PCD. Finally, the prevailing hypothesis suggests that GABA has an excitatory role during the first of postnatal week of development, hence loss of GABA release should in theory result in reduced pyramidal cell participation and not in their increased participation as suggested by the above results.

Several questions emerge from the aforementioned observations including 1) why so many cINs undergo such an extensive migration to the cortex, to then die, 2) what function cINs destined to die have prior to their elimination, and 3) what are the molecules that regulate PCD

among cINs in the cortex. My thesis work begins to explore key molecules that regulate PCD in cINs.

Before introducing my thesis work I will further discuss the main bodies of work that attempt to explain how PCD is regulated in the cortex, including work that refutes BDNF-drive survival, work that supports activity-driven survival and work from the Alvarez-Buylla laboratory that proposes a cell or population model for the regulation of cIN numbers in the cortex.

## **CHAPTER 2: THESIS STRUCTURE**

### **a. Regulation of programmed cell death through a cell or population mechanism**

Subpallial immature cINs show a unique capacity to migrate, differentiate, and integrate into neural circuits following heterochronic transplantation (Southwell et al. 2014; Larimer et al. 2016, 2017; Southwell et al. 2012, 2010; Tang et al. 2014), a feature that largely reflects their ontogeny: during development subpallial-derived cINs must migrate long distance, differentiate and survive in an environment that is distinct from their site of birth. Remarkably, transplanted MGE and CGE progenitors closely follow the developmental time-course of endogenous cINs, including timing of migration (H. Wichterle et al. 2001), the extent and timing of PCD (Southwell et al. 2012), the timing of differentiation and proportions of cIN subtypes that emerge (Larimer et al. 2016). Together these observations point to an intrinsic clock regulating the development of cINs, including their period of developmental cell death. Indeed, the heterochronic transplantation of MGE precursor cells shows that cIN cell death occurs in accordance with the age of the grafted cells, that is 7 to 21 days after birth (Southwell et al. 2012), and not according to the age of the host.

Heterochronic transplantation experiments of MGE precursor cells suggest that the regulation of PCD is not dependent on BDNF availability; however these experiments did not exclude a role in survival for other local trophic support. In order to decouple the activation of PCD in cINs from other local factors that could play a role in its regulation, heterochronic transplantation was used to introduce varying numbers of embryonic cIN precursor cells into the neocortex of WT mice. The rationale behind this was that if survival of cINs occurred in a trophic signal-dependent state, the amount of cIN cell death should increase with larger transplant sizes **if** survival is determined by intercellular competition for extrinsically derived signals. Surprisingly, the proportion of transplanted surviving cINs in the host brain microenvironment is constant across grafts of various sizes, arguing against an extrinsic trophic-dependent survival mechanism (Southwell et al. 2012).

Together, heterochronic transplantation experiments of cIN precursor cells suggest that PCD among cINs in the cortex is largely regulated through intrinsic mechanisms at the cell or population level. Furthermore, heterochronic transplantation of cIN precursor cells decouples the age of the grafted cells from that of host cells (cINs and ENs), and also uncouples early postnatal host activity from that of the grafted cells. Since heterochronically transplanted cINs undergo PCD in a proportion that closely resembles that of host cINs (~40% reduction in cell number, see Figure 9 and Supplement Figure 10. ), and the amount of cell death does not scale up with increasing graft sizes, then host activity fails to explain why the same fraction of cINs survive across multiple graft sizes. Under the trophic or host activity-dependent mechanism, higher proportions of cells are expected to survive in small grafts, assuming a finite supply of trophic factors or activity is provided by the local microenvironment. One potential explanation for the above observations is that a secreted molecule or the activity within the grafted cINs scales up to regulate survival among the transplanted cells. Together these observations

suggest that while activity is key to cIN survival, transplantation experiments suggest that regulation of PCD occurs through a cell or population mechanism within cINs.

From the above work, several cell or population intrinsic mechanistic models have been proposed to account for the adjustment of cINs in the cortex during PCD including 1) a proportion of cINs may carry defects possibly produced during their production in the MGE and these cells are eliminated postnatally by PCD, 2) an intrinsic molecular clock is activated in cINs postnatally that triggers apoptosis in a transient population of cINs that have a transitory function and 3) cINs in the cortex compete among themselves for survival factors that include molecules secreted among themselves, activity or through contact dependent mechanisms.

#### **b. Thesis hypothesis**

My thesis work explores the latter mechanistic hypothesis: cINs compete for survival among themselves using cell-adhesion molecules that allow them to interact among themselves. I proposed that clustered protocadherins(Pcdhs), which have been implicated in PCD in retina and spinal cord (see below) could be involved in such a mechanism. Note that interactions of cIN among themselves, possibly mediated by protocadherins, does not preclude additional interactions with other cell types including the ENs; given the diversity and function of clustered Pcdhs, these set of adhesion proteins could be also involved in informing individual young cINs what other cells they are interacting with. Given that cINs undergo long migration from the subpallium to reach the cortex where they interact with local ENs, we reason that cell-adhesion molecules might play a role in PCD.

#### **c. The Clustered Protocadherins**

The clustered protocadherins (Pcdhs) (Wu and Maniatis, 1999, Add Yagi) are a set of cell surface homophilic-binding proteins implicated in neuronal tiling, arborization, survival and axon



targeting (Wang et al., 2002b; Lefebvre et al., 2012, Lefebvre et al., 2008; Katori et al., 2017; Mountoufaris et al., 2017; Chen et al., 2017). In the mouse, the clustered Pcdh gene locus encodes a total of 58 isoforms that are arranged in three tandemly arranged gene clusters, alpha, beta and gamma: *Pcdh $\alpha$* , *Pcdh $\beta$* , and *Pcdh $\gamma$*  (Wu et al., 2001). The *Pcdh $\alpha$*  and *Pcdh $\gamma$*  isoforms are each composed of a set of 14 and 22 large variable exons respectively, each coding for the extracellular, transmembrane, and most-proximal intracellular segment of a protocadherin. Each Pcdh variable exon is transcribed from its own promoter (Canzio et al. 2019; Esumi et al. 2005; Tasic et al. 2002; Wang, Su, and Bradley 2002; Wu and Maniatis 1999). Three additional exons, found at the 3' end of the *Pcdh $\alpha$*  or *Pcdh $\gamma$*  gene clusters, are alternatively spliced to each variable exon, and code for the most-distal intracellular domain of a Pcdh, providing a common cytoplasmic region to all Pcdh isoforms within each subcluster (Wu and Maniatis, 1999, Tasic et al., 2002; Wang et al., 2002a). The 22 *Pcdh $\beta$*  isoforms are encoded by single exon genes encoding both extracellular, transmembrane, and cytoplasmic domains (Wu and Maniatis, 1999).

Single cell RT-PCR studies in cerebellar Purkinje cells suggest that each neuron expresses around 15 clustered Pcdh isoforms that include 10 stochastically expressed alternate *Pcdh $\alpha$* , *Pcdh $\beta$* , and *Pcdh $\gamma$*  isoforms in addition to 5 constitutively expressed C-type isoforms (*Pcdhac1*, *Pcdhac2*, *Pcdhyc3*, *Pcdhyc4* and *Pcdhyc5*) (Esumi et al., 2005; Kaneko et al., 2006; Mountoufaris et al., 2017). This mode of expression potentially endows each neuron with a unique combinatorial Pcdh code (Canzio et al., 2019), but also suggests an important role for the constitutive C-type Pcdh genes. Indeed, the C-type isoforms in the *Pcdh $\gamma$*  cluster (*Pcdhyc3*, *Pcdhyc4*, and *Pcdhyc5*) are required for the postnatal survival of mice (Wang et al., 2002b; Hasegawa et al., 2016; Chen et al., 2012).

In this thesis work, I used a series of genetic deletions of the cluster *Pcdh* gene locus to probe the role of clustered *Pcdhs* in the regulation of cIN cell death in mice. In the first part of my thesis work, we show that *Pcdhy* genes, but not *Pcdha* or *Pcdhb* genes, are required for the survival of approximately 50% of cINs through a BAX-dependent mechanism. I probe whether cINs compete for survival using clustered PCHDs by employing a co-transplantation assay I developed. My data suggest that indeed *Pcdhy*-deficient and wild-type (WT) cINs of the same age compete for survival in a mechanism that involves *Pcdhy*. Using the co-transplantation assay, I also study postnatally the effect of clustered *Pcdh* mutations that cause lethality in neonatal mice. While mice with constitutive deletion of *Pcdhyc3*, *Pcdhyc4*, and *Pcdhyc5* isoforms (*Pcdhy*<sup>tko</sup>) die perinatally, cINs precursors cells from *Pcdhy*<sup>tko/tko</sup> mice were transplanted with cells carrying WT *Pcdhy*. Deletion of the three C-type isoforms in the *Pcdhy* cluster was sufficient to increase cell death of MGE-derived cINs to levels comparable to the deletion of the whole *Pcdhy* cluster. Surprisingly, three-dimensional reconstructions and patch-clamp recordings indicate that the *Pcdhy* mutant cells have similar morphology, excitability and receive similar numbers of inhibitory and excitatory synaptic inputs compared to wild type cINs.

In the second part of my thesis work, I use a combination of *Pcdhy* KO lines to investigate the function of the C-type isoforms in the regulation of cIN survival. Results clearly show that the 19 alternate A- and B-type *Pcdhy* isoforms do not play a role in the regulation of cIN survival. Additionally, two of the C-type *Pcdhy* isoforms (*Pcdhyc3* and *Pcdhyc5*) do not seem to play an important role in the regulation of PCD. The sole removal of *Pcdhyc4* is sufficient to increase the death of cINs and expression of *Pcdhyc4* alone in cINs lacking the entire *Pcdhy* cluster prevents cINs from dying

We conclude that survival of most cINs in the cortex depends solely on the expression of one of the fifty-eight *Pcdh* isoforms (PCDH<sub>Y</sub>C4). Further, the regulation of *Pcdhyc4*-mediated

survival is independent of the structural complexity or intrinsic physiological properties of the cell or the strength of its excitatory and inhibitory synaptic inputs. Expression of *Pcdhyc4* in cINs lacking all *Pcdhy* isoforms prevents cell death in those cINs, strongly suggesting that expression of *Pcdhyc4* is key to the regulation of cIN cell death.

#### **d. Thesis organization:**

In the first part I describe the expression of the alpha, beta, and gamma clustered *Pcdhs* in the brain. I initially assayed the expression of the fifty-eight *Pcdh* isoforms using whole cortex extracted RNA and real time RT-PCR. I show in a non-cell type specific way that all *Pcdh* isoforms are expressed in the cortex of P30 mice. I also show expression of a select group of the *Pcdhy* isoforms at various time points during the first two weeks of postnatal development in isolated cINs. For this particular experiment cINs were extracted from the cortex, isolated from the rest of the cells using Fluorescence Activated Cell Sorting (FACS) and RT-PCR was used to assay gene expression.

In the second part I investigated which of the *Pcdh* gene clusters (*Pcdha*, *Pcdhb*, or *Pcdhy*) is involved in the survival of cINs. I use mice with entire *Pcdh* gene cluster loss of function or deletion and crossed to MGE reporter mice to label the cINs in the cortex derived from the MGE. I analyze the density of cINs in two regions of the cortex, the visual and somatosensory cortex. I find that the loss of function of *Pcdhs* from the *Pcdhy* gene cluster, but not from the *Pcdha* or *Pcdhb*, results in approximately 50% reduction in the density of cINs in the areas analyzed. I next remove the function of *Pcdhy* isoforms using the conditional FCON3 allele by crossing to either the *Gad2<sup>Cre</sup>*, *Nkx2.1<sup>Cre</sup>*, *SST<sup>Cre</sup>* or *PV<sup>Cre</sup>* mouse reporter lines. I found similar reductions in cIN density in the cortex of the *Gad2<sup>Cre</sup>*, *Nkx2.1<sup>Cre</sup>* and *SST<sup>Cre</sup>* mice, but not in *PV<sup>Cre</sup>* mice, suggesting that the *Pcdhy* gene cluster function to cIN density is restricted early postnatal or embryonic deletion. In order to understand the origin of the reduced cIN density in

*Pcdhy* loss of function mice, I look at whether these mice had defects in the production of cINs, their migration to the cortex or the numbers of cells undergoing apoptosis. I found that both the proliferative capacity of cIN precursor cells and the migratory ability of young cINs was similar in mice with WT *Pcdhy* or with loss of function of the *Pcdhy* genes. However, I found a heightened period of cell death in cINs from mice lacking *Pcdhy* function when compared to cINs carrying WT *Pcdhy*. Notably, the heightened levels of apoptosis in the mutant mice occurred during the first and second postnatal week of development, and overlaps with the naturally occurring period of cIN cell death. In order to validate whether the *Pcdhy*-mediated reduction in cIN destiny in the cortex of P30 mice stemmed from a heightened PCD wave, I cross *Pcdhy* mutant mice to *Bax* null mice. Indeed, in the double mutant mice (*Pcdhy* cKO and *Bax* cKO) the *Pcdhy*-mediated decrease in cIN density was rescued. Surprisingly, in these double mutant mice, cells that are normally eliminated in the period of cell death were also rescued. Data from this part of my thesis work effectively demonstrates that genes in the *Pcdhy* cluster, but not those in the *Pcdha* or *Pcdhb*, play a key role in cIN survival during PCD.

In part three I evaluate whether the survival role *Pcdhy* isoforms play is through contact mediated interactions. To this end, I test directly whether cINs regulate their survival using *Pcdhy*. To test this hypothesis, I developed a co-transplantation assay to study, in the same host microenvironment, the survival of cINs carrying WT or mutant *Pcdhy* alleles. The co-transplantation technique was also instrumental to the postnatal study of alleles that cause neonatal lethality and to the study of the morphological and electrophysiological properties of cINs within the same preparation. Using these techniques, I discovered that MGE-derived cINs lacking *Pcdhy* function are eliminated in much greater proportions when mixed with cINs carrying WT *Pcdhy* when compared to survival of cINs in mice with conditional deletion of *Pcdhy* in all cINs. Surprisingly, in these co-transplants the cINs carrying WT *Pcdhy* also died at increased proportions when compared to cINs of transplants carrying only *Pcdhy*. These data

suggest that when young cINs have mismatched PCDHys at the population level as in the case of the co-transplants, the survival of the cINs is compromised.

In the fourth part I interrogate whether all the twenty-two isoforms encoded from the *Pcdhy* gene cluster are required for cIN survival. I used a series of genetic deletions of the *Pcdhy* gene locus to probe the role of *Pcdhy* isoforms in the regulation of cIN cell death in the mouse cortex. I found that the nineteen alternate *Pcdhy* isoforms (*Pcdhy* A- and B-type) do not play a role in survival. Previous work from other laboratories have shown that deletion of the three constitutively expressed *Pcdhy* C-type isoforms (*Pcdhyc3*, *Pcdhyc4* and *Pcdhyc5*) leads to perinatal death of mice. To test the role of the *Pcdhy* C-type isoforms to postnatal cIN survival, I transplanted cIN precursors cells lacking *Pcdhyc3*, *Pcdhyc4* and *Pcdhyc5* into the cortex of WT neonate mice. I found that similarly to the loss of function of the entire *Pcdhy* cluster (22 *Pcdhy* genes), the removal of the three *Pcdhy* C-type isoforms lead to marked reduction in cIN survival.

I next investigated whether all the C-type isoforms in the *Pcdhy* gene cluster conform survival properties to cINs. Surprisingly, loss of the *Pcdhyc3* and *Pcdhyc5* did not significantly affect the survival of transplanted cINs. However, cINs which were solely lacking *Pcdhyc4* underwent increased cell death to levels comparable to the deletion of the entire *Pcdhy* gene cluster, suggesting cIN use *Pcdhyc4* to regulate PCD. Lastly, to directly test the survival properties of *Pcdhyc4*, I reintroduced the *Pcdhyc4* gene using lentivirus to cINs that lack the function of all 22 *Pcdhy* isoforms. Indeed, the sole expression of *Pcdhyc4* via lentiviral approach prevented the *Pcdhy* mutant cells from dying.

In the final part of my thesis, I summarize the findings from the work I performed during my PhD, discuss the implications of my work regarding how brain size and final number of

neurons is determined in development, discuss the relevance of activity-dependent mechanisms for my work, and the implications for human biology and disease.

## CHAPTER 3: RESULTS

### PART I - Expression of clustered Pcdhs in cINs

#### Expression of clustered Pcdhs (*Pcdh $\alpha$* , *Pcdh $\beta$* , and *Pcdhy*) in the cerebral cortex and *Pcdhy* isoforms in cINs.

Expression of clustered protocadherins (Pcdh) in the brain starts in the embryo and continues postnatally (Hirano et al. 2012; Frank et al. 2005; Wang et al. 2002; Kohmura et al. 1998). RT-PCR analysis revealed the expression of each of the fifty-eight isoforms from the clustered Pcdh gene locus in the adult cortex (P30) (**Figure 1A**). Of the 58 Pcdh genes, those in the Pcdhy cluster are essential for postnatal survival (Hasegawa et al. 2016; W. V. Chen et al. 2012), and are implicated in cell death in the retina and spinal cord (Lefebvre et al. 2008; Prasad et al. 2008). We, therefore, determined whether Pcdhy genes are expressed in cINs in the cortex during the period of cIN cell death. Using *Gad67-GFP* mice to label GABAergic cINs (Nobuaki Tamamaki et al. 2003), we FACS-sorted GFP-positive (GFP+) and GFP-negative (GFP-) cells from P7 mice at the peak of cIN cell death (**Supplement Figure 1A**). We confirmed that GABAergic cell markers (*Gad1*, *Gad2*) were enriched in the GFP+ population, while markers of excitatory neurons (*Tbr1*, *Satb2*, *Otx1*), astrocytes (*GFAP*, *Aldh1L1*), and oligodendrocytes (*Olig2*, *MBP*) were enriched in the GFP- population (**Supplement Figure 1B**). With the exception of A9 Pcdhy isoform, we detected the expression of all other 21 Pcdhy (RT-PCR) in the cIN population (**Figure 1B**). To determine the expression pattern of Pcdhy at various stages during the period of cell death cINs, we measured the expression level of 8 Pcdhy mRNAs (*Pcdhyc3-5*, *Pcdhya1-A3* and *Pcdhyb6-7*) at P2, P5, P8, P12 and P15 using qPCR (**Figure 1C**). All eight isoforms were expressed at each of the 5 ages studied. Interestingly, the expression of *Pcdhyc5* increased dramatically between P8 and P15. An increase in expression of Pcdhy isoforms *Pcdhya1*, *Pcdhya2*, and *Pcdhyc4* was also observed at P12, compared to

other ages, but this increase was less pronounced than that observed for *Pcdhyc5*. The above results show that all Pcdh isoforms are expressed in cINs and that the expression of Pcdhy isoforms *Pcdhya1*, *Pcdhya2*, *Pcdhyc4*, and *PcdhyC5* increases during the period of postnatal cell death.



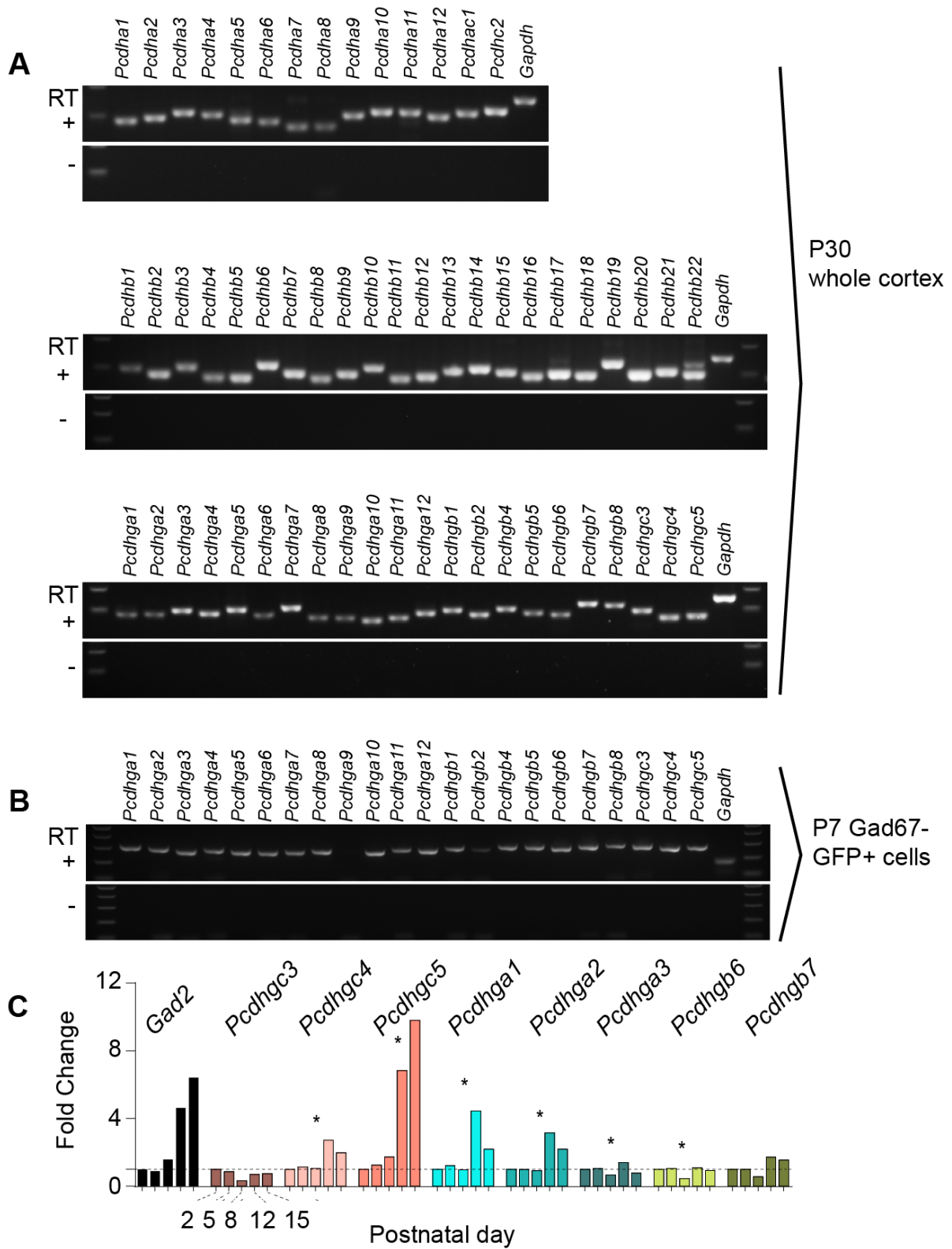
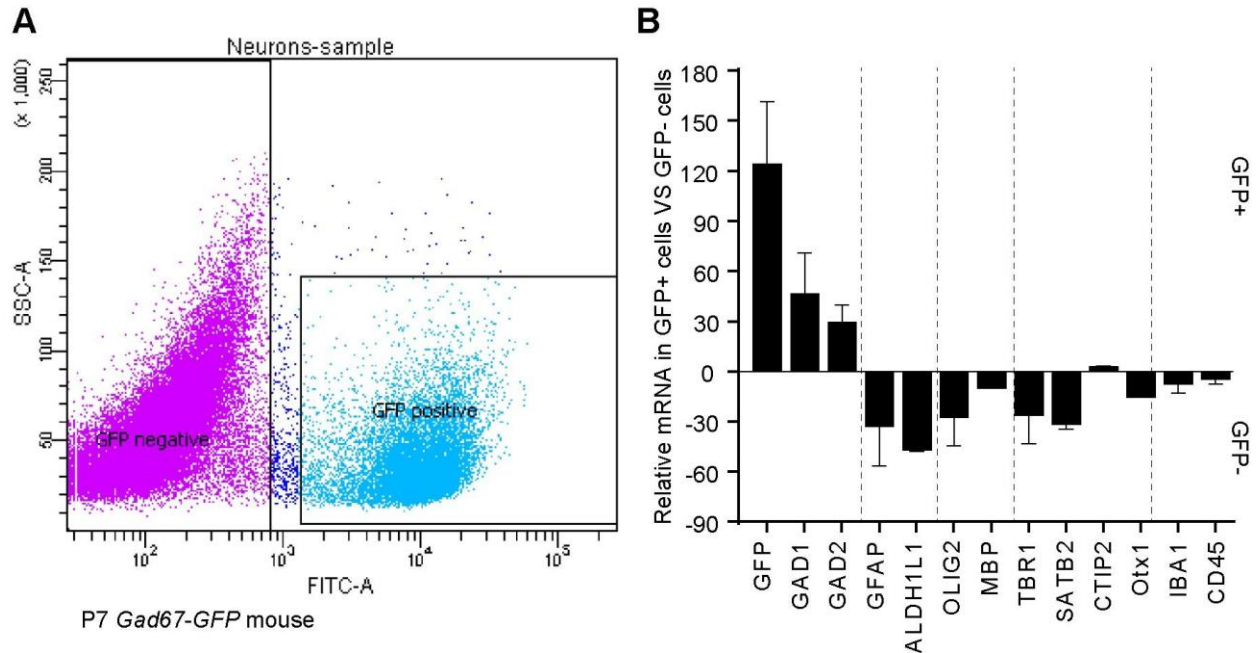


**Figure 1.1** - Expression of clustered Pcdhs in the mouse cortex and purified cortical GABAergic cells.

**Figure 1.1** - (A) PCR analysis of clustered *Pcdh* and *Gapdh* gene expression in P30 whole cortex extracts. (B) PCR analysis of *Pcdhy* and *Gapdh* gene expression in purified P7 cortical GABAergic cells. (C) Quantification of target gene mRNA levels at various postnatal stages (P2, P5, P8, P12, P15) in purified cortical GABAergic cells. P2 mRNA levels used as a reference for each gene (Kruskal-Wallis test, P value = 0.0007 [*Pcdhyc4*], P value < 0.0001 [*Pcdhyc5*], P value = 0.015 [*Pcdhya1*], P value = 0.024 [*Pcdhya2*], P value = 0.003 [*Pcdhya3*], P value = 0.038 [*Pcdhyb6*]; n = 3 technical replicas]. Significant p values are marked with\*. See Figure 1—source data 1 for follow-up of comparisons.



**Supplement Figure 1.1 - GABAergic markers are enriched in GFP positive FACS-sorted cells from *Gad1-GFP* mice.** – (Related to Figure 1.1) - (A) Representative flow cytometry plot, sorting GFP-positive cIN from *Gad1-GFP* mice. (B) Real-time RT-PCR analysis of GABAergic and non- GABAergic markers in positive and negative FACS-sorted GFP cells from P7 *Gad1-GFP* mice.

## **PART II - The clustered Pcdhs and their role in the regulation of cIN programmed cell death.**

### **PCDHY expression is lost in $Pcdhy^{fcon3}$ mice that also express CRE.**

As mentioned above, isoforms encoded from the *Pcdhy* gene cluster are essential for postnatal survival (Hasegawa et al. 2016; W. V. Chen et al. 2012), and are implicated in cell death in the retina and spinal cord (Lefebvre et al. 2008; Prasad et al. 2008). Therefore, while I do interrogate the function of all the clustered *Pcdh* genes in the regulation of cIN cell death in the cortex, we first probe the function of those genes in the *Pcdhy* cluster.

Most cINs are produced between embryonic days (E) 10.5 and 16.5 by progenitors located in the medial and caudal ganglionic eminences (MGE and CGE) (S. A. Anderson et al. 1997; H. Wichterle et al. 2001; Nery, Fishell, and Corbin 2002; Miyoshi et al. 2010). To address the potential role of *Pcdhy* in cIN development, we used the *Pcdhy* conditional allele ( $Pcdhy^{fcon3}$ ) to block production of all 22 *Pcdhy* isoforms (Lefebvre et al. 2008). In the  $Pcdhy^{fcon3}$  allele, the third constant common exon shared by all *Pcdhy* isoforms contains the sequence coding for GFP and is flanked by loxP sites (Lefebvre et al. 2008)(**Figure 3A**). In unrecombined  $Pcdhy^{fcon3}$  mice, all *Pcdhy* isoforms are thus fused to GFP. However, when these animals are crossed to a Cre driver line, expression of all the 22 *Pcdhy* genes in the cluster is abolished in Cre-expressing cells (Prasad et al. 2008).

In E13.5 embryos homozygous for the  $Pcdhy^{fcon3}$  allele, robust GFP expression was detected throughout the brain, including cells in the MGE and CGE (**Figure 3B**), indicating expression of *Pcdhy* isoforms in cIN progenitor cells. In order to validate that recombination of the  $Pcdhy^{fcon3}$  allele occurs in cells that express the CRE protein, we crossed  $Pcdhy^{fcon3}$  mice to *Nkx2.1<sup>Cre</sup>* mice that also carried the Ai14 allele to conditionally ablate expression of all *Pcdhy*

genes in GABAergic cells derived from the MGE and POA. NKX2.1 expression is detected in the ventral telencephalon from E9.5 (Sandberg et al. 2016; Shimamura et al. 1995) and is downregulated in most cINs as they migrate into the developing neocortex (Nóbrega-Pereira et al. 2008). Recombined cells were visualized thanks to the conditional tdTomato reporter allele Ai14 (Figure 3A). Homozygous *Nkx2.1::Cre-Ai14-Pcdhy<sup>fcon3/fcon3</sup>* embryos lost GFP expression specifically in the MGE and the preoptic regions (**Figure 3B**), consistent with full recombination and loss of Pcdhy function in cells derived from the Nkx2.1 lineage.

### Reduced number of cIN in the cortex of Pcdhy mutants

The initial goal was to investigate the function of all the genes in the Pcdhy cluster in all the brain cINs. To this end, we crossed *Pcdhy<sup>fcon3</sup>* mice to *Gad2<sup>Cre</sup>* mice (Taniguchi et al. 2011) to conditionally ablate expression of all Pcdhy genes in GABAergic cells throughout the CNS at an early embryonic stage (E10.5)(Katarova et al. 2000). As above, the recombined cells were visualized thanks to the conditional tdTomato reporter allele Ai14 (**Figure 2A**). Heterozygous *Gad2<sup>Cre</sup>-Ai14-Pcdhy<sup>fcon3/+</sup>* mice were viable and fertile. However, homozygous *Gad2<sup>Cre</sup>-Ai14-Pcdhy<sup>fcon3/fcon3</sup>* mice displayed growth retardation after birth, a hind limb paw-clasping phenotype when held by the tail and were infertile (**Figure 2B**). Brain size as well as cerebral cortex thickness of homozygous *Gad2<sup>Cre</sup>-Ai14-Pcdhy<sup>fcon3/fcon3</sup>* was similar to those of control mice (**Figure 2B'**). However, the density of tdTomato positive cells in somatosensory and visual cortex was roughly halved in homozygous *Gad2<sup>Cre</sup>-Ai14-Pcdhy<sup>fcon3/fcon3</sup>* animals, compared to wild type and heterozygous littermates (**Figure 2C & C'**). The density of cINs stained positive for parvalbumin (PV) and somatostatin (SST) (MGE-derived), vasoactive intestinal peptide (VIP) (CGE-derived) or reelin (RLN) (derived from both the MGE and CGE) was significantly reduced in the visual cortex of homozygous *Gad2<sup>Cre</sup>-Ai14-Pcdhy<sup>fcon3/fcon3</sup>* mice (**Figure 2D & Supplement Figure 2**). Consistent with the above observations, we found significant reductions of tdTomato positive cells in all layers of the visual cortex of *Gad2<sup>Cre</sup>-Ai14-Pcdhy<sup>fcon3/fcon3</sup>* mice, but the layer

distribution of cINs in these mice was similar to control mice, except for a significant change in the distribution of cells in layer V (**Supplement Figure 3**). Taken together, these experiments indicate that the embryonic loss of Pcdhy function in GABAergic progenitor cells leads to a drastically reduced number of cINs in the neocortex, affecting all cIN subtypes similarly.

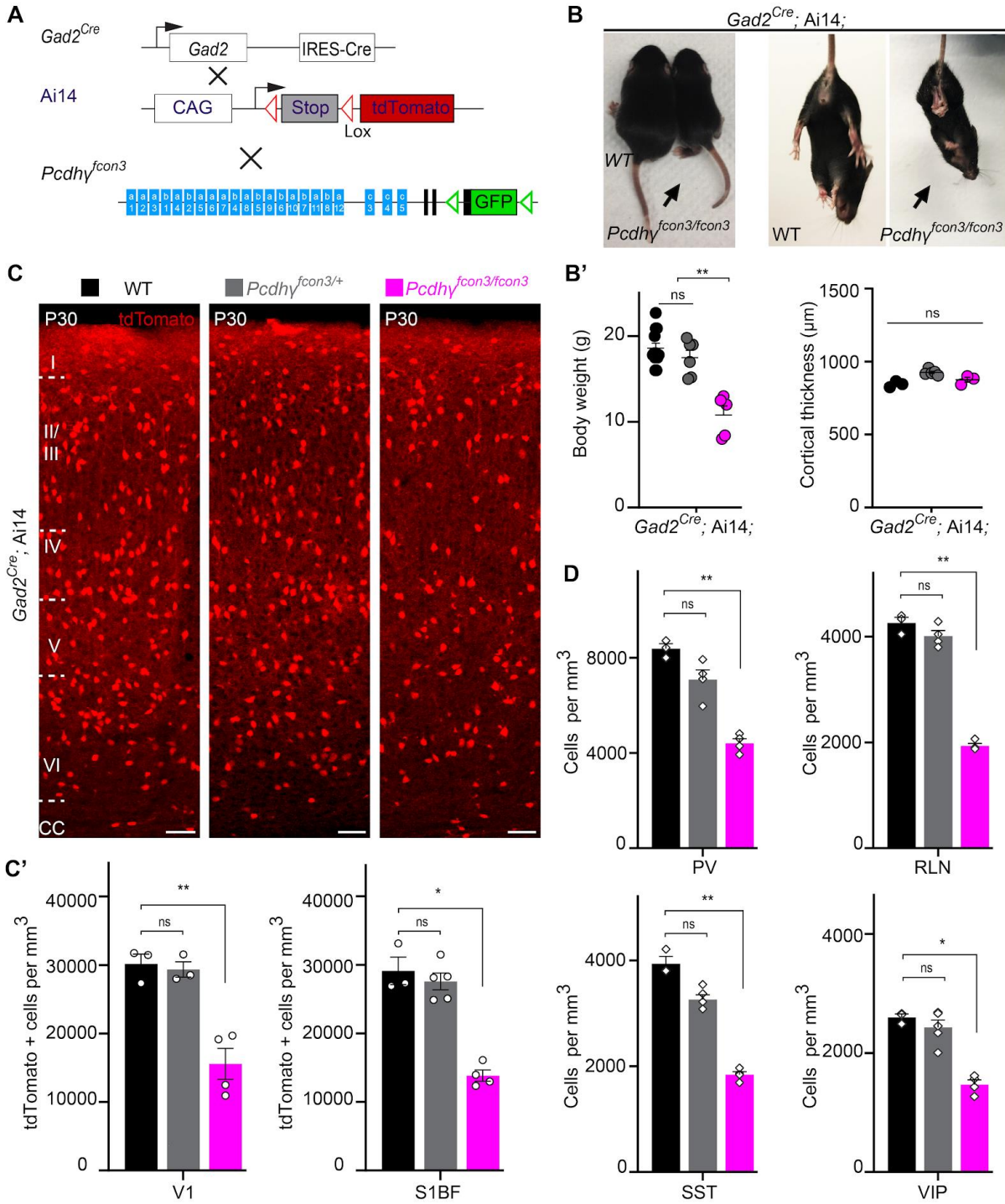
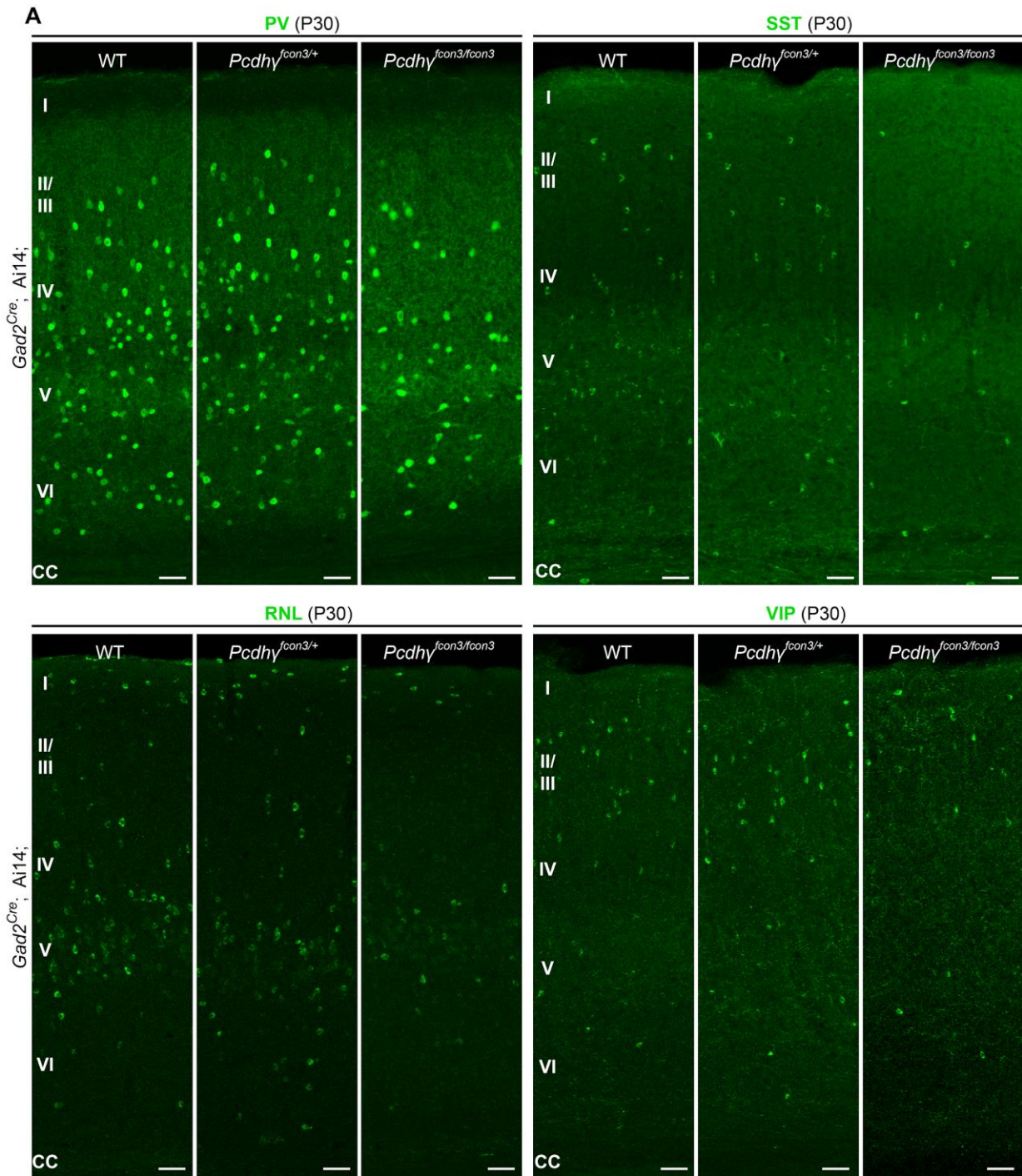


**Figure 2.1 - Reduced number of GABAergic cINs in Pcdhy-deficient mice.**

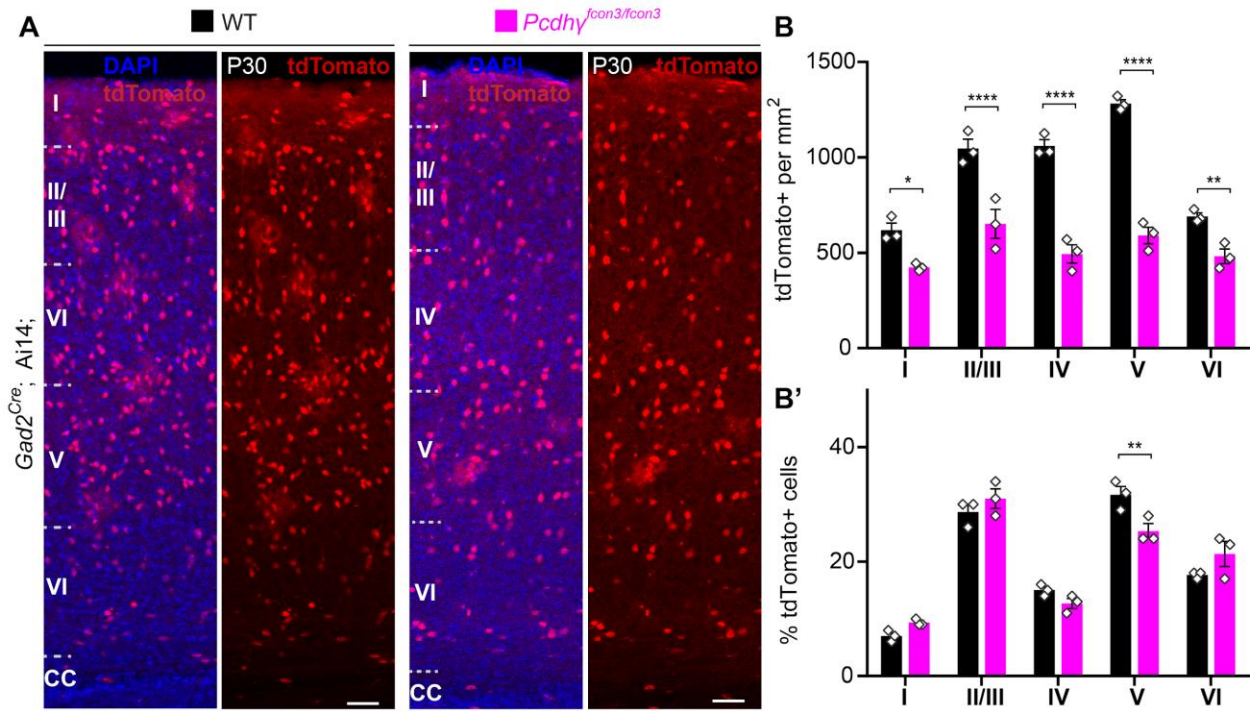
**Figure 2.1** - (A) Mutant mice with loss of *Pcdhy* in GABAergic neurons were generated by crossing conditional *Pcdhy*<sup>fcon3</sup> mice to Pan-GABAergic Cre driver (*Gad2*) mice. The conditional Ai14 reporter was used to fluorescently label *Gad2*-expressing cells. (B) Photographs of P21 *Gad2*<sup>Cre</sup>-*Ai14* mice that are wild type (WT) or mutant (*Pcdhy*<sup>fcon3/fcon3</sup>) for *Pcdhy*. (B') Body weight and cortical thickness measurements in P30 *Gad2*<sup>Cre</sup>-*Ai14*-*Pcdhy*<sup>+/+</sup> (*Pcdhy* WT), *Gad2*<sup>Cre</sup>-*Ai14*-*Pcdhy*<sup>fcon3/+</sup> (*Pcdhy* HET), and *Gad2*<sup>Cre</sup>-*Ai14*-*Pcdhy*<sup>fcon3/fcon3</sup> (*Pcdhy* mutant) mice (Kruskal-Wallis test, P value=0.0027, adjusted p values \*\*p=0.0017, n = 12 mice [*Pcdhy* WT], n = 7 mice [*Pcdhy* HET] and n = 5 mice [*Pcdhy* mutant]). (C) Photographs of coronal sections in primary visual cortex (V1) of P30 *Gad2*<sup>Cre</sup>-*Ai14*-*Pcdhy* WT (left), *Pcdhy* HET (middle) and *Pcdhy* mutant (right) mice. All cortical layers are similarly affected (**Supplement Figure 3**). Scale bar, 100  $\mu$ m. (C') Quantifications of tdTomato+ cell density in V1 and somatosensory (S1BF) cortex of P30 *Gad2*<sup>Cre</sup>-*Ai14* *Pcdhy* WT (black), *Pcdhy* HET (grey), and *Pcdhy* mutant (magenta) mice (Kruskal-Wallis test; for V1 (P value = 0.006), for S1BF (P value = 0.009); adjusted p values \*\*p=0.0180, \*p=0.036, n = 3–5 mice of each genotype). (D) Quantifications of cIN subtype density in V1 cortex at P30. All four non-overlapping cIN subtypes (PV, SST, RLN, and VIP) were similarly reduced in numbers in *Gad2*<sup>Cre</sup>-*Ai14*-*Pcdhy*<sup>fcon3/fcon3</sup> mice (*Pcdhy* mutant, magenta) compared to WT controls (Kruskal-Wallis test; for PV (P value = 0.0002), for SST (P value=0.0021), for RLN (P value = 0.0012), and for VIP (P value=0.0093); adjusted p values \*\*p=0.004 (PV), \*\*p=0.0073 (SST), \*\*p=0.0093 (RLN), \*p=0.0365 (VIP), n = 3–5 mice of each genotype).





**Supplement Figure 2.1** - Reduced number of GABAergic cIN subtypes in *Pcdhy*-deficient mice.

**Supplement Figure 2.1** - (Related to Figure 2.1) - (A) Representative photographs of the primary visual cortex (V1) in *Gad2<sup>Cre</sup>-Ai14 Pcdhy* WT, *Pcdhy* heterozygote and *Pcdhy* mutant mice. *Gad2<sup>Cre</sup>-Ai14* sections were stained for PV, SST, RLN or VIP. Scale bars, 50  $\mu$ m.



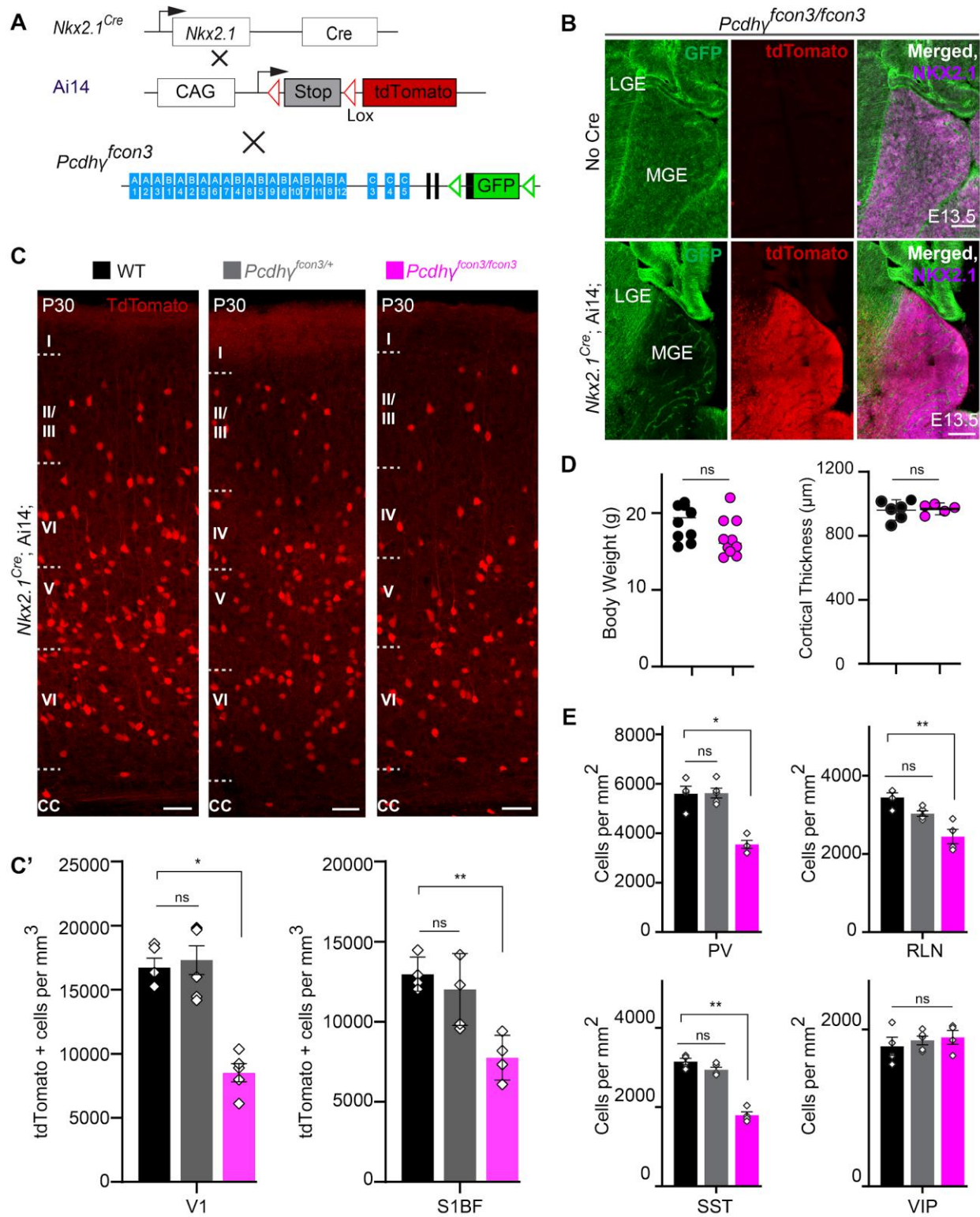
**Supplement Figure 3.1** - Reduced number of GABAergic cINs across cortical layers in *Pcdhy*-deficient mice.

**Supplement Figure 3.1** (Related to Figure 2.1 ) - (A) Representative photographs of the primary visual cortex (V1) in *Gad2<sup>Cre</sup>-Ai14-Pcdhy+/+* (*Pcdhy* WT) and *Gad2<sup>Cre</sup>-Ai14-Pcdhy<sup>fcon3/fcon3</sup>* (*Pcdhy* mutant) mice. Sections stained for tdTomato and DAPI. Scale bars, 50  $\mu$ m. (B) Quantification of tdTomato+ *Gad2<sup>Cre</sup>*-derived cINs in layers I-VI of visual cortex (V1) in *Pcdhy* WT (black bars) and *Pcdhy* mutant mice (magenta bars) (2-way ANOVA, Fgenotype = 244.83, P value < 0.001; adjusted p values \*p=0.02, \*\*p=0.01, \*\*\*p<0.0001; n = 3 mice per genotype). (B') Layer distribution of tdTomato+ *Gad2<sup>Cre</sup>*-derived cINs shown as percentage from total tdTomato+ cells in V1 of *Pcdhy* WT and *Pcdhy* mutant mice (2-way ANOVA, Fgenotype = 0.01, P value = 0.93, adjusted p values \*\*p=0.01; n = 3 mice per genotype).

The global *Pcdhy* loss of function in cINs may have indirectly affected the survival of cINs in a non-cell autonomous manner. In addition, and as mentioned above several developmental defects were observed in *Gad2Cre-Ai14-Pcdhy<sup>fcon3/fcon3</sup>* mice. Many of the *Pcdhy* mutant mice that showed growth retardation died before P21. Therefore, we decided to restrict the *Pcdhy* loss of function to MGE/POA (preoptic area) progenitors by means of the *Nkx2.1<sup>Cre</sup>* mouse (Xu, Tam, and Anderson 2008). MGE/POA progenitors give rise to the majority of mouse cINs, including PV and SST cINs. NKX2.1 expression is detected in the ventral telencephalon from E9.5 (Sandberg et al. 2016; Shimamura et al. 1995) and is downregulated in most cINs as they migrate into the developing neocortex (Nóbrega-Pereira et al. 2008). *Pcdhy<sup>fcon3</sup>* mice were crossed to *Nkx2.1<sup>Cre</sup>* mice. As described above, the Ai14 allele was again used to visualize the recombined cells (**Figure 3A**).

At P30, the number of MGE-derived tdTomato+ cells in *Nkx2.1<sup>Cre</sup>-Ai14-Pcdhy<sup>fcon3/fcon3</sup>* mice was dramatically reduced (~50%) in both the visual and somatosensory cortex (**Figure 3C & C'**). We also found reductions of tdTomato positive cells in layers II-VI of the visual cortex of *Nkx2.1<sup>Cre</sup>-Ai14-Pcdhy<sup>fcon3/fcon3</sup>* mice, consistent with the notion that MGE-derived cINs preferentially localize to deeper layers of the cortex (**Supplement Figure 6**). The layer distribution of the tdTomato positive cINs in these mutant mice was similar to control mice, except for a small change in layer V and VI (**Supplement Figure 6**). MGE-derived PV and SST positive cIN number was similarly reduced in these animals. However CGE-derived VIP cIN density was similar to that of control animals (**Figure 3E & Supplement Figure 4**). A smaller, but significant reduction in the RLN positive cIN population was observed, in agreement with the notion that a subpopulation of RLN positive cells is born in the MGE (Miyoshi et al. 2010). Consistently, layer 1 RLN+ cells, which are largely derived from the CGE (Miyoshi et al. 2010), were not affected by *Pcdhy* loss of function, but RNL cells in deeper layers 2-6 (many of which are MGE-derived and also positive for SST) showed reduced numbers (**Supplement Figure 5**).

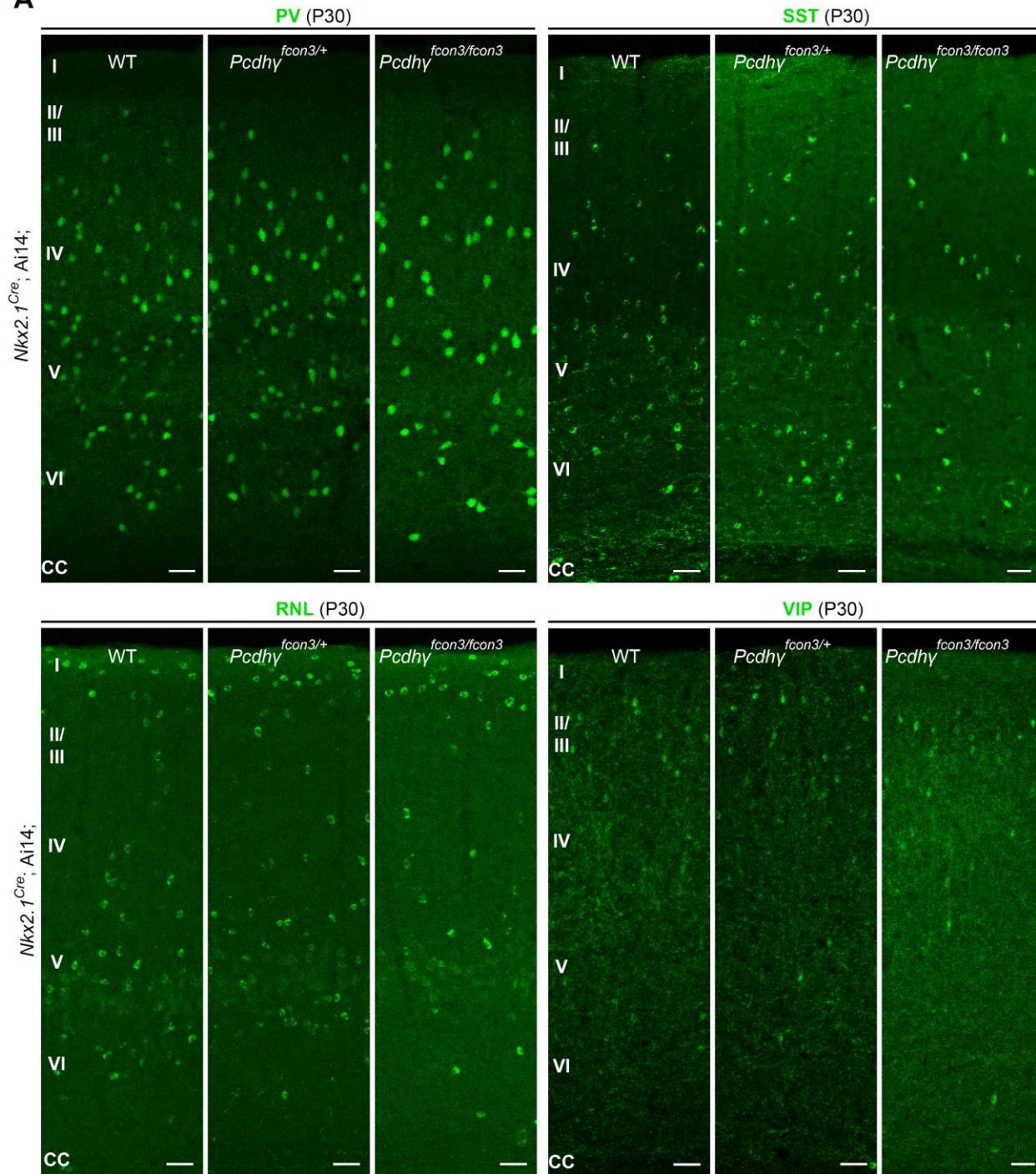
Interestingly, we observed that in *Nkx2.1<sup>Cre</sup>-Ai14-Pcdhy<sup>fcon3/fcon3</sup>* mice, the number of un-recombined PV and SST (PV+/Ai14- and SST+/Ai14-) cells was significantly increased compared to WT mice (**Supplement Figure 7**), a result consistent with recent observations (Carriere et al., 2020). PV+/tdTomato- and SST+/tdTomato- cells are likely derived from the most dorsal MGE at the interface with LGE from progenitor cells expressing NKX6.2 in a region of low, or no expression of NKX2.1 (Hu, Vogt, Sandberg, et al. 2017; Fogarty et al. 2007; Sousa et al. 2009; Hu, Vogt, Lindtner, et al. 2017). It is unclear if the presence of the conditional FCON3 allele results in increased production of these cells or if un-recombined cells from this domain increase their survival in compensation for the loss of cIN that lack Pcdhy function. If the latter is true, the behavior of these un-recombined PV and SST cINs differs from that observed for WT cells co-transplanted with MGE cells lacking Pcdh- $\gamma$  function (see below). Together the above results show that embryonic loss of Pcdhy function in Nkx2.1 positive progenitors results in a significant reduction in the number of MGE/POA-derived cINs.



**Figure 3.1** - Loss of *Pcdhy* genes targeted to *Nkx2.1* expressing cells results in selective loss of cIN derived from the MGE.

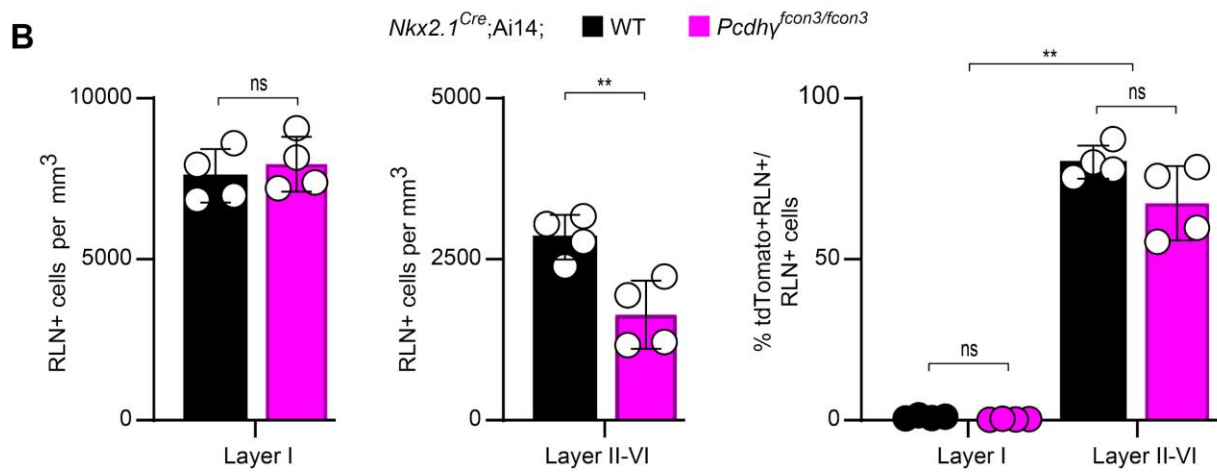
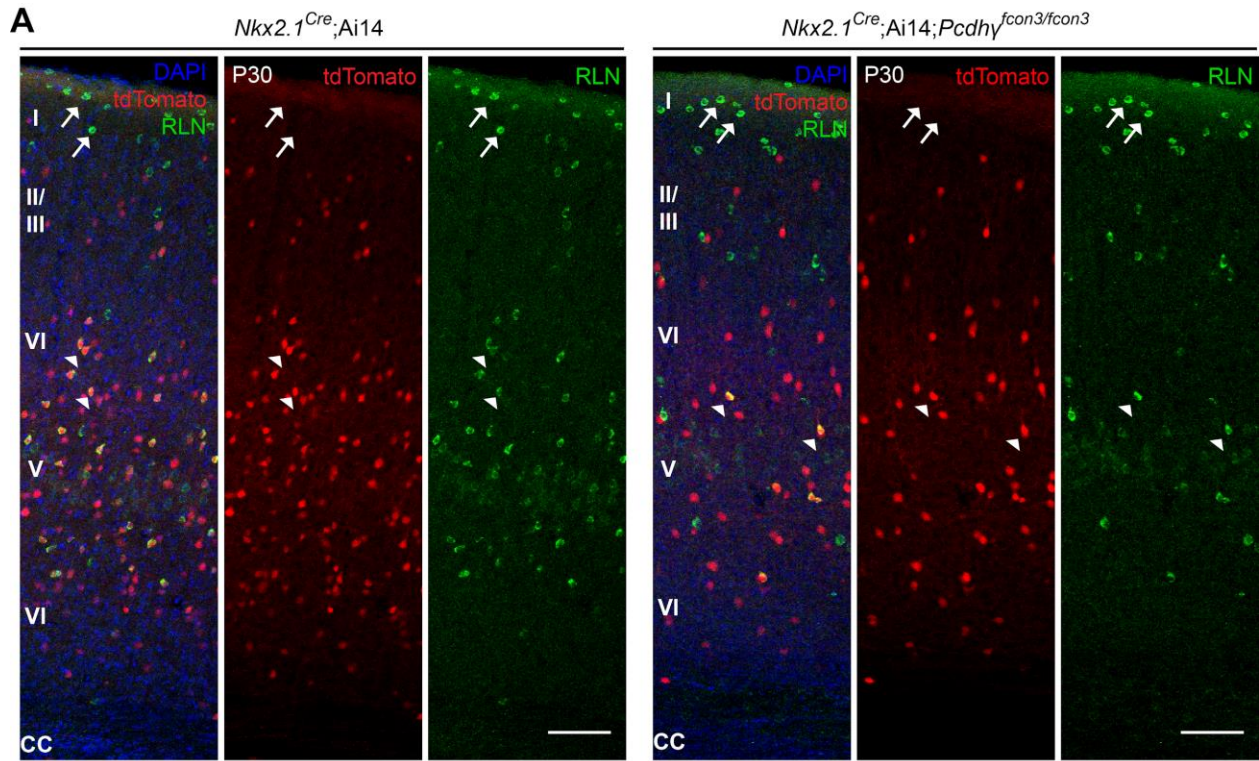
**Figure 3.1 -** (A) Mutant mice with loss of *Pcdhy* in MGE-derived cIN were generated by crossing *Pcdhy<sup>fcon3</sup>* mice to *Nkx2.1<sup>Cre</sup>* mice. The conditional Ai14 line was used to fluorescently label MGE-derived cells. (B) *Pcdhy<sup>fcon3/fcon3</sup>* mice (at E13.5; top panels) carrying the *Pcdhy* mutant allele, but not Cre, show robust expression of GFP in the MGE. In contrast, in *Nkx2.1<sup>Cre</sup>-Ai14-Pcdhy<sup>fcon3/fcon3</sup>* mice (at E13.5; bottom panels), carrying the *Pcdhy* mutant allele and expressing Cre, GFP expression was eliminated from the MGE. Note NKX2.1 staining (magenta) in the panels on the right delineates MGE/POA (preoptic area). The few cells left expressing GFP in the MGE are blood vessels and are tdTomato negative. (C) Photographs of coronal sections of the primary visual cortex (V1) in *Nkx2.1<sup>Cre</sup>-Ai14-Pcdhy<sup>+/+</sup>* (*Pcdhy* WT), *Nkx2.1<sup>Cre</sup>-Ai14-Pcdhy<sup>fcon3/+</sup>* (*Pcdhy* HET) and *Nkx2.1<sup>Cre</sup>-Ai14-Pcdhy<sup>fcon3/fcon3</sup>* (*Pcdhy* mutant). Scale bar, 100  $\mu$ m. (C') Quantification of the density of tdTomato+ cells in V1 and S1BF cortex of P30 *Nkx2.1<sup>Cre</sup>-Ai14 Pcdhy* WT (black), *Pcdhy* HET (grey) and *Pcdhy* mutant (magenta) mice. The number of *Nkx2.1*-derived cells was significantly reduced in *Nkx2.1<sup>Cre</sup>-Ai14 Pcdhy* mutant mice compared to WT controls (Kruskal-Wallis test; for V1 (P value=0.002), for S1BF (P value=0.0065), adjusted p values \*p=0.0232, \*\*p=0.0168 (S1), n = 4–6 mice of each genotype). (D) Body weight and cortex thickness measurements in *Nkx2.1<sup>Cre</sup>-Ai14 Pcdhy* WT (black) and *Pcdhy* mutant (magenta) mice at P30. Body weight and cortical thickness were not significantly affected by loss of *Pcdhy* (Mann-Whitney test, body weight (p=0.0547, n = 10 mice of each genotype), cortical thickness (p=0.2857, n = 4–5 mice of each genotype). (E) Quantification of tdTomato+ cIN subtypes in V1 mouse cortex at P30. *Nkx2.1<sup>Cre</sup>-Ai14 Pcdhy* mutant mice (magenta) had significantly reduced numbers of MGE-derived parvalbumin (PV)+, somatostatin (SST)+, and Reelin (RLN)+ cells compared to WT controls. In contrast VIP+ cells, which are derived from the CGE, were not significantly affected (Kruskal-Wallis test; for PV (P value = 0.0113), for SST (P value=0.0009), for RLN (P value = 0.0014), and for VIP (P value=0.636); adjusted p values \*p=0.0113 (PV), \*\*p=0.0055 (SST), \*\*p=0.0055 (RLN), n = 4–5 mice of each genotype).



**A**

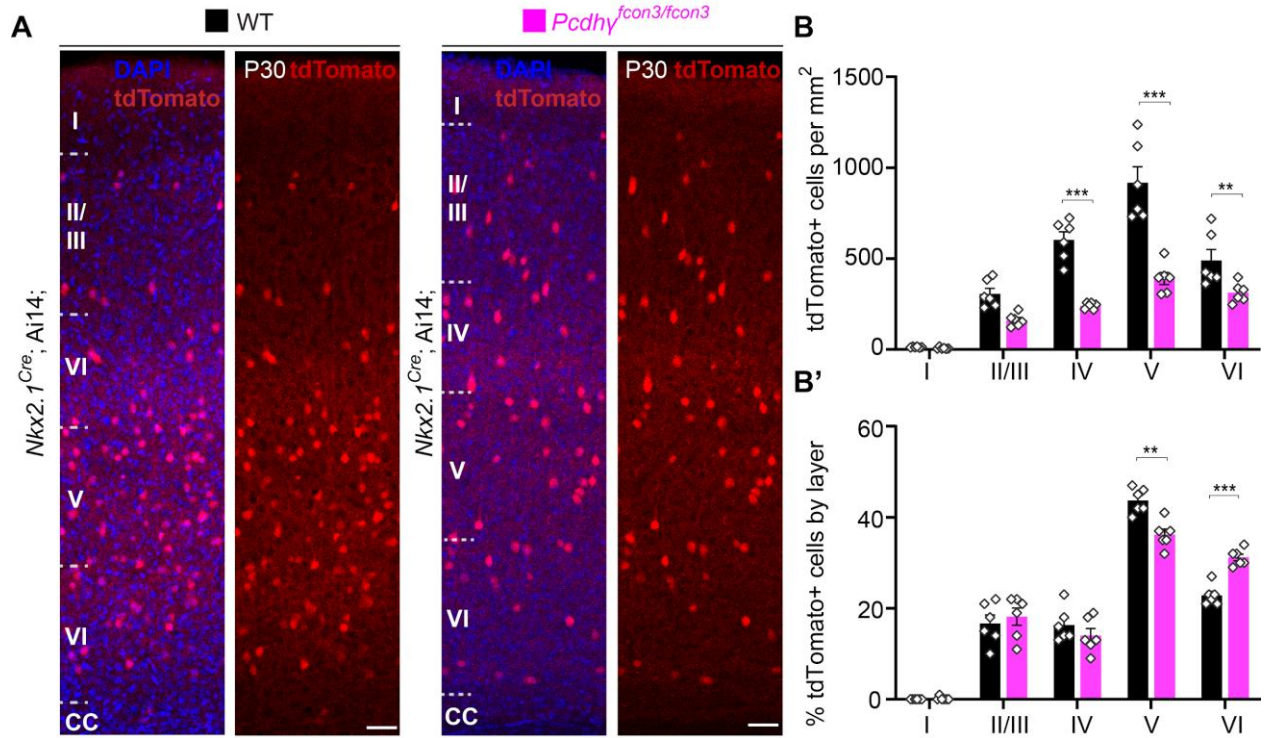
**Supplement Figure 4.1** - Reduced number of MGE cIN subtypes after loss of *Pcdhy* in *Nkx2.1*-derived cells.

**Supplement Figure 4.1** – (Related to Figure 3.1) - (A) Representative photographs of visual cortex (V1) in *Nkx2.1<sup>Cre</sup>-Ai14 Pcdhy* WT, *Pcdhy* heterozygote or *Pcdhy* mutant mice. Sections were stained for PV, SST, RLN or VIP. Scale bars, 50  $\mu$ m



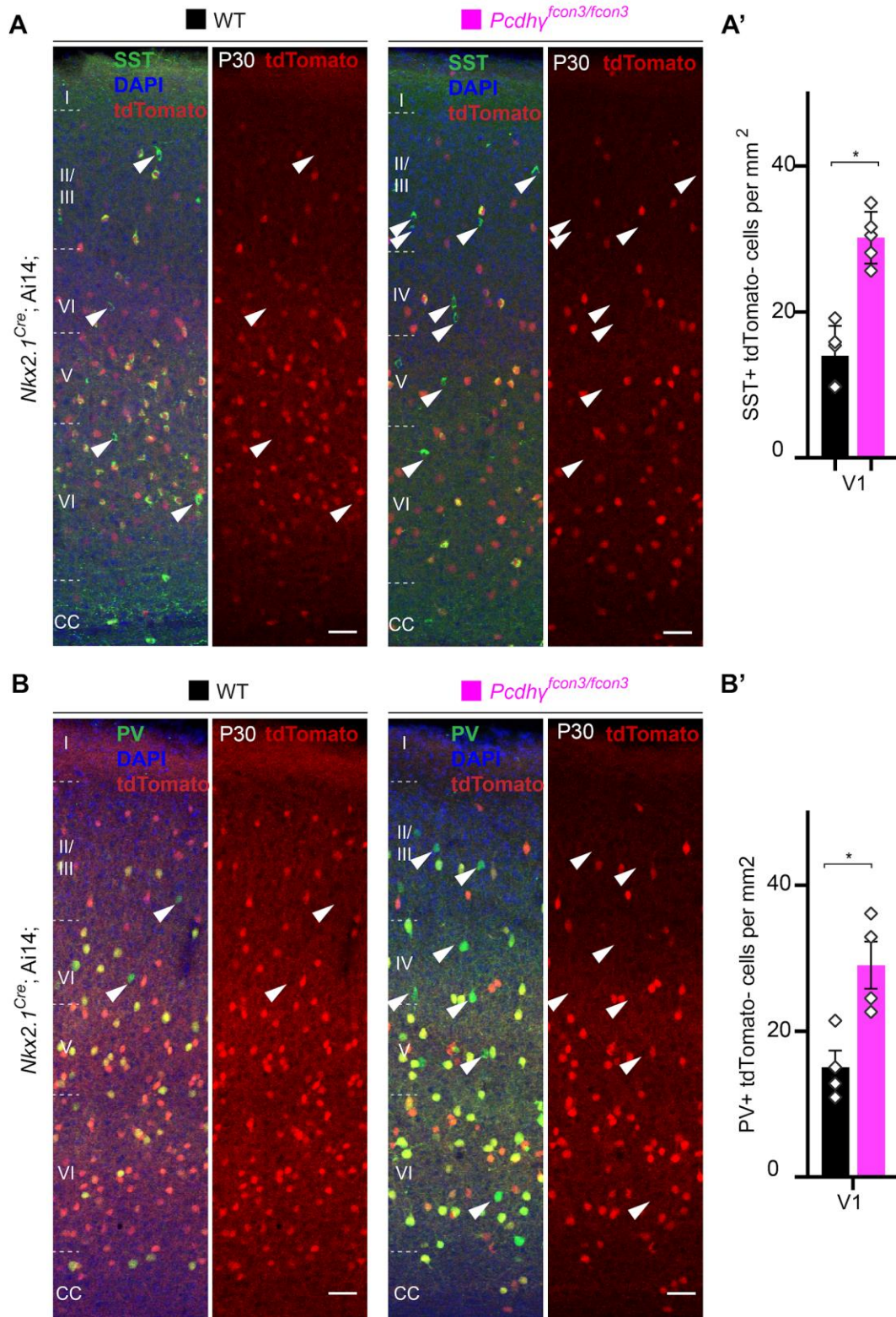
**Supplement Figure 5.1** - Numbers of *Nkx2.1*-derived RLN positive cINs are reduced in layers II-VI in *Pcdhy*-deficient mice.

**Supplement Figure 5.1** – (Related to Figure 3) - (A) Representative photographs of visual cortex (V1) in *Nkx2.1<sup>Cre</sup>-Ai14-Pcdhy<sup>+/+</sup>* (*Pcdhy* WT, left panels) and *Nkx2.1<sup>Cre</sup>-Ai14-Pcdhy<sup>fcon3/fcon3</sup>* (*Pcdhy* mutant, right panels) mice. Sections were stained for RLN, tdTomato, and DAPI. Arrows point to RLN+/tdTomato- cells and arrowhead points to RLN+/tdTomato+ positive cells. Scale bars 100  $\mu$ m. (B) Quantifications of RLN+ cells in layer I and layers II-VI represented as density (left and middle graphs) and as percentage of Nkx2.1-derived cells by cortical layer (right graph) in the primary visual cortex (Mann-Whitney,  $p=0.4857$  (Layer I, left graph),  $**p=0.0286$  (Layers II-VI, middle graph); Kruskal-Wallis test  $P$  value $<0.0001$ , adjusted  $p$  values  $**p=0.005$  (right graph);  $n = 4$  mice of each genotype).



**Supplement Figure 6.1** - Cortical layer distribution of Nkx2.1-derived cINs in Pcdhy WT and mutant mice.

**Supplement figure 6.1** – (Related to Figure 3) - (A) Representative photographs of the primary visual cortex (V1) in *Nkx2.1<sup>Cre</sup>-Ai14-Pcdhy<sup>+/+</sup>* (*Pcdhy* WT) and *Nkx2.1<sup>Cre</sup>-Ai14-Pcdhy<sup>fcon3/fcon3</sup>* (*Pcdhy* mutant) mice at P30. Scale bar 50  $\mu$ m. (B) Quantification of tdTomato+ Nkx2.1-derived cINs in layers I-VI of visual cortex of *Pcdhy* WT and mutant mice at P30 (2-way ANOVA, Fgenotype = 91.70, P value<0.0001, adjusted p values \*\*\*p<0.0001, \*\*p=0.015, n = 6 mice of each genotype). (B') Layer distribution of tdTomato+ Nkx2.1-derived cINs shown as percentage tdTomato+ cells per layer in V1 of *Pcdhy* WT and *Pcdhy* mutant mice at P30 (2-way ANOVA, Fgenotype = 1.75e-003, P value=0.95, adjusted p values \*\*\*p=0.0001, \*\*p=0.0005, n = 6 mice of each genotype).



**Supplement Figure 7.1** - Increased survival of non-*Nkx2.1*-derived SST and PV cINs in *Pcdhy*-deficient mice.

**Supplement Figure 7.1** – (Related to figure 3) - (A,B) Representative photographs of the primary visual cortex (V1) in *Nkx2.1<sup>Cre</sup>-Ai14-Pcdhy<sup>+/+</sup>* (*Pcdhy* WT) and *Nkx2.1<sup>Cre</sup>-Ai14-Pcdhy<sup>fcon3/fcon3</sup>* (*Pcdhy* mutant) mice at P30. Sections were stained for SST and PV. Arrowheads (in A and B) indicate SST+ or PV+ unrecombined (tdTomato-) cINs. Scale bar 50  $\mu$ m. (A', B') Quantifications of SST+/tdTomato- (A) and PV+/tdTomato- (B) cells in V1 of *Pcdhy* WT and *Pcdhy* mutant mice at P30 (Mann-Whitney test, for SST+/tdtomato- \*p=0.0079, n = 5 mice of each genotype; for PV+/tdTomato- \*p=0.0286, n = 4 mice of each genotype)



### **Pcdhy function is not required for the proliferation and migration of cIN precursor cells**

The reduction in the number of cINs in the cortex of *Nkx2.1<sup>Cre</sup>-Ai14-Pcdhy<sup>fcon3/fcon3</sup>* mice was not a result of abnormal cortical thickness or abnormal layer distribution of cINs, as these measures were similar across *Pcdhy* genotypes in P30 mice (**Figure 3C**). We then asked whether proliferation defects in the cIN progenitor population or defects in the migration of young cINs could lead to a reduced cIN density in *Pcdhy* mutant mice. Quantification of the number of dividing cells in the ventricular or subventricular zones at E13.5 and E15.5, using the mitotic marker Phosphohistone H3 (PH3), showed no difference in the number of mitotic cells in the MGE between *Nkx2.1<sup>Cre</sup>-Ai14-Pcdhy<sup>fcon3/fcon3</sup>* and *Nkx2.1<sup>Cre</sup>-Ai14* controls mice (**Figure 4A & B**). Migration of young cINs into cortex was also not affected in the *Nkx2.1::Cre-Ai14-Pcdhy<sup>fcon3/fcon3</sup>* mice. The tdTomato+ cells in the cortex displayed a similar migratory morphology between *Nkx2.1<sup>Cre</sup>-Ai14-Pcdhy<sup>fcon3/fcon3</sup>* and *Nkx2.1<sup>Cre</sup>-Ai14* control embryos. Consistent with the absence of an effect of *Pcdhy* on cIN migration, the number of migrating cells in cortex in the marginal zone (MZ), the subplate (SP), and the intermediate and subventricular zone (IZ/SVZ) was equivalent between *Pcdhy* mutant embryos and controls at E15.5 (**Figure 4C & D**). These findings indicate that loss of *Pcdhy* did not affect the proliferation of MGE progenitors or the migration of young MGE-derived cINs into the developing neocortex.

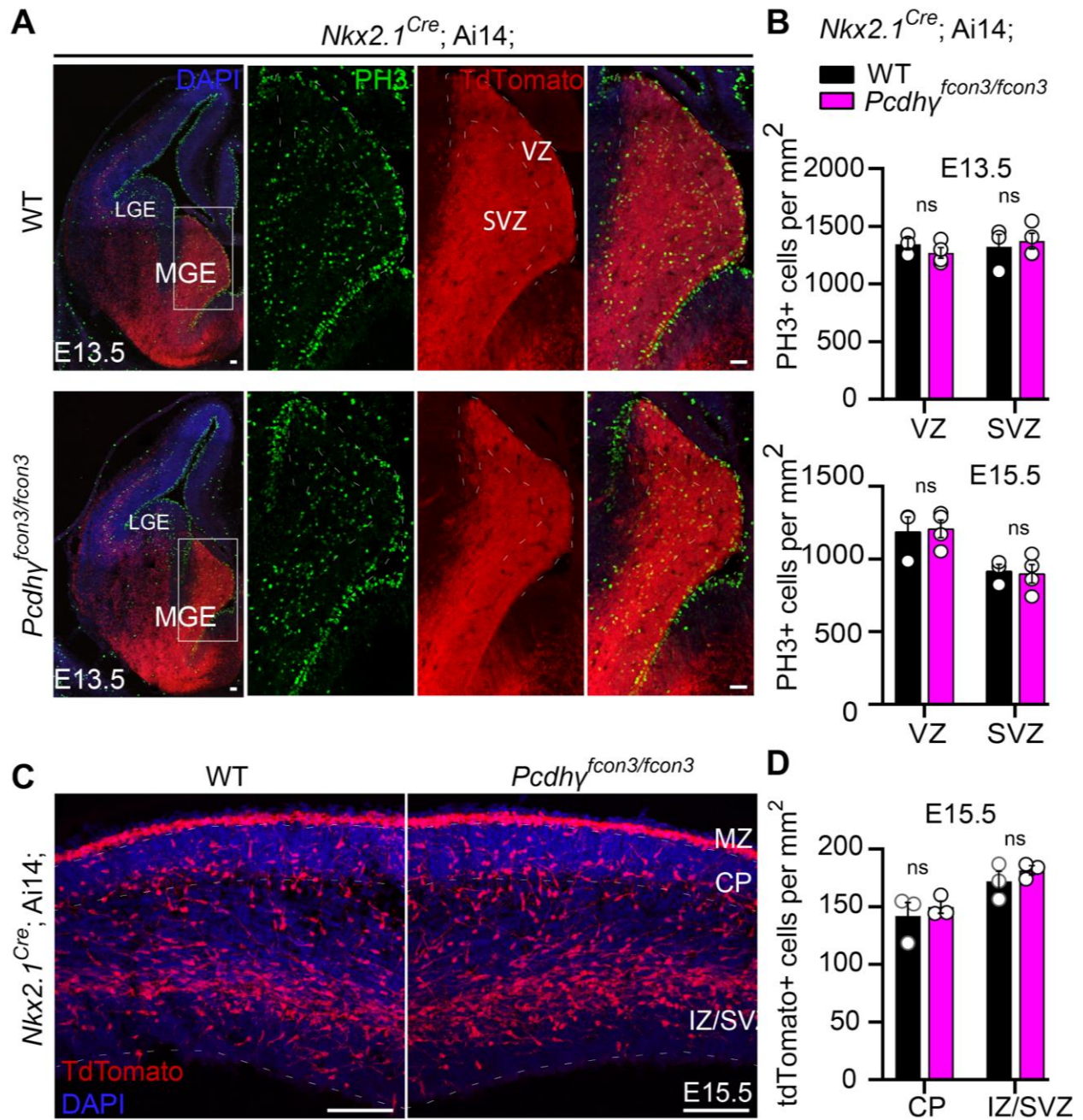


**Figure 4.1** - Proliferation and migration are not affected by the loss of *Pcdhy* in *Nkx2.1* expressing cells.

**Figure 4.1** - (A) Photographs of coronal sections through the embryonic forebrains of E13.5 *Nkx2.1<sup>Cre</sup>-Ai14-Pcdhy<sup>+/+</sup>* (*Pcdhy* WT, top panels) and *Nkx2.1<sup>Cre</sup>-Ai14-Pcdhy<sup>fcon3/fcon3</sup>* (*Pcdhy* mutant, bottom panels). Close-up photographs of the MGE from *Nkx2.1<sup>Cre</sup>-Ai14 Pcdhy* WT (right panels) and *Pcdhy* mutant (bottom, right panels) embryos. Robust reporter activity (tdTomato) was observed in the MGE. Dividing cells were labeled using the mitotic marker PH3. Note that the size and number of PH3+ cells in the MGE was similar in the mutant and control brains. Scale bars, 50  $\mu$ m. (B) Quantification of PH3+ cells from MGE ventricular (VZ) and subventricular zone (SVZ) in E13.5 (top) and E15.5 (bottom) *Nkx2.1<sup>Cre</sup>-Ai14 Pcdhy* WT (black bars) and *Pcdhy* mutant (magenta bars) embryos (Mann-Whitney test,  $p=0.4000$  (E13.5 VZ),  $p=0.8571$  (E13.5 SVZ),  $p=0.8571$  (E15.5 VZ),  $p>0.999$  (E15.5 SVZ),  $n = 3-4$  embryos of each genotype). (C) Photographs of coronal sections of dorsal cortex at E15.5 showing the migrating MGE-derived cIN in *Nkx2.1<sup>Cre</sup>-Ai14 Pcdhy* WT (left) and *Pcdhy* mutant (right) embryos. Note the robust migratory streams of young neurons in the SVZ and in the marginal zone (MZ). From these regions, cells disperse into the intermediate zone (IZ) and cortical plate (CP). Similar numbers of migrating cIN were observed in mutants and controls. Scale bar, 100  $\mu$ m. (D) Quantifications of number of migrating MGE-derived cINs in the CP and in the IZ/SVZ of *Nkx2.1<sup>Cre</sup>-Ai14 Pcdhy* WT (black) and *Pcdhy* mutant (magenta) mice. No significant differences were detected in the number of tdTomato+ migrating cells in *Pcdhy* mutant and WT controls (Mann-Whitney test,  $p>0.990$  (E15.5 CP),  $p=0.7000$  (E15.5 IZ-SVA),  $n = 3$  embryos of each genotype).

### **Loss of Pcdhy function results in increased cIN programmed cell death.**

A wave of PCD eliminates ~40% of the young cINs shortly after their arrival in the cortex (Southwell et al. 2012; Wong et al. 2018). This wave starts at ~P0, peaks at P7, and ends at ~P15. We asked if the reduced cIN density observed in Pcdhy mutant mice could stem from a heightened number of mutant cINs undergoing apoptosis at the normal time of PCD. Such cells were immunolabeled using an antibody directed against cleaved-Caspase 3 (cc3). Since CC3 positive cells are relatively rare, our analysis was performed throughout the entire neocortex at P0, 3, 7, 10, and 15. Similarly to their control Pcdhy wild type littermates, *Nkx2.1<sup>Cre</sup>-Ai14-Pcdhy<sup>fcon3/fcon3</sup>* homozygous mice displayed a wave of PCD peaking at P7 (**Figure 5A & B**). However, Pcdhy mutant mice had significantly higher numbers of tdTomato+/cc3+ cells compared to controls. We also examined the proportion of CC3+ cells that were tdTomato negative (un-recombined cells that would notably include pyramidal cells, CGE-derived cINs, and glial cells). With the exception of a small, but significant increase observed at P0, we found no significant difference in the number of CC3+/tdTomato- cells between genotypes (**Figure 5B, bottom graph**). This suggests that the survival of neighboring Pcdhy-expressing cells is not impacted by the loss of Pcdhy-deficient MGE/POA-derived cINs. Importantly, the homozygous deletion of the pro-apoptotic Bcl-2-associated X protein (BAX) rescued the density of cINs in the Pcdhy mutant mice to levels similar to those observed in control *BAX<sup>-/-</sup>;Pcdh<sup>fcon3/+</sup>* mice or in mice carrying only the *Bax* mutation (*Bax<sup>-/-</sup>*) (Southwell et al. 2012) (**Figure 5C**). The above results indicate that loss of Pcdhy in MGE/POA-derived cIN enhances their demise through PCD during the developmental period when these cells are normally eliminated.

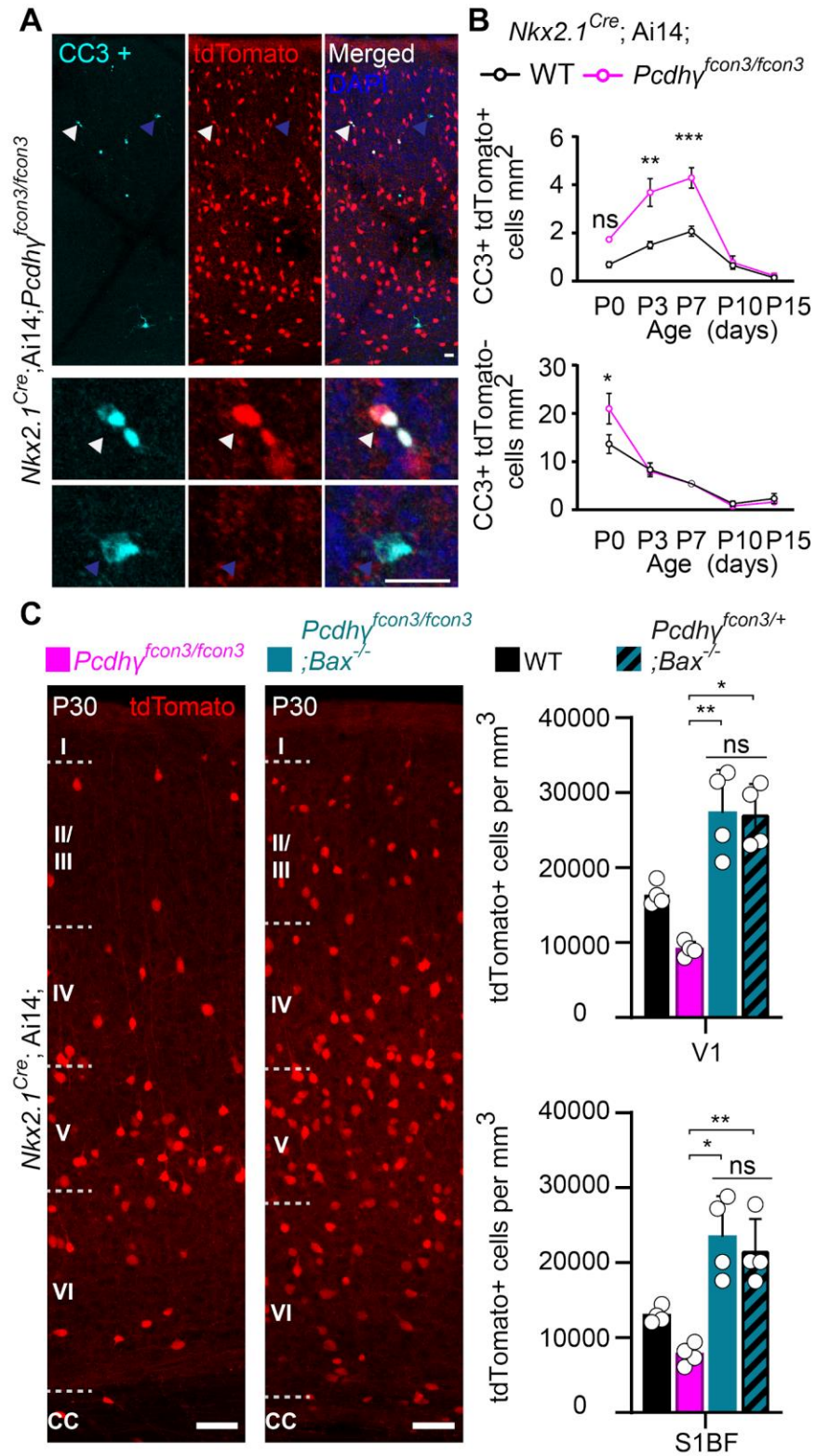


**Figure 5.1** - Increased PCD in *Pcdhy* mutants is rescued in *Pcdhy*-*Bax* null animals.

**Figure 5.1** - (A) Photographs of coronal sections through a *Nkx2.1<sup>Cre</sup>-Ai14-Pcdhy<sup>fcon3/fcon3</sup>* (*Pcdhy* mutant) P7 mouse cortex (top), showing tdTomato+ cINs and cleaved caspase 3 positive cells (CC3+). Close-up photographs (bottom) of tdTomato+, CC3+ (white Arrowheads) and tdTomato-, CC3+ (blue Arrowheads) cells. Scale bar 25  $\mu$ m. (B) Quantification of the density of tdTomato+, CC3+ (MGE-derived, top graph) cells from *Nkx2.1<sup>Cre</sup>-Ai14 Pcdhy* WT (black line) and *Pcdhy* mutant (magenta line) mice. Quantification of the density of tdTomato-, CC3+ (non-MGE-derived, bottom graph) cells from *Nkx2.1<sup>Cre</sup>-Ai14 Pcdhy* WT (black line) and *Pcdhy* mutant (magenta line) mice. Note that the number of CC3+ cells was significantly increased in the MGE-derived population in *Pcdhy* mutant mice, and coincides with the normal period of PCD for cINs in WT mice (Each age was analyzed with a nested 1-way ANOVA (mouse ID nested within genotype), P value<0.0001. Significant comparisons are marked with \*; \*p=0.0004 \*\*p=0.0014, \*\*\*p=0.0009, n = 3–5 mice of each genotype). (C) Coronal sections through the primary visual cortex (V1) of *Nkx2.1<sup>Cre</sup>-Ai14-Pcdhy<sup>fcon3/fcon3</sup>* (*Pcdhy* mutant, left) and *Nkx2.1<sup>Cre</sup>-Ai14-Pcdhy<sup>fcon3/fcon3</sup>;Bax<sup>-/-</sup>* (*Pcdhy* mutant, *Bax* null, right) mice at P30. Quantifications of the density of cINs in V1 (top) and S1BF (bottom) cortex. Note that genetic removal of *Bax* in both *Pcdhy<sup>fcon3/+</sup>* (*Pcdhy* HET) and *Pcdhy<sup>fcon3/fcon3</sup>* (*Pcdhy* mutant) mice rescues cell death to similar levels (Kruskal-Wallis test, P value<0.001 (for V1 an S1BF), adjusted p values for V1 (\*p=0.01 , \*\*0.005 ) and for S1BF (\*\*p=0.0109 , \*p=0.0286); n = 4–5 mice of each genotype).

### **Loss of *Pcdhy* does not affect survival of cINs after the period of PCD.**

We then asked whether *Pcdhy* expression is also required for the survival of cINs past the period of PCD. To address this question we took advantage of the *PV<sup>Cre</sup>* transgene (Hippenmeyer et al. 2005) that becomes activated specifically in PV cINs starting at around ~P16 (**Figure 6 & Supplement Figure 8**). Quantifications of tdTomato+ cell density in *PV<sup>Cre</sup>-Ai14- Pcdhy<sup>fcon3/fcon3</sup>* and *PV<sup>Cre</sup>-Ai14* mice at P60-P100 revealed no significant differences between homozygous and control mice (V1 and S1BF) (**Figure 6D & E**). In contrast, the *SST<sup>Cre</sup>* line, like *Nkx2.1<sup>Cre</sup>*, induces recombination at embryonic stages. The *SST<sup>Cre</sup>* allele in *Ai14- Pcdhy<sup>fcon3/fcon3</sup>* reduced the density of SST cINs measured at P30 to a similar level as found using the *Nkx2.1<sup>Cre</sup>* line (**Figure 6A-C**). Together, our results demonstrate that *Pcdhy* loss of function reduces cIN survival specifically during the endogenous period of cIN cell death, resulting in a reduced cortical density of cINs.

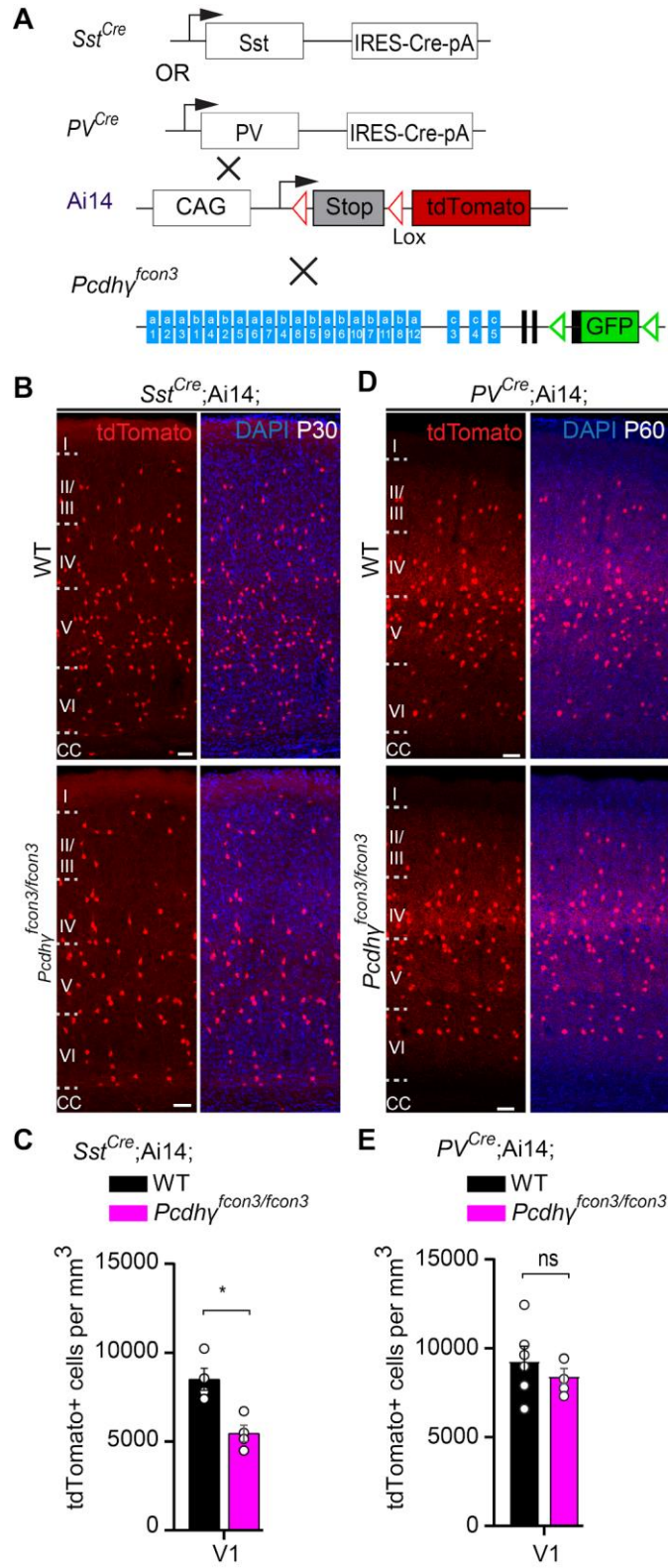
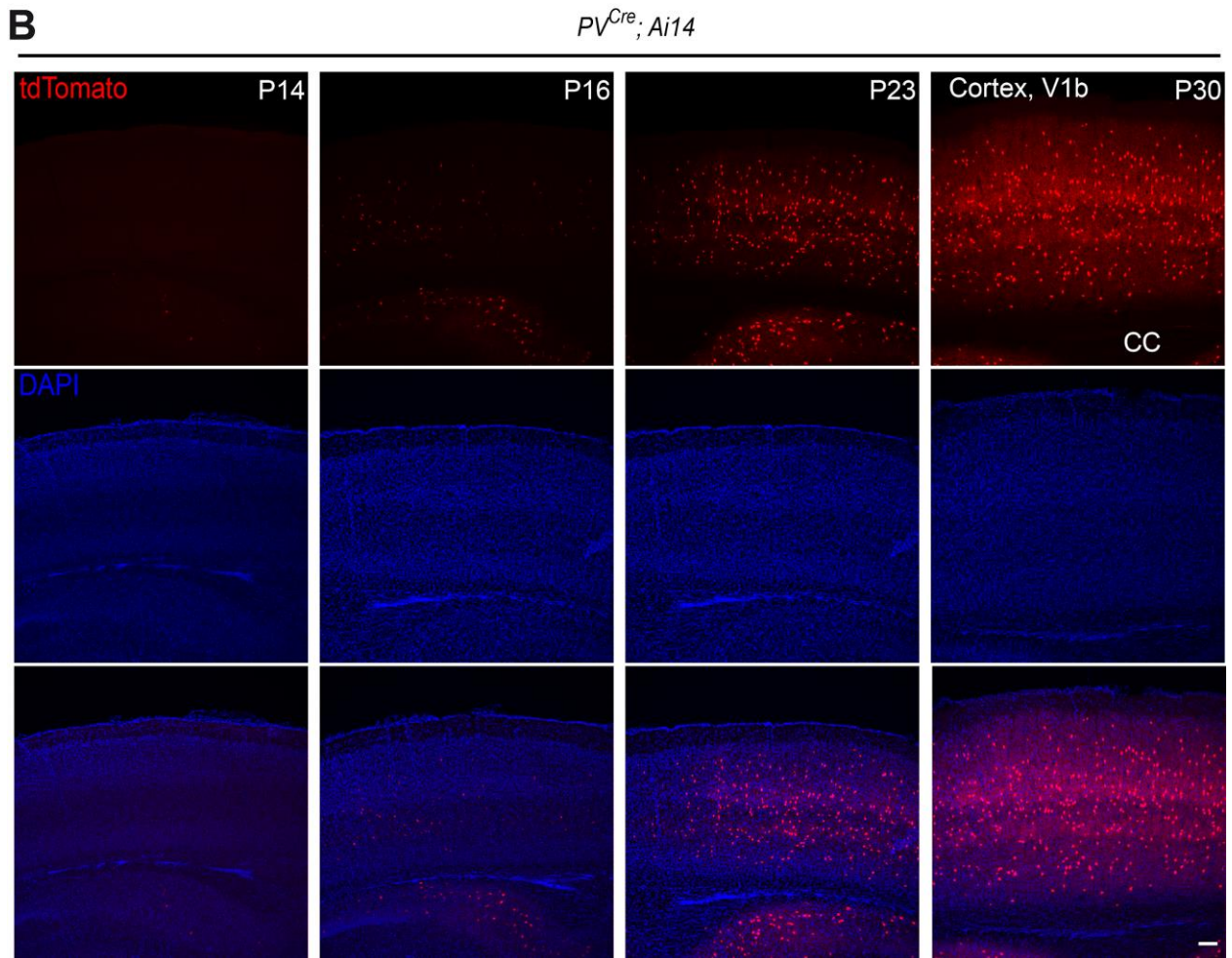
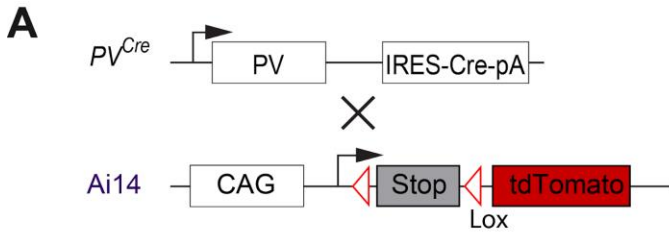


**Figure 6.1** - *Pcdhy* function is not required for the survival of PV cINs after the period of PCD.



**Figure 6.1** - (A) Mutant mice with loss of *Pcdhy* in SST or PV cells were generated by crossing conditional *Pcdhy*<sup>fcon3</sup> mice to mice carrying Cre under *SST* (*Somatostatin*, *SST*<sup>Cre</sup>) or *Pvalb* (*Parvalbumin*, *PV*<sup>Cre</sup>). The conditional Ai14 line was used to fluorescently label SST or PV cells. (B) Photographs of coronal sections of the primary visual cortex (V1) of P30 *Sst*<sup>Cre</sup>-*Ai14*-*Pcdhy*<sup>+/+</sup> (*Pcdhy* WT, top left) and *Sst*<sup>Cre</sup>-*Ai14*-*Pcdhy*<sup>fcon3/fcon3</sup> (*Pcdhy* mutant, bottom left) mice. Scale bars, 50  $\mu$ m. (C) Quantifications of the density of tdTomato+ cINs in V1 cortex of *Pcdhy* WT (black) and *Pcdhy* mutant (magenta) *Sst*<sup>Cre</sup>-*Ai14* mice at P30 (Mann-Whitney test, \*\*p=0.0286, n = 4 mice of each genotype). (D) Photographs of coronal sections of V1 in *PV*<sup>Cre</sup>-*Ai14*-*Pcdhy*<sup>+/+</sup> (*Pcdhy* WT, top right) and *PV*<sup>Cre</sup>-*Ai14*-*Pcdhy*<sup>fcon3/fcon3</sup> (*Pcdhy* mutant, bottom right) mice at P60. Scale bars, 50  $\mu$ m. (E) Quantifications of the density of tdTomato+ cIN in V1 cortex of *Pcdhy* WT and *Pcdhy* mutant *PV*<sup>Cre</sup>-*Ai14* mice at P60-100 (Mann-Whitney test, p=0.4206, n = 5 mice of each genotype).



**Supplement Figure 8.1** - Late postnatal expression of Parvalbumin in cINs.

**Figure 8.1** - (Related to Figure 6.1) - (A) PV reporter mice ( $PV^{Cre}$ ) were crossed to conditional Ai14 mice to label PV expressing cINs. (B) Representative photographs of primary visual cortex (V1) in  $PV^{Cre}$ -Ai14 mice at P14, 16, 23 and 30. CC = corpus callosum. Scale bars, 100  $\mu$ m.

### ***Pcdh $\alpha$* or *Pcdh $\beta$* do not affect cIN survival**

Our data thus far suggests that *Pcdhy* genes are involved in the regulation of PCD in cINs. We wondered whether the involvement of *Pcdh* genes in this process was unique to those isoforms encoded from the gamma cluster. Additionally, PCDHY proteins can form tetrameric units with members of the  $\alpha$  and  $\beta$  gene clusters (Dietmar Schreiner 2010; Thu et al. 2014). We, therefore reasoned that removal of the  $\alpha$  and  $\beta$  *Pcdh* genes might also contribute to cIN cell death.

Mice that carry conditional alleles for the deletion of the entire *Pcdh $\alpha$*  gene cluster (*Pcdh $\alpha$ <sup>acon/acon</sup>*) were crossed to mice that carry the *Nkx2.1<sup>Cre</sup>* and *Ai14* transgenes, resulting in removal of all twelve *Pcdh $\alpha$*  genes from MGE/POA progenitor cells (**Figure 7A**). The resulting transgenic mice carrying all three transgenes *Nkx2.1<sup>Cre</sup>*, *Ai14* and *Pcdh $\alpha$ <sup>acon/acon</sup>* (hereon referred to as *Nkx2.1<sup>Cre</sup>-Ai14-Pcdh $\alpha$ <sup>acon/acon</sup>*) were viable, fertile, and displayed normal weight (**Figure 7 B, top graph**). The cIN density in the visual cortex of *Nkx2.1<sup>Cre</sup>-Ai14-Pcdh $\alpha$ <sup>acon/acon</sup>* mice at P30 was similar to that of *Nkx2.1<sup>Cre</sup>-Ai14* mice (**Figure 7B**).

To determine whether *Pcdh $\beta$*  isoforms encoded in the *Pcdh $\beta$*  gene cluster affected MGE/POA-derived cIN survival, mice with constitutive deletion of the entire *Pcdh $\beta$*  gene cluster (*Pcdh $\beta$ <sup>del/del</sup>*) were crossed to *Nkx2.1<sup>Cre</sup>-Ai14* mice (**Figure 7A**). The resulting *Nkx2.1<sup>Cre</sup>-Ai14-Pcdh $\beta$ <sup>del/del</sup>* mice were viable, fertile and of normal weight (**Figure C, top graph**) (W. V. Chen et al. 2017). Similarly to the results obtained from the removal of *Pcdh $\alpha$*  gene cluster, deletion of the *Pcdh $\beta$*  gene cluster did not alter the density of cINs in the visual cortex of P30 mice compared to control mice that carry WT *Pcdh $\beta$*  genes (**Figure 7C**). The above results indicate that unlike the genes in the *Pcdhy* cluster, which is essential for the regulation of cIN elimination, the function of PCDH proteins encoded from the *Pcdh $\alpha$*  or *Pcdh $\beta$*  gene clusters is dispensable for the survival of MGE/POA-derived cINs.

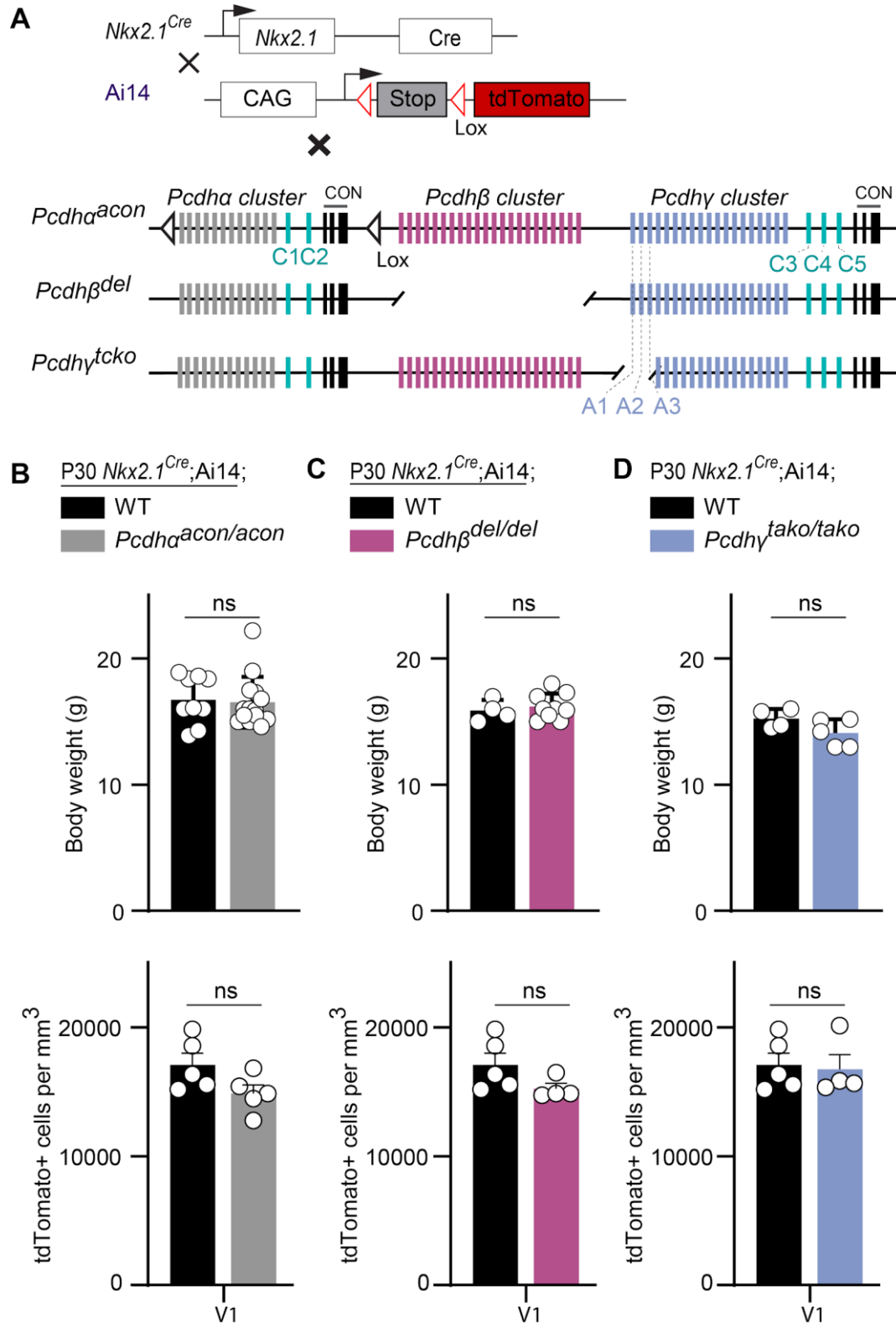


**Figure 7.1** - Loss of *Pcdha*, *Pcdhb*, or *Pcdhya1*, *Pcdhya2*, and *Pcdhya3* genes does not affect the survival of MGE-derived cINs.

**Figure 7.1** - (A) Mutant mice with loss of *Pcdh $\alpha$* , *Pcdh $\beta$*  or *Pcdhya1*, *Pcdhya2*, and *Pcdhya3* genes in MGE-derived cINs were generated by crossing *Pcdh $\alpha$ <sup>acon</sup>*, *Pcdh $\beta$ <sup>del</sup>*, and *Pcdhy<sup>tako</sup>* mice to the *Nkx2.1<sup>Cre</sup>* mouse line. The conditional Ai14 line was used to fluorescently label MGE-derived cells. (B) Measurements of body weight (top graph) in P30 *Nkx2.1<sup>Cre</sup>-Ai14-Pcdh $\alpha$ <sup>+/+</sup>* (*Pcdh $\alpha$*  WT, black bar) and *Nkx2.1<sup>Cre</sup>-Ai14-Pcdh $\alpha$ <sup>acon/acon</sup>* (*Pcdh $\alpha$*  mutant, grey bar) mice (Mann-Whitney test, p=0.545, n = 9–14 mice of each genotype). Quantification of the density of MGE-derived cINs (bottom graph) in primary visual cortex (V1) of *Pcdh $\alpha$*  WT (black bar) and *Pcdh $\alpha$*  mutant (grey bar) P30 mice (Mann-Whitney test, p=0.9603, n = 4–5 mice of each genotype). (C) Measurements of body weight (top bar) in P30 *Nkx2.1<sup>Cre</sup>-Ai14-Pcdh $\beta$ <sup>+/+</sup>* (*Pcdh $\beta$*  WT, black bar) and *Nkx2.1<sup>Cre</sup>-Ai14-Pcdh $\beta$ <sup>del/del</sup>* (*Pcdh $\beta$*  mutant, pink bar) mice (Mann-Whitney test, p=0.712, n = 4–9 mice of each genotype). Quantification of the density of MGE-derived cIN (bottom graph) in primary visual cortex (V1) of *Pcdh $\beta$*  WT (black bar) and *Pcdh $\beta$*  mutant (pink bar) P30 mice (Mann-Whitney test, p=0.1111, n = 4–5 mice of each genotype). (D) Measurements of body weight (top graph) in *Nkx2.1<sup>Cre</sup>-Ai14-Pcdhy<sup>+/+</sup>* (*Pcdhy* WT, black) and *Nkx2.1<sup>Cre</sup>-Ai14-Pcdhy<sup>tako/tako</sup>* (*Pcdhya1*, *Pcdhya2*, and *Pcdhya3* mutant, blue bar) P30 mice (Mann-Whitney test, p=0.175, n = 4–5 mice of each genotype). Quantification of the density of MGE-derived cINs (bottom graph) in in primary visual cortex (V1) of *Pcdhy* WT (black bar) and *Pcdhya1*, *Pcdhya2*, and *Pcdhya3* mutant (blue bar) P30 mice (Mann-Whitney test, p=0.9048, n = 4–5 mice of each genotype).

### **PART III - cINs compete for survival using PCDHy.**

The genomic architecture and regulation of clustered *Pcdh* genes creates an enormous diversity of PCDH molecules that potentially endows each neuron with a unique cell-surface PCDH barcode and potentially allows each neuron to engage in homophilic cell-cell interactions. In order to test whether cINs use *Pcdhy* to compete for survival, we designed a co-transplantation assay that allowed us to compare the migration and maturation of cINs of different *Pcdhy* genotypes within the same environment. This assay also allowed us to study the timing and extent of survival of cINs of different genotypes

#### **Heterochronic transplantation recapitulates timing and extent of PCD in cINs.**

Before we could test the hypothesis that cINs compete for survival using *Pcdhy*, we co-transplanted into the cortex of host animals cIN precursor cells expressing WT *Pcdhy* but labeled with red and green fluorescent proteins. Both GFP-labeled and RFP-labeled cells were obtained from the MGEs of *Gad67-GFP* or *Nkx2.1<sup>Cre</sup>-Ai14* embryos respectively at E13.5 (**Figure 8A**). We first confirmed that MGE cells WT *Pcdhy*, but labeled with the two different fluorescent reporters, displayed no differences in their survival. We co-transplanted equal proportions of GFP-labeled and RFP-labeled MGE cells into the neocortex of neonatal recipient mice. While the absolute number of cells transplanted between mice varied, red and green cells were mixed before being transplanted so that the proportions of GFP-labeled and RFP-labeled cells would be equivalent between mice. In order to compare survival, we use the fraction of green or red cells, among all co-transplanted cells (red+green). The fraction of surviving GFP positive and tdTomato positive cells at 3, 6, 13, and 21 days after transplantation (DAT) was measured (**Figure 8A & B, top graph**). The contribution of each cell population to the overall pool of surviving cells was found to be ~ 50% at 3 DAT, and remained constant at 6, 13, and 21 DAT (**Figure 8B, top graph**). This experiment indicates that the fluorescent reporters (GFP or

tdTomato) or breeding background does not affect the survival of MGE cINs in this assay. Importantly, in the above experiment a fraction of both the GFP and tdTomato labeled cells underwent cell death.

In order to determine the absolute extent of cell death in the MGE transplanted cells that carry WT *Pcdhy*, we co-transplanted 50K cells of each fluorescently labeled population (GFP and tdTomato) into WT host mice (**Figure 9A**). Our baseline for survival was established at 6 DAT, before the period of cIN PCD (6DAT is roughly equivalent to P0 and 21DAT is roughly equivalent to P15, (Southwell et al. 2012). In this control experiments where cIN precursors WT for the *Pcdhy* allele, derived from *Nkx2.1<sup>Cre</sup>-Ai14* or *Gad67-GFP* embryos, were transplanted, 39% of the transplanted cIN population was eliminated between 6 and 21 DAT (**Figure 9A-C and Supplement Figure 10**). Therefore transplanted MGE cINs not only undergo PCD during a period defined by their intrinsic cellular age but are also eliminated in a proportion that is strikingly similar to that observed during normal development (Wong et al. 2018; Southwell et al. 2012).



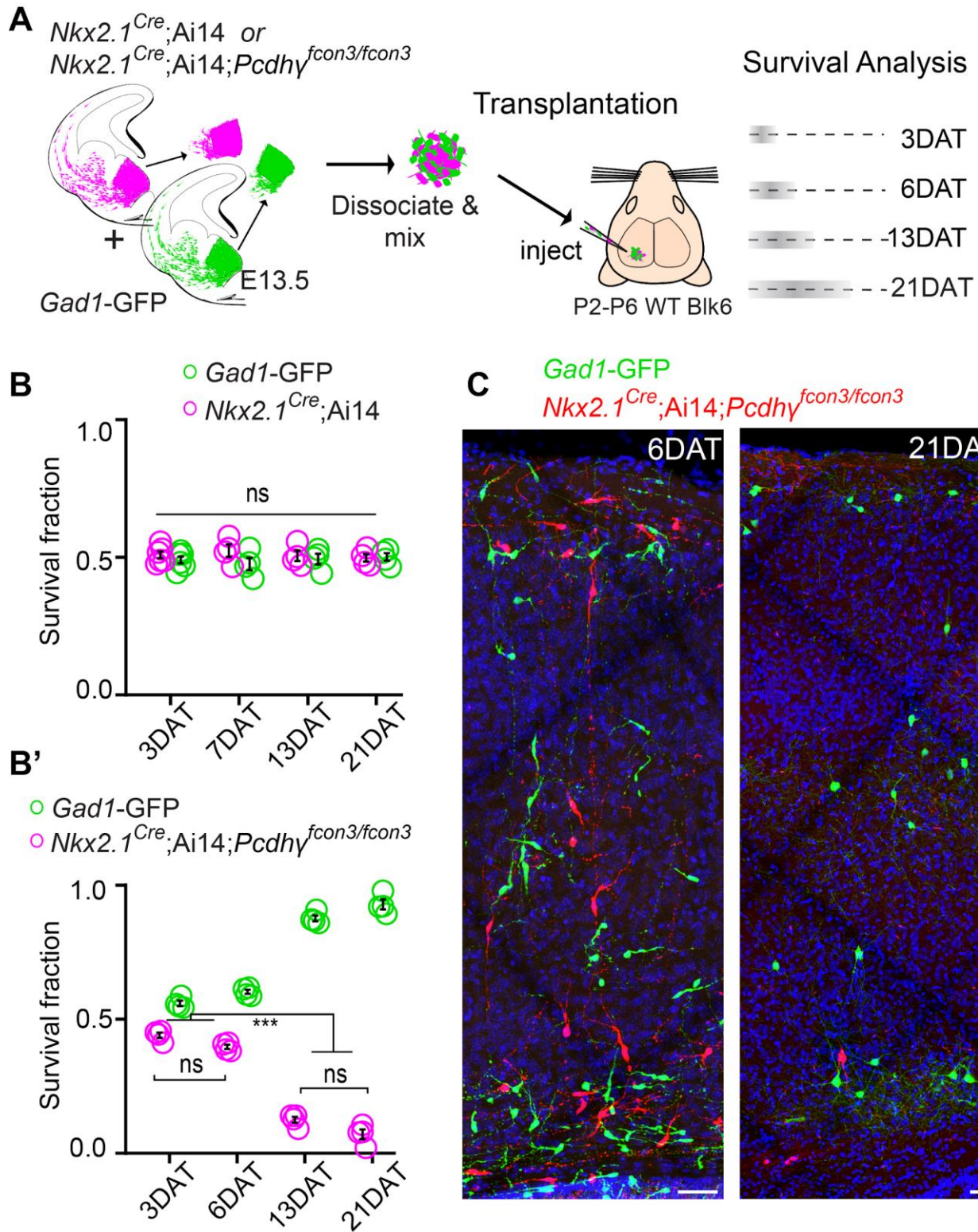
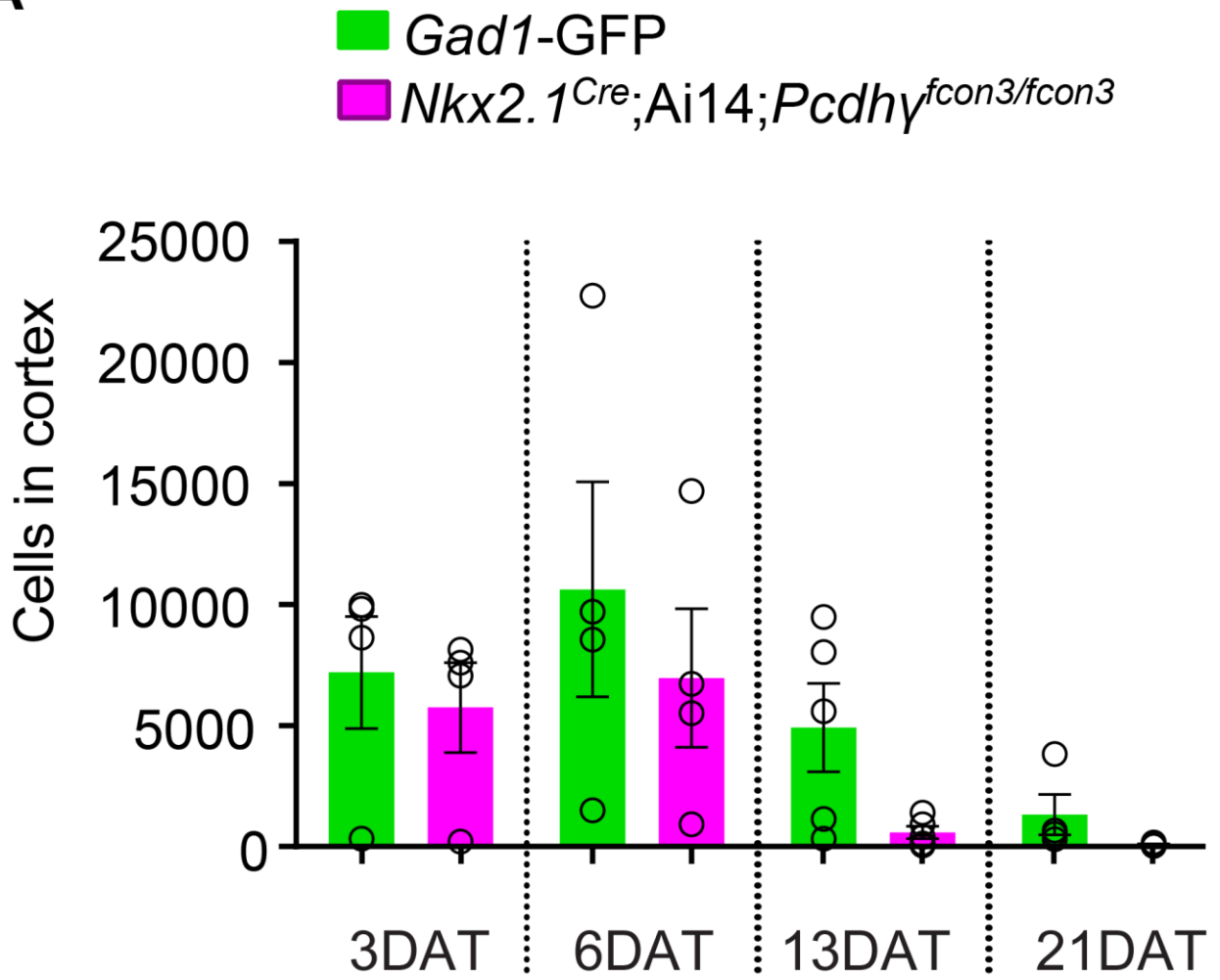


**Figure 8.1** - *Pcdhy* are required for cIN survival after transplantation.

**Figure 8.1** - (A) Schematic of co-transplantation of MGE-derived cIN precursors. MGE cells were derived from *Nkx2.1<sup>Cre</sup>-Ai14-Pcdhy<sup>+/+</sup>* (*Pcdhy* WT) or *Nkx2.1<sup>Cre</sup>-Ai14-Pcdhy<sup>fcon3/fcon3</sup>* (*Pcdhy* mutant) embryos. These cells were mixed in equal proportions with MGE cells from *Gad1-GFP* embryos (*Pcdhy* WT, green) and transplanted into WT black (Blk) six host recipient mice. Cell survival was analyzed before (3 DAT) and throughout the period of cell death (6–21 DAT). (B,B') Survival fraction of co-transplanted MGE-derived cIN precursors. (B) MGE cells were derived from *Gad1-GFP* (green) and *Nkx2.1<sup>Cre</sup>-Ai14-* (magenta) embryos; both GFP+ and tdTomato+ cells carry WT *Pcdhy*. In this control experiment the survival fraction was similar for both genotypes carrying the different fluorescent reporters (2-way ANOVA,  $F_{\text{genotype}} = 2.54$ , P value > 0.999; n = 4–6 mice per time point from two transplant cohorts). (B') MGE cells were derived from *Gad1-GFP* WT (green) and *Nkx2.1<sup>Cre</sup>-Ai14 Pcdhy* mutant (magenta) embryos. GFP+ and tdTomato+ cells showed dramatic differences in their survival; the majority of cells carrying the *Pcdhy* mutant allele (magenta) were eliminated between 6 and 21 DAT (2-way ANOVA,  $F_{\text{genotype}} = 2738.02$ , P value < 0.0001; adjusted p values \*\*\*p<0.0001; n = 4–5 mice per time point from two transplant cohorts. Quantifications in (B and B') were done at 3, 6, 13 and 21 DAT and are represented as fractions of GFP+ or tdTomato+ cells from total cells (GFP + tdTomato+) per brain section. The increase in the proportion of WT cells during this period is not a reflection of increased cell numbers (WT cIN also undergo elimination by PCD (See **Supplement Figure 9**), but rather that WT cells account for a larger fraction of all transplant-derived cells (WT + *Pcdhy* mutant). (C) Representative photographs of cortical sections from transplanted host mice at 6 (left) and 21 (right) DAT. Transplanted MGE cells were derived from *Gad1-GFP* (*Pcdhy* WT, green) and *Nkx2.1<sup>Cre</sup>-Ai14-Pcdhy<sup>fcon3/fcon3</sup>* (*Pcdhy* mutant, red) embryos. Scale bars, 50  $\mu\text{m}$ .

A



**Supplement Figure 9.1** - Number of cIN drops for both the *Pcdhy* WT and *Pcdhy* mutant transplanted population.

**Supplement Figure 9.1** - (Related to Figure 8) - (A) Quantification of the GFP (green bars) and tdTomato (magenta bars) positive cells in the cortex of Blk six recipient mice at 3, 6, 13, and 21 DAT. The GFP and tdTomato-labeled cells were derived from E13.5 MGEs of *Nkx2.1<sup>Cre</sup>-Ai14-Pcdhy<sup>fcon3/fcon3</sup>* (*Pcdhy* mutant) and *Gad1-GFP* (*Pcdhy* WT) embryos, and were co-transplanted in similar proportions into Blk6 WT recipients. Note that both WT and *Pcdhy* mutant cell numbers decrease over time.

### **cINs compete for survival using Pcdhy.**

After determining that the fluorophore (GFP or tdTomato) does not negatively impact the survival of transplanted cINs, and that cINs that express WT Pcdhy undergo apoptosis to levels comparable to those observed during the normal period of cell death, we investigated the survival of cINs lacking Pcdhy and mixed with cINs expressing WT Pcdhy. We co-transplanted equal numbers of Gad67-GFP cells (Pcdhy WT) and *Nkx2.1-Cre-Ai14-Pcdhy<sup>fcon3/fcon3</sup>* cells (Pcdhy mutant) into the cortex of neonatal recipient mice. As above, we measured the proportion of surviving GFP positive and tdTomato positive cells at 3, 6, 13, and 21 DAT (**Figure 8A**). Similar numbers of GFP positive and tdTomato positive cells were observed at 3 and 6 DAT. However, the fraction of Pcdhy mutant cINs (tdTomato+) surviving was dramatically lower by 21 DAT, when the transplanted cells reached a cellular age equivalent to that of endogenous cINs after the normal wave of PCD (21DAT is roughly equivalent to P15). Note that in this experiment the proportion of WT cells increases during this same period (from 6 to 21 DAT). This change in proportion is not a reflection of increased survival, as these cells also undergo elimination by PCD (see below)(**Supplement Figure 9**), but that, with the increased loss of mutant cells, the WT cells account for a larger fraction of the total surviving cells.

We next determined the extent to which the Pcdhy loss of function affected the survival of cINs using the co-transplant assay. As above, we co-transplanted 50K cells of each genotype (Pcdhy WT and Pcdhy mutant) into the cortex of host mice (**Figure 9A**) and compared the survival of each population at 6 and 21 DAT. At 6 DAT the total number of tdTomato positive cells in the cortex of recipient mice was similar to that of GFP positive cells (**Figure 9A, D & E**). However, between 6 and 21 DAT the total number of GFP positive cells that express WT Pcdhy had decreased by an average of ~63% (**Figure 9E, compared to Figure 9C**). This surprising result contrasted with the results above, where the population of either GFP or tdTomato labeled cells but expressing WT Pcdhy was reduced by ~40% between 6 and 21 DAT. This

result also suggests that WT cells die at a higher rate (63%) when co-transplanted with Pcdhy mutant MGE cells. However, this observation would require additional animals for statistical confirmation. Regardless, the number of Pcdhy mutant (tdTomato+ cells) cINs in these co-transplants decreased drastically, by ~96% (**Figure 9E**). This experiment confirms that MGE cells lacking Pcdhy function are eliminated in far greater numbers than control MGE cells and show that the presence of Pcdhy WT cINs within a mixed population also affects the survival of mutant cINs (**compare Figure 8 and Figure 9**). However, this observation would require the assessment of the total change in cIN numbers between 6 and 21 DAT when Pcdhy mutant cells are transplanted alone. Altogether, these observations are consistent with the hypothesis that cINs interact with other cINs of the same age(discussed below).

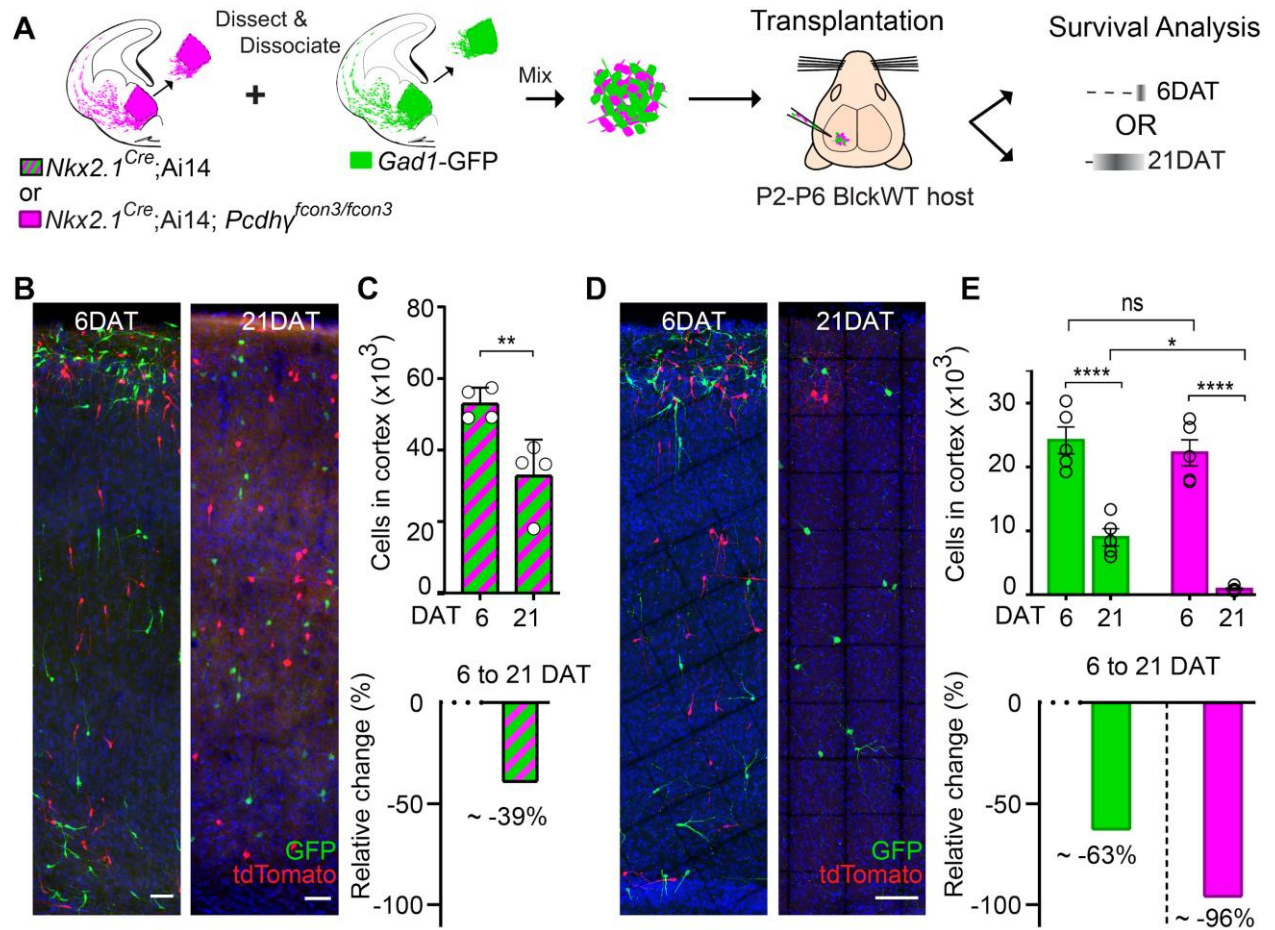
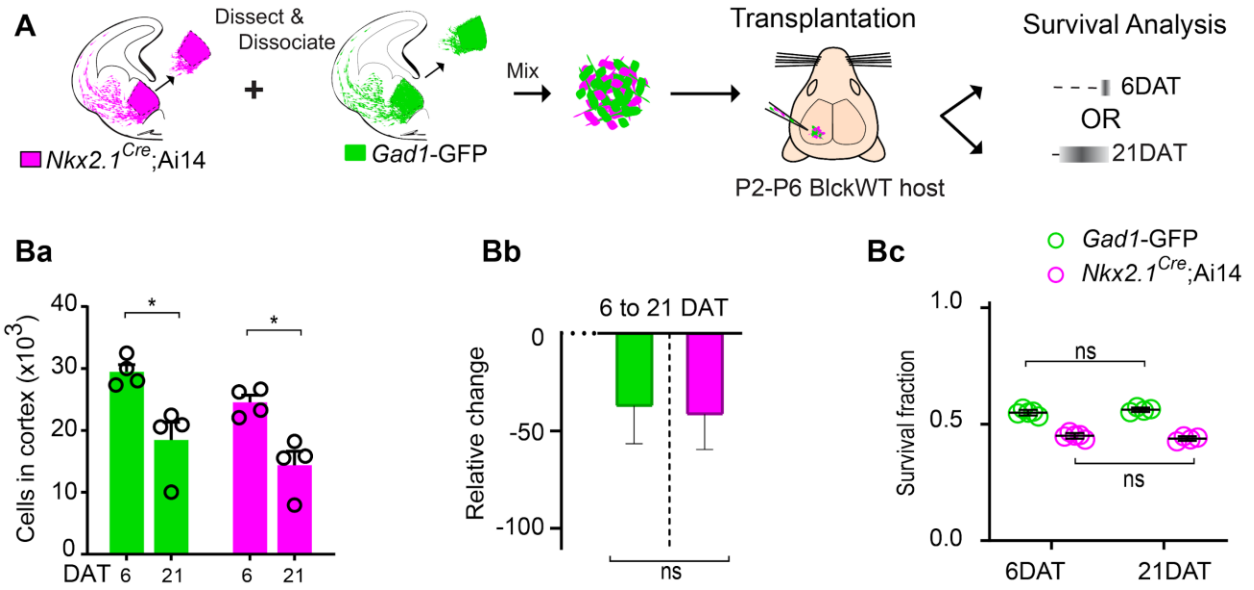


**Figure 9.1** - MGE cell transplantation reveals a non-cell autonomous effect of *Pcdhy* on cIN survival.

**Figure 9.1** - (A) Schematic of co-transplantation experiment for quantification of absolute number of transplanted MGE cells derived from (1) *Nkx2.1<sup>Cre</sup>-Ai14* and *Gad1-GFP* embryos WT for *Pcdhy* or (2) *Nkx2.1<sup>Cre</sup>-Ai14-Pcdhy<sup>fcon3/fcon3</sup>* (*Pcdhy* mutant, magenta) and *Gad1-GFP* (*Pcdhy* WT, green) embryos. The total numbers of transplanted-derived cINs were counted at 6 and 21 DAT throughout the cortical volume were transplanted cells dispersed. (B) Photographs of representative coronal sections of co-transplanted tdTomato and GFP-labeled cells, both *Pcdhy* WT, at 6 and 21 DAT. Scale bar 100  $\mu$ m. (C) Absolute number of surviving tdTomato and GFP-labeled *Pcdhy* WT cIN at 6 and 21 DAT (top graph) (Mann-Whitney test, \*\* $p=0.0286$ ,  $n = 4$  mice per time point from one transplant cohort). The drop in number of transplant derived cells was similar for WT-GFP+ and WT-tdTomato+ (**Supplement Figure 10**). A 39% drop in cIN number was observed between 6 and 21 DAT (bottom graph). (D) Photographs of representative coronal sections of transplanted tdTomato-labeled *Pcdhy* mutant (magenta) and GFP-labeled *Pcdhy* WT (green) cells at 6 and 21 DAT. Survival of the cINs drops for both genotypes, but the tdTomato-labeled cells were nearly eliminated by 21 DAT. Scale bar 100  $\mu$ m. (E) Absolute number of surviving cINs at 6 and 21 DAT (top graph)(2-way ANOVA; Fage = 128.65, P value < 0.0001, adjusted p value \*\*\*\* $p<0.0001$ ); F-genotype = 9.74 (p value=0.0066, adjusted p value \* $p=0.0126$ );  $n = 5$  mice per time point from one transplant cohort). Comparing 6 and 21 DAT a drop of ~63% and of 96.0% was observed, respectively, for cells WT and mutant for *Pcdhy* (bottom graph).





**Supplement Figure 10.1** - Fluorescent reporter or breeding background does not affect the survival of transplanted MGE-derived cINs.

**Supplement Figure 10.1** - (Related to Figure 9.1) - (A) Schematic of co-transplantation of MGE-derived cIN precursors. MGE precursor cells were derived from *Nkx2.1<sup>Cre</sup>-Ai14-* (tdTomato+) and *Gad1-GFP* (GFP+) E13.3 embryos that carry WT *Pcdhy*. The GFP and tdTomato positive cells were mixed in similar proportions and transplanted into WT black six (C57Bl6) host recipients. Survival of the transplanted cells was analyzed at 6 and 21 DAT. (Ba-Bc) Quantification of the GFP (green bars) and tdTomato (magenta bars) positive cells in the cortex of Blk6 recipient mice at 6 and 21 DAT. The number of GFP+ (green bars) and tdTomato+ (magenta bars) cells decreases over time (Ba), but the relative change in cell number from 6 to 21 DAT (Bb) and the survival fraction (Bc) is similar in both the GFP+ and tdTomato+ population. Note here that the initial ratio was not 50/50 with slightly more GFP+ cells transplanted compared to the tdTomato+ cells. This indicates that the fluorophore and driver of the fluorophore do not affect survival. Note that a similar survival between 6 DAT and 21 DAT (shown in Bc) is not a reflection of unchanged cell numbers, but rather that GFP or tdTomato cells account for a similar fraction of all the transplant-derived cells (Mann-Whitney test, \*p=0.0286 (Ba), n = 4–5 mice per time point).

We next determined whether the survival of the Pcdhy WT or Pcdhy mutant cells labeled with GFP or tdTomato respectively would be affected by their density. At 6 DAT, the Pcdhy WT or Pcdhy mutant MGE-derived cINs had migrated away from the injection site establishing a bell-shaped distribution of density as a function of tangential distance from the injection site (**Figure 10B & B'**). The dispersion of developing cINs lacking Pcdhy was indistinguishable from that of control WT cells at this time (**Figure 10B', top graph**), consistent with our observation that Pcdhy expression is not required for the migration of MGE-derived cINs. Strikingly, the survival fraction at 6 DAT of control Pcdhy WT and Pcdhy mutant cINs at the injection site or at multiple locations anterior or posterior to the site of injection were also similar (**Figure 10B', bottom graph**). By 21 DAT the survival of Pcdhy mutant cells was dramatically reduced, and to a similar extent at all distances from the injection site (**Figure 10B & B'**). Since the density of cIN varies fivefold over regions measured, we conclude that the survival of control Pcdhy WT and Pcdhy mutant cINs does not depend on their density over this range.

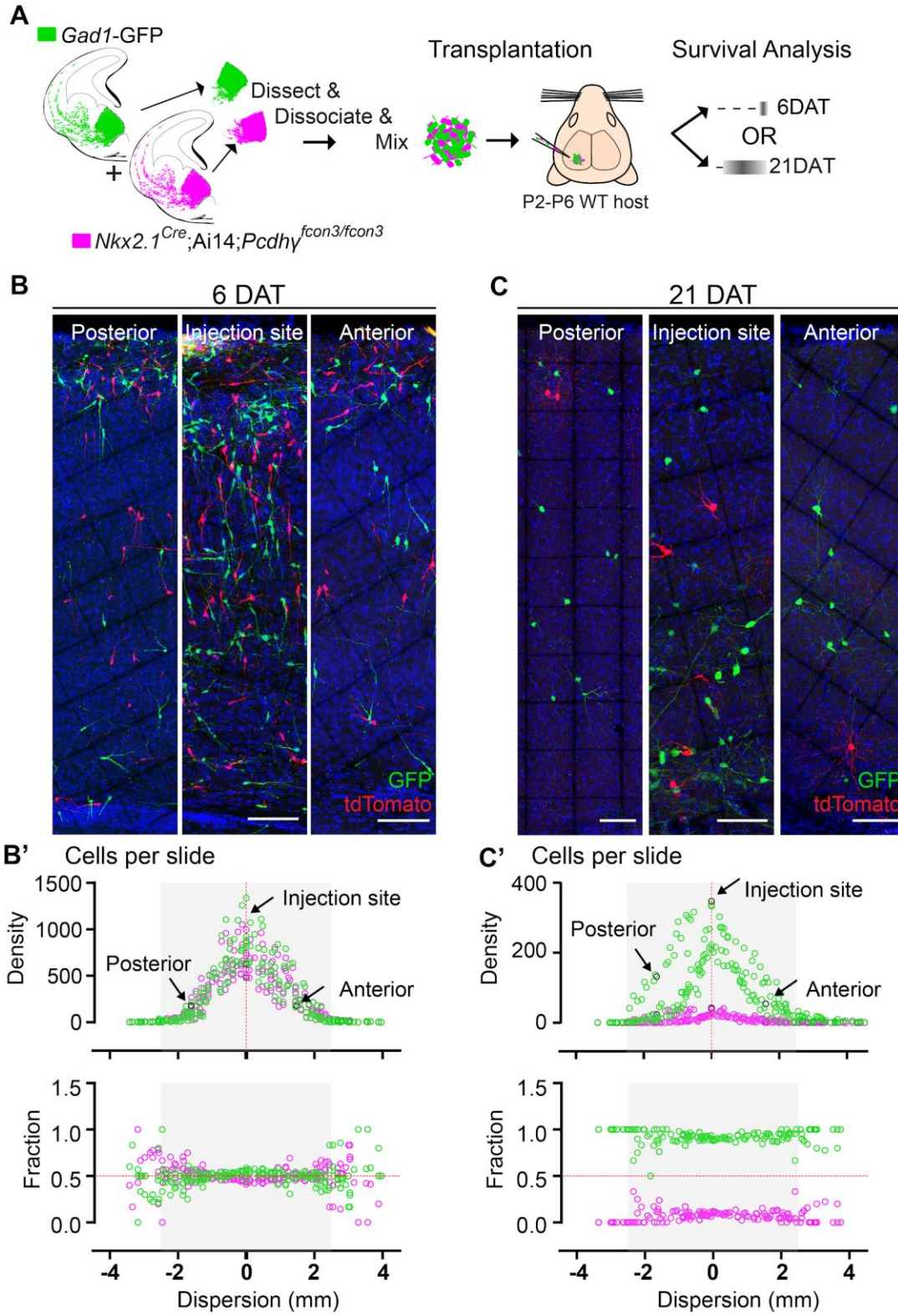


**Figure 10.1** - Survival of cINs, WT, or mutant for *Pcdhy*, was not affected by cell density.

**Figure 10.1** (A) MGE cells derived from *Nkx2.1<sup>Cre</sup>-Ai14-Pcdhy<sup>fcon3/fcon3</sup>* embryos (*Pcdhy* mutant, magenta) and from *Gad1-GFP* embryos (*Pcdhy* WT, green) were mixed in equal numbers and transplanted into WT hosts. The survival of tdTomato and GFP- labeled cINs was analyzed in every other section throughout the brain region of the transplant dispersal. (B) Photographs of representative coronal sections at the injection site, anterior and posterior to it, from host mice at 6DAT. At this time, similar numbers of tdTomato and GFP-labeled cINs were observed at each location. Scale bar 100  $\mu$ m. (B') Dispersion analysis at 6 DAT of the *Pcdhy* WT (green) or *Pcdhy* mutant (magenta) cells, represented as density (top) or survival fraction (bottom) as a function of distance from the site of injection. Note that the density of cells decreases as one moves anteriorly or posteriorly with respect to the injection site. At 6 DAT, the dispersal and survival were similar for both WT and *Pcdhy* mutant cells. (C) Photographs of representative coronal sections at the injection site, or anterior and posterior to it, from host mice at 21DAT. Note the dramatic reduction in the number of *Pcdhy* mutant cells (magenta) compared to the *Pcdhy* WT cells (green). Scale bar 100  $\mu$ m. (C') Dispersion analysis at 21DAT of the *Pcdhy* WT (green) or *Pcdhy* mutant (magenta) cells, represented as density (top) or survival fraction (bottom) as a function of distance from the site of injection in the host recipients. At 21 DAT, the survival fraction for the *Pcdhy* mutant cells (magenta) was dramatically reduced and similarly affected at different locations with respect to the injection site.

## Morphological and Physiological maturation of cINs lacking Pcdhy

The above results indicate that cINs lacking Pcdhy genes have increased cell death, specifically when the transplanted cells reach an age equivalent to that of endogenous cINs undergoing their normal period of PCD. However, transplantation experiments showed that the proportion of cell death was constant across varying cell densities, suggesting potential increased cell-cell contacts due to higher cell density might not be a factor in determining cIN survival. Still we wondered whether the loss of Pcdhy in cINs affected their morphological maturation during this period. We first determined the survival fraction for the co-transplanted Pcdhy WT and Pcdhy mutant cINs labeled with GFP or tdTomato respectively. To this end, we mixed similar proportions of *Gad67-GFP* (Pcdhy WT) and *Nkx2.1<sup>Cre</sup>-Ai14-Pcdhy<sup>fcon3/fcon3</sup>* (Pcdhy mutant) MGE-derived cIN precursor cells, and transplanted this mix into the cortex of neonate mice. We measured the survival of the transplanted cells at several time points during the period when cell death occurs in the transplanted population (6, 8, 10, 12 and 21 DAT). We found that the proportion of the Pcdhy mutant cINs dropped steadily throughout the period of cell death (**Figure 11B**). We next imaged the transplanted cells using confocal microscopy, and performed morphological reconstructions of the transplanted cINs between 6 and 12 DAT when the majority of the transplanted cINs underwent PCD (**Figure 11A**). We found no obvious differences between Pcdhy mutant and control Pcdhy WT cINs in neuritic complexity, including neurite length (**Figure 11C**), the number of neurites (**Figure 11D**), number of nodes (**Figure 11E**) and number of neurites ends (**Figure 11F**). These results suggest that Pcdhy genes do not play a major role in the morphological maturation of cINs during the period of cIN death.

Next, we investigated whether the loss of Pcdhy affected the integration or intrinsic physiological properties of the transplanted cells at time points around the peak of Pcdhy-mediated cell death. Again, we utilized the co-transplantation assay of cINs that were either Pcdhy deficient (labeled with tdTomato) or carried WT Pcdhy (labeled with GFP). To test how

integration was affected, we made acute cortical slices of mouse visual cortex at 8, 9, 10, 11, and 12 DATs and measured the frequency of spontaneous excitatory (glutamatergic) and inhibitory (GABAergic) synaptic events, comparing mutant and WT cINs within the same slice. There was no effect to the loss of Pcdhy function on the frequency of spontaneous excitatory (glutamatergic) synaptic events or on the frequency of spontaneous inhibitory (GABAergic) synaptic events (**Figure 12B** and **Tables 1 and 2**). We next investigated whether the loss of Pcdhy altered intrinsic physiological properties in co-transplanted cINs. There was no effect to the loss of Pcdhy on the maximum firing rate (**Figure 12C** and **Tables 1 and 2**), membrane time constant (Tau) (**Figure 12D** and **Table 1**), or input resistance (**Figure 12F** and **Table 1**). A difference in capacitance was observed at 8DAT between the WT Pcdhy and mutant Pcdhy cINs, but this difference was not statistically significant following multiple comparisons correction and was not seen at later time points (**Figure 12E** and **Table 1**). While we conclude that the synaptic integration and morphological - functional maturation of cINs lacking Pcdhy is similar to that of cINs with WT Pcdhy controls, we cannot rule out the possibility that Pcdhy mediate interactions among cINs or between cINs and ENs that might be important for other neuronal activity.

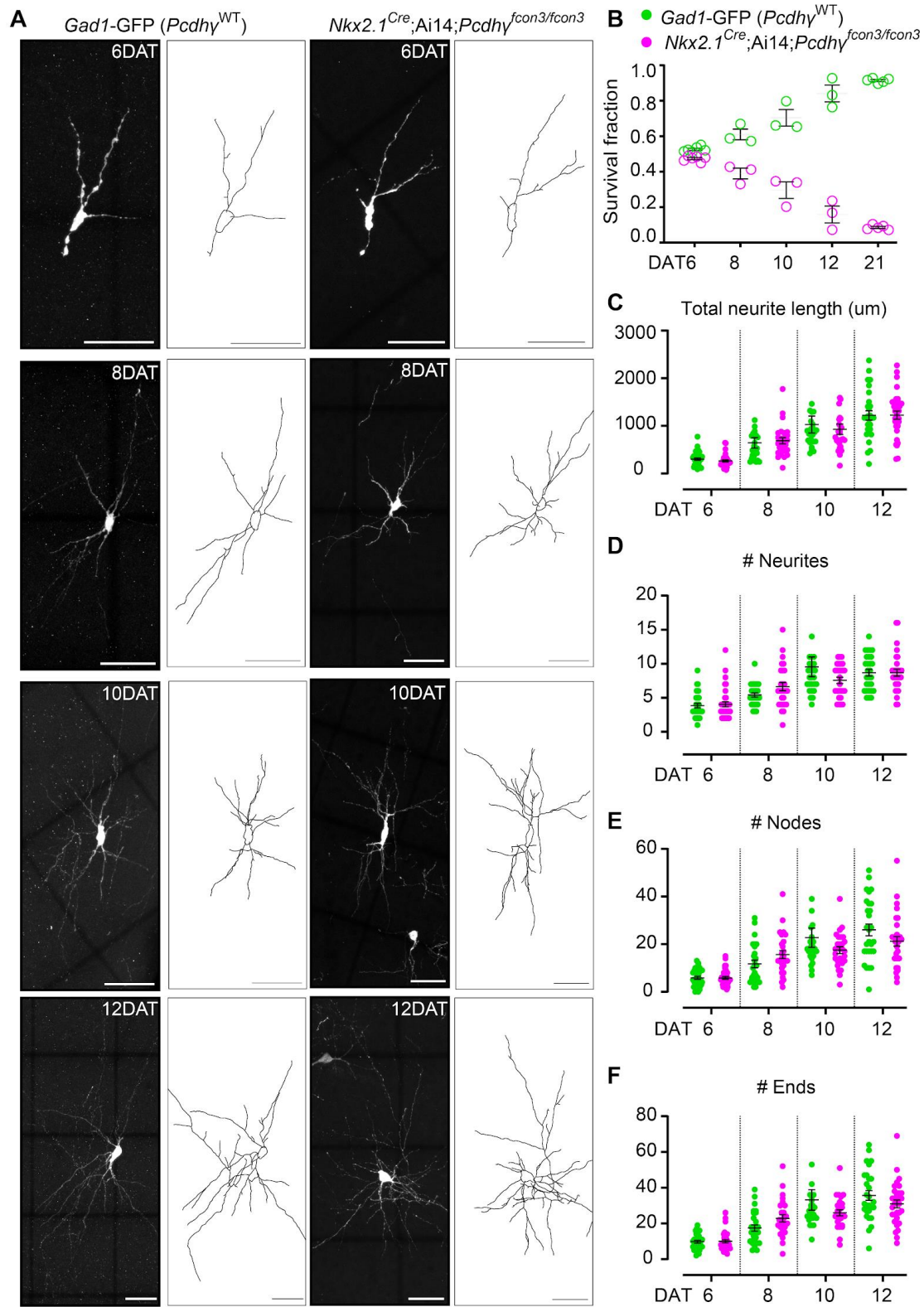


**Figure 11.1** - Loss of *Pcdhy* does not affect the morphological maturation of cIN during the period of PCD.



**Figure 11.1** - (A) Photographs of representative images and morphological reconstructions of co-transplanted *Gad1*-GFP cells (*Pcdhy* WT, left columns) with *Nkx2.1<sup>Cre</sup>-Ai14-Pcdhy<sup>icon3/fcon3</sup>* cells (*Pcdhy* mutant, right columns) at 6, 8, 10 and 12DAT. Scale bars, 50  $\mu$ m. (B) Quantifications of *Pcdhy* WT (green) and *Pcdhy* mutant cells (magenta) from co-transplanted animals, represented as survival fraction from total number of cells per section at 6, 8, 10, 12, and 21 DAT. *Pcdhy* mutant cells show increased cell death between 6 and 8 DAT and this increase in neuronal elimination occurs through 21 DAT. (C–F) Measurements of neurite complexity during the period of PCD: neurite length (C), neurite number (D), node number (E), and neurite ends (F) in *Pcdhy* WT (green) and *Pcdhy* mutant (magenta) neurons at 6, 8, 10, and 12 DAT. Two-tailed unpaired *Student's t-test*, n = 32 (WT), n = 35 (*Pcdhy* mutant) cells at 6 DAT, n = 27 (WT and *Pcdhy* mutant) cells at 8 DAT, n = 26 (WT), n = 27 (*Pcdhy* mutant) cells at 10 DAT, and n = 27 (WT), n = 31 (*Pcdhy* mutant) cells at 12 DAT; cells analyzed from two transplant cohorts. All statistical comparisons were not significant following Benjamini-Hochberg multiple comparisons correction at alpha of 0.05.

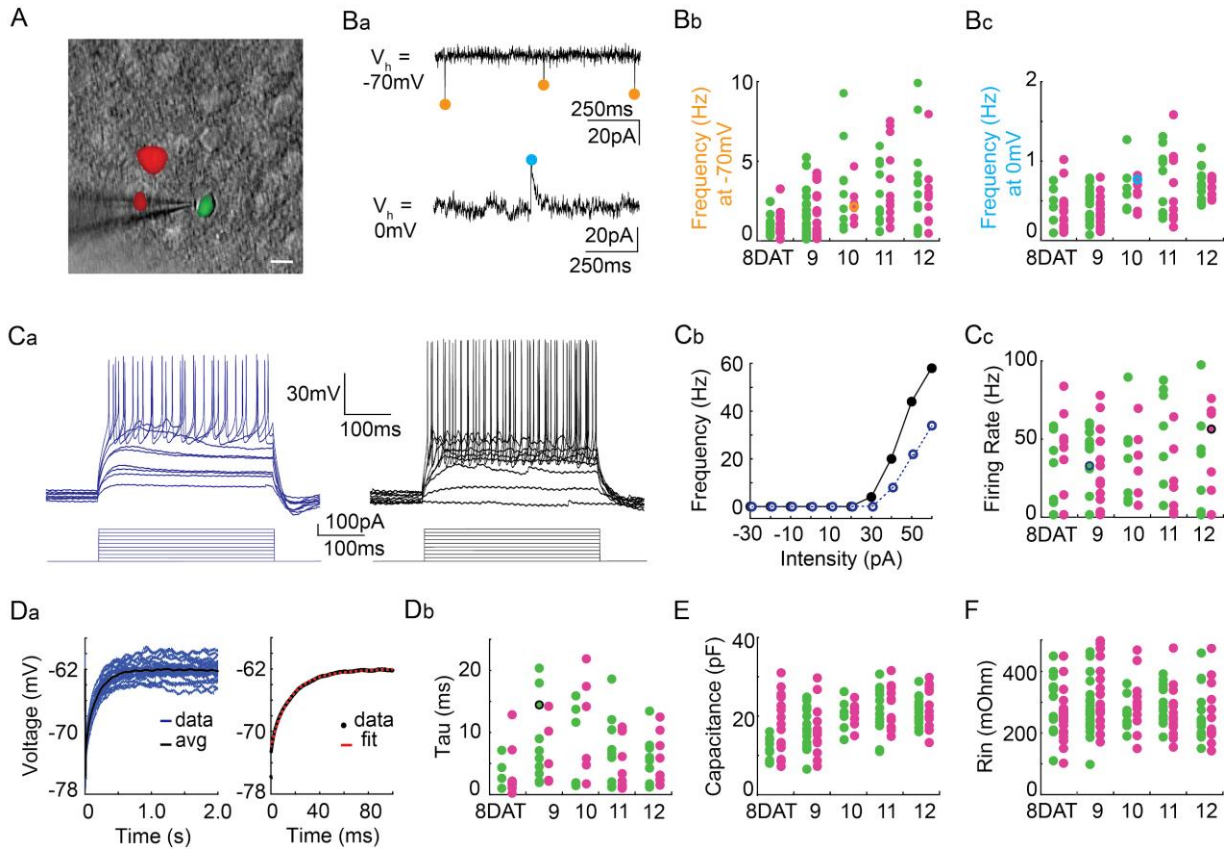


**Figure 12.1** - Pcdhy deletion does not affect the physiological properties of cINs during the period of PCD.

**Figure 12.1** - (A) DIC image with fluorescence image overlaid showing co-transplanted cINs from the MGE of *Gad1*-GFP (*Pcdhy* WT, green) or *Nkx2.1<sup>Cre</sup>-Ai14-Pcdhy<sup>fcon3/fcon3</sup>* (*Pcdhy* mutant, red) embryos, recorded in an acute brain slice taken from visual cortex (scale bar 10  $\mu$ m). (Ba) Representative voltage-clamp recordings (1 s) from a *Nkx2.1<sup>Cre</sup>-Ai14-Pcdhy<sup>fcon3/fcon3</sup>* (*Pcdhy* mutant) cINs held at  $-70$  mV (top) to record glutamatergic events (orange circles) and 0 mV (bottom) to record GABAergic events (cyan circles). Bb, Bc. Group data from cINs recorded at 8, 9, 10, 11, and 12 DAT showed that co-transplanted *Gad1*-GFP cINs (WT, green circles) and *Nkx2.1<sup>Cre</sup>-Ai14-Pcdhy<sup>fcon3/fcon3</sup>* cINs (*Pcdhy* mutant, magenta circles) have similar rates of glutamatergic events (measured at  $-70$  mV, Bb) and similar rates of GABAergic events (measured at 0 mV, Bc). The voltage clamp recordings from (Ba) are represented within the group data by the orange ( $-70$  mV) and cyan (0 mV) circles in Bb and Bc) respectively. Ca, Cb. Representative current clamp traces showing a range of firing rates from a *Gad1*-GFP cIN (WT, blue trace) and a *Nkx2.1<sup>Cre</sup>-Ai14-Pcdhy<sup>fcon3/fcon3</sup>* (*Pcdhy* mutant, black trace) cIN responding to intracellular current injections (Ca), and the corresponding FI curves (Cb). (Cc) Group data from cINs recorded at 8, 9, 10, 11, and 12 DAT showed that co-transplanted *Gad1*-GFP cINs (WT, green circles) and *Nkx2.1<sup>Cre</sup>-Ai14-Pcdhy<sup>fcon3/fcon3</sup>* cINs (*Pcdhy* mutant, pink circles) have similar maximum spike rates. The current clamp traces from (Ca and Cb) are represented within the group data by the blue and black circles. (Da) Left: *Gad1*-GFP (WT) cIN voltage responses to repeated current injections (blue traces). Right: The membrane time constant ( $\tau$ ) is calculated by fitting an exponential to the average voltage trace (black line). (Db) Group data from current-clamp recordings of co-transplanted *Gad1*-GFP cINs (WT, green circles) and *Nkx2.1<sup>Cre</sup>-Ai14-Pcdhy<sup>fcon3/fcon3</sup>* cINs (*Pcdhy* mutant, magenta circles) at 8, 9, 10, 11, and 12 DAT shows that *Pcdhy* deletion does not affect membrane time constant. The current clamp recording from (Da) is represented within the group data by a black circle. (E and F) Group data from current-clamp recordings of co-transplanted *Gad1*-GFP cINs (WT, green circles) and *Nkx2.1<sup>Cre</sup>-Ai14-Pcdhy<sup>fcon3/fcon3</sup>* cINs (*Pcdhy* mutant, magenta circles) at 8, 9, 10, 11, and 12 DAT shows that *Pcdhy* deletion does not affect either capacitance (E) or input resistance (F). Cells analyzed in A–F were taken from at least three transplant cohorts.

## **PART IV - Genomic complexity of Pcdhy and its role in cIN survival**

### **Genomic complexity of Pcdhy is not required for the regulation of PCD.**

The genomic complexity of the Pcdhy gene cluster and the low protein expression levels of PCDHY isoforms in neurons have made it difficult to assay the expression profile of Pcdhy in single cells. Our results above indicate that the loss of function of all 22 Pcdhy isoforms encoded from the Pcdhy gene cluster significantly increased cell death among cINs. Whether all 22 Pcdhy are equally involved in the regulation of cIN survival remains unclear. To dissect the Pcdhy gene cluster complexity and its role in cIN survival, we use a series of genetic deletions in the Pcdhy gene locus and probe the role of various Pcdhy isoforms in the regulation of cIN cell death in mice.

### **Loss of Pcdhy C-type isoforms is sufficient to increase cell death.**

Our qPCR expression analysis suggested that the expression of Pcdhya1, Pcdhya2, Pcdhyc4, and Pcdhyc5 in cINs increases during, or soon after, the period of cell death (**Figure 1C**). In collaboration with the laboratory of Professor Tom Maniatis at Columbia University, we obtained mice with constitutive deletions of Pcdhya1, Pcdhya2 and Pcdhya3 (Pcdhy<sup>tako</sup>) or Pcdhyc3, Pcdhyc4 and Pcdhyc5 (Pcdhy<sup>tko</sup>). Using these mice, we tested if Pcdhya1 and Pcdhya2 or Pcdhyc4 and Pcdhyc5 were required for the normal survival of MGE-derived cINs.

We first crossed the Pcdhy<sup>tako/tako</sup> mouse line to *Nkx2.1<sup>Cre</sup>-Ai14* mice to label MGE-derived cINs (**Figure 7A**). The resulting *Nkx2.1<sup>Cre</sup>-Ai14-Pcdhy<sup>tako/tako</sup>* mice (Pcdhya1, Pcdhya2, and Pcdhya3 mutant) develop and breed normally, are born in normal Mendelian ratios had normal weight and showed no evidence of brain abnormalities. At P30, the density of cINs in both somatosensory and visual cortex of *Nkx2.1<sup>Cre</sup>-Ai14-Pcdhy<sup>tako/tako</sup>* mice was not significantly different from that of control *Nkx2.1<sup>Cre</sup>-Ai14* mice that are WT for Pcdhy (**Figure 7D**). Consistent

with this finding, co-transplanted MGE cells obtained from Gad67-GFP and *Nkx2.1<sup>Cre</sup>-Ai14-Pcdhy<sup>tako/tako</sup>* E13.5 MGE donor embryos displayed similar surviving cIN fractions (**Figure 13A, B & B'**). Therefore, the removal of the first three isoforms (A1, A2, and A3) of the *Pcdhy* gene cluster does not significantly affect cIN survival.

We next tested the function of C-type *Pcdhy* isoforms (*Pcdhyc3*, *Pcdhyc4* and *Pcdhyc5*) for cIN survival. Since homozygous *Pcdhy<sup>tcko</sup>* mice die shortly after birth (W. V. Chen et al. 2012), *Pcdhy<sup>tcko</sup>* heterozygous mice were crossed to the *Nkx2.1-Cre-Ai14* mouse line to label MGE/POA-derived cINs (**Figure 13A**). Even though homozygous *Nkx2.1-Cre-Ai14-Pcdhy<sup>tcko/tcko</sup>* mice develop normally (normal weight and no evidence of brain abnormalities) and are born in normal Mendelian ratios, these mice die shortly after birth (W. V. Chen et al. 2012). To bypass neonatal lethality, and study the role of *Pcdhyc3-c4-c5* isoforms during the normal period of postnatal cIN cell death, we co-transplanted *Pcdhyc3-c4-c5* homozygous mutant E13.5 MGE cells and *Pcdhy* WT (GFP+) cells into the cortex of WT neonatal recipients (**Figure 13A**). At 6 DAT, the dispersion and density of tdTomato+ and GFP+ cells was indistinguishable. However, the number of tdTomato+ MGE-derived *Pcdhyc3-c4-c5* mutant cINs dropped dramatically between 6 and 21 DAT, compared to the *Pcdhy* WT (GFP+) population (**Figure 13C**). The survival of *Pcdhyc3-C4-C5* mutant cINs at 21 DAT was strikingly similar to that observed after transplantation of MGE cells lacking the entire *Pcdhy* gene cluster (*Nkx2.1-Cre-ai14-Pcdhy<sup>fcon3/fcon3</sup>*); compare **Figure 8 and Figure 13**. These results indicate that unlike *Pcdhy* isoforms A1, A2, and A3, the *Pcdhy* isoforms C3, C4, and C5 are essential for cIN survival.

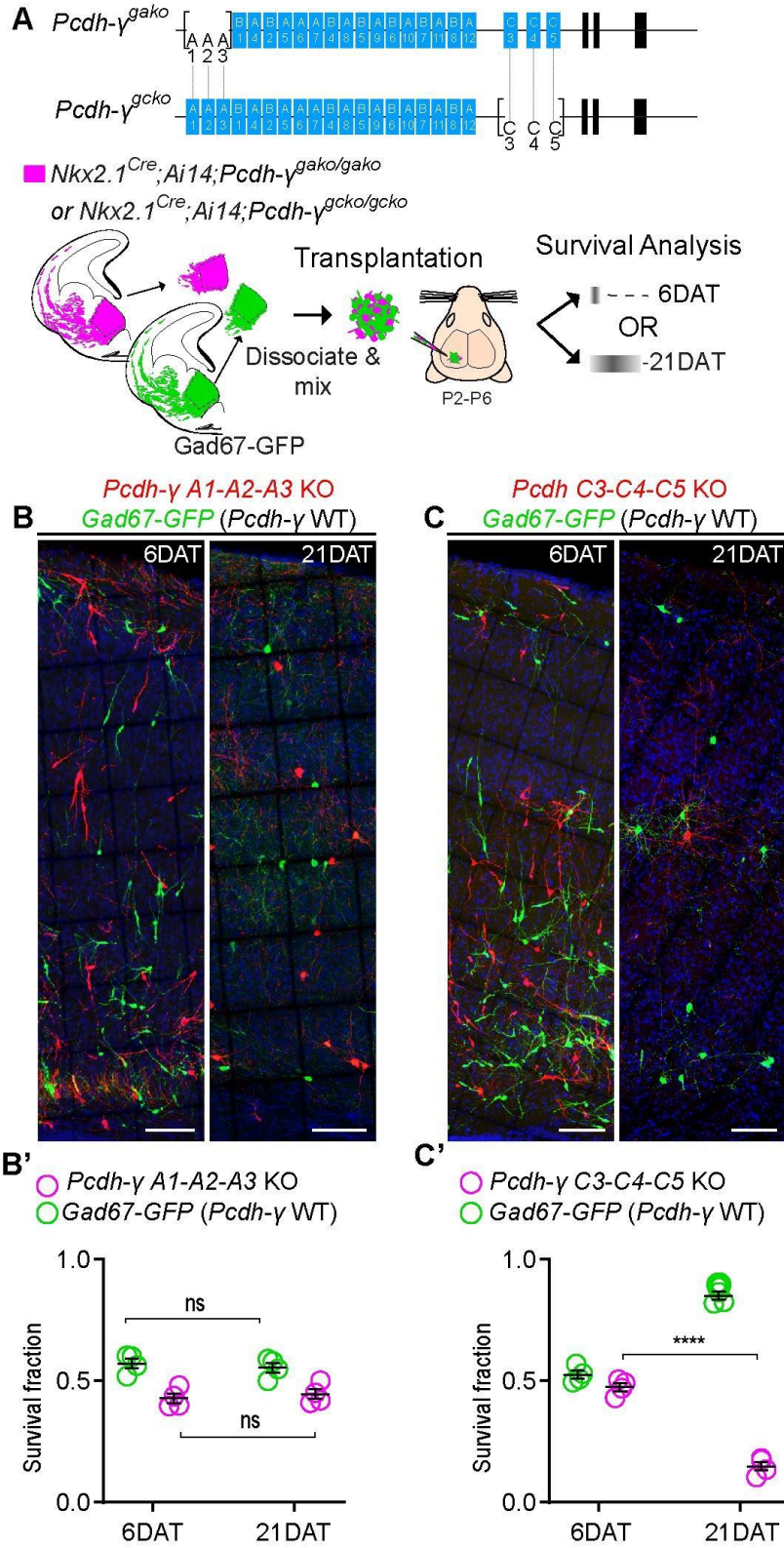


**Figure 13.1** - Loss of Pcdhyc3, Pcdhyc4, and Pcdhyc5 is sufficient to increase cIN cell death.

**Figure 13.1** - (A) Diagram of the mutant alleles *Pcdhy*<sup>tako</sup> (*Pcdhya1*, *Pcdhya2*, and *Pcdhya3* KO) and *Pcdhy*<sup>tcko</sup> (*Pcdhyc3*, *Pcdhyc4*, and *Pcdhyc5* KO). Below - schematic of transplantation of MGE cIN precursors from *Nkx2.1*<sup>Cre</sup>-*Ai14-Pcdhy*<sup>tako/tako</sup> (*Pcdhya1*, *Pcdhya2*, and *Pcdhya3* deleted) and *Nkx2.1*<sup>Cre</sup>-*Ai14-Pcdhy*<sup>tcko/tcko</sup> (*Pcdhyc3*, *Pcdhyc4*, and *Pcdhyc5* deleted) embryos. These cells were mixed in equal proportions with MGE cells from *Gad1*-GFP embryos (*Pcdhy* WT, green) and transplanted into WT Blk6 host recipients. Survival of the GFP and tdTomato-labeled cells was analyzed at 6 and 21 DAT. (B, B') Representative photographs of cortical sections from transplanted host animals at 6 (left) and 21 (right) DAT. Note the similar proportions of *Pcdhy* WT (GFP+) and *Pcdhya1*-, *Pcdhya2*-, and *Pcdhya3*- deleted cells (tdTomato+) at 6 and 21DAT. Scale bars, 100  $\mu$ m. (B') Quantifications of the survival fraction of the GFP (green) and tdTomato (magenta)-labeled MGE-derived cells at 6 and 21 DAT. Note, survival fraction remains similar and constant for both genotypes (*Pcdhy* WT and *Pcdhya1*-, *Pcdhya2*-, and *Pcdhya3*- deleted cells) between 6 and 21 DAT (Mann-Whitney test,  $p=0.6571$ ,  $n = 4$  mice per time point from one transplant cohort). (C, C') Representative photographs from coronal brain sections of transplanted host animals at 6 (left) and 21 (right) DAT. Scale bars, 100  $\mu$ m. Survival of MGE-derived cINs from *Pcdhyc3*-, *Pcdhyc4*-, and *Pcdhyc5*-deleted embryos (tdTomato+) is markedly different from MGE-derived cINs from *Pcdhy* WT embryos (GFP+). (C') Survival fraction at 6 and 21 DAT of the *Pcdhy* WT (green) and *Pcdhyc3*-, *Pcdhyc4*-, and *Pcdhyc5*- deleted cells (magenta) (Mann-Whitney test, \*\*\*\* $p=0.0286$ ,  $n = 4$  mice per time point from one transplant cohort).

**Pcdhyc4, but not the A-, B- or other C-type isoforms, plays a key role in the regulation of cIN PCD.**

As mentioned above, the *Pcdhy* gene locus encodes for the expression of 22 distinct PCDHY proteins. The 22 *Pcdhy* genes are subclassified into A-, B- or C-type isoforms. The A- and B-type isoforms comprise 19 of the 22 *Pcdhy* genes. The remaining three isoforms are the C-type *Pcdhy* (*Pcdhyc3*, *Pcdhyc4* and *Pcdhyc5*). The above experiment suggested that the *Pcdhy* C-type isoforms are key to cIN survival, but it did not exclude that the 19 *Pcdhy* A- and B-type isoforms are dispensable in the regulation of cIN cell death. It was also unclear whether one, some or all C-type *Pcdhy* isoforms participate in the regulation of cIN cell death. To determine whether *Pcdhy* diversity and expression of all 22 *Pcdhy* isoforms is required for cIN survival, we obtained a series of *Pcdhy* deletions in the A-, B- and C-type isoforms in collaboration with the laboratory of Joshua Wiener from the University of Iowa.

Using the CRISPR/Cas9 genome editing tool, a group from the Jackson Laboratory and University of Iowa developed a large cohort of new mouse lines with mutations or deletions in one or several clustered *Pcdh* genes (Garrett et al. 2019). We obtained three of these newly generated mouse lines: the *Pcdhy*<sup>1R1</sup>, *Pcdhy*<sup>C4KO</sup> and *Pcdhy*<sup>3R2</sup> (**Figure 14A**). Mice carrying the *Pcdhy*<sup>1R1</sup> allele solely express *Pcdhyc4* and have a constitutive deletion of 21 of the 22 *Pcdhy* isoforms. Conversely, mice with the *Pcdhy*<sup>C4KO</sup> allele have a constitutive deletion of *Pcdhyc4* but express the remaining 21 *Pcdhy* isoforms. Lastly, the *Pcdhy*<sup>3R2</sup> mice express *Pcdhyc3* and *Pcdhyc4* but lack *Pcdhyc5* and all of the *Pcdhy*A- and *Pcdhy*B- type isoforms, with the exception of B8. Importantly, all three lines carry intact alleles of the *Pcdha* and *Pcdhb* gene clusters. Together, experiments using these mouse lines helped us determine whether one, some or all of the *Pcdhy* C-type isoforms are required for the regulation of cIN cell death. In



addition, results using the above lines will help determine whether the alternate PcdhyA- and PcdhyB-type isoforms contribute to cIN survival.

The Pcdhy<sup>1R1</sup>, Pcdhy<sup>C4KO</sup> and Pcdhy<sup>3R2</sup> mice do not carry a fluorescent reporter to label cINs. Thus we took two approaches to study the function of these mutations in cINs. In the first approach, we used a lentivirus expressing GFP to label MGE precursor cells (**Figure 14A-B**). In the second approach, we crossed two of the above lines (Pcdhy<sup>1R1</sup> and Pcdhy<sup>C4KO</sup>) to an MGE reporter mouse line to fluorescently labeled cINs derived from the MGE (**Figure 15A-B**).

MGE precursors cells obtained from Pcdhy<sup>1R1/1R1</sup> homozygous embryos at E13.5, and infected with lentivirus expressing GFP driven by the CAG promoter (**Figure 14B**, see methods for infection details). The virus infected Pcdhy<sup>1R1/1R1</sup> MGE cells were mixed with Pcdhy WT MGE cells obtained from Nkx21.Cre-Ai14 embryos(**Figure 14B**). In this co-transplantation experiment, cells lacking all Pcdhy except C4 were carried using GFP-labeled and WT cells carried tdTomato. The mixture of cells was transplanted into the cortex of neonate WT mice, and the host mice were sacrificed at 7 and 21 DAT (n=3), at an age equivalent to P1 and P15 for the transplanted cells. The proportion of GFP and tdTomato labeled cells was compared at these timepoints. At 7DAT the fraction of Pcdhy<sup>1R1/1R1</sup> GFP labeled cells was ~40% while the Pcdhy WT tdTomato labeled cells was roughly 60% of the of the total number of cells in each brain slice analyzed (**Figure 14C**). By the 21 DAT, the proportion of Pcdhy<sup>1R1/1R1</sup> GFP population dropped slightly to ~33% and that of WT tdTomato cells increased slightly to ~67% (**Figure 14C**). This suggests that if the 19 Pcdhy A- and B-type, and Pcdhyc3 and C5 contribute to the regulation of cIN cell death, their contribution is small.

We next tested the function of Pcdhyc5 using embryos that are homozygous for the Pcdhy<sup>3R2</sup> allele. These mice carry only B8, C3 and C4, but lack all other Pcdhy isoforms

including C5. MGE precursor cells from E13.5  $Pcdhy^{3R2/3R2}$  embryos were infected with GFP-expressing lentivirus, and mixed with  $Pcdhy$  WT MGE cells obtained from  $Nkx21.Cre-Ai14$  embryos (**Figure 14A-B**). The mixture of cells was transplanted into the cortex of neonate mice, and the fraction of GFP and tdTomato cells analyzed at 6 and 21 DAT. At 6 DAT (n=3) the  $Pcdhy^{3R2/3R2}$  GFP positive cells accounted for an average of 70% while the  $Pcdhy$  WT tdTomato positive cells made-up 30% of the total cell number in each of the brain slices analyzed (**Figure 14D**). By 21 DAT (n=4) the proportion of  $Pcdhy^{3R2/3R2}$  GFP positive cells decreased from 70% to 60% while the  $Pcdhy$  WT tdTomato positive increased from 30% to 40% (**Figure 14D**). These results suggest that  $Pcdhy^{c5}$ , and most of the 19  $Pcdhy$  A- and B-type isoforms do not contribute significantly to cIN survival.

We next tested the deletion of  $Pcdhy^{c4}$  to cIN survival. These mice have a deletion of all of the  $Pcdhy$  cluster, with the exception of C4. For breeding purposes we used mice that carry a heterozygous  $Pcdhy^{C4KO}$  allele, since mice homozygous for the deletion of the  $Pcdhy^{c4}$  die shortly after birth (Garrett et al. 2019). As above, MGE precursor cells from E13.5  $Pcdhy^{C4KO/C4KO}$  embryos were infected with GFP-expressing lentivirus, and mixed with  $Pcdhy$  WT MGE cells obtained from  $Nkx21.Cre-Ai14$  embryos (**Figure 14A-B**). The mixture of cells was transplanted into the cortex of neonate mice, and the fraction of GFP and tdTomato cells analyzed at 6 and 21 DAT (n=1). At 6 DAT, the GFP positive cells accounted for 49% of all the transplant-derived cells, while tdTomato positive cells made up 51% of the total transplanted cells in each brain slice (**Figure 14E**). By 21 DAT, the proportion of the GFP cells had dramatically dropped to 17% and at this time the majority (83%) of the transplant-derived cells were WT tdTomato positive (**Figure 14E**). In these co-transplants, carry-over virus particles infected a portion of the grafted tdTomato-labeled cells expressing  $Pcdhy$  WT. The proportion of the tdTomato cells that were also labeled with GFP (double labeled:tdtomato+GFP+) remained similar between 6 and 21 DAT, suggesting virus infection or viral-driven GFP

expression does not cause changes in survival. These initial results using retroviral labeling suggests that the loss of Pcdhyc4 is sufficient to induce the elimination of high numbers of cINs

The above results suggest that the Pcdhy A-type and B-type (19 isoforms) in addition to the Pcdhyc3 and Pcdhyc5 isoforms do not play a major role in the regulation of cIN PCD. Since these preliminary experiments were carried out using viruses to infect and label the mutant cells, some of the host cells were also labeled due to viral particles that are carried along with the cell mixture used for transplantation. Therefore, we cannot exclude the possibility that some GFP labeled host cells could have been included in our analysis.

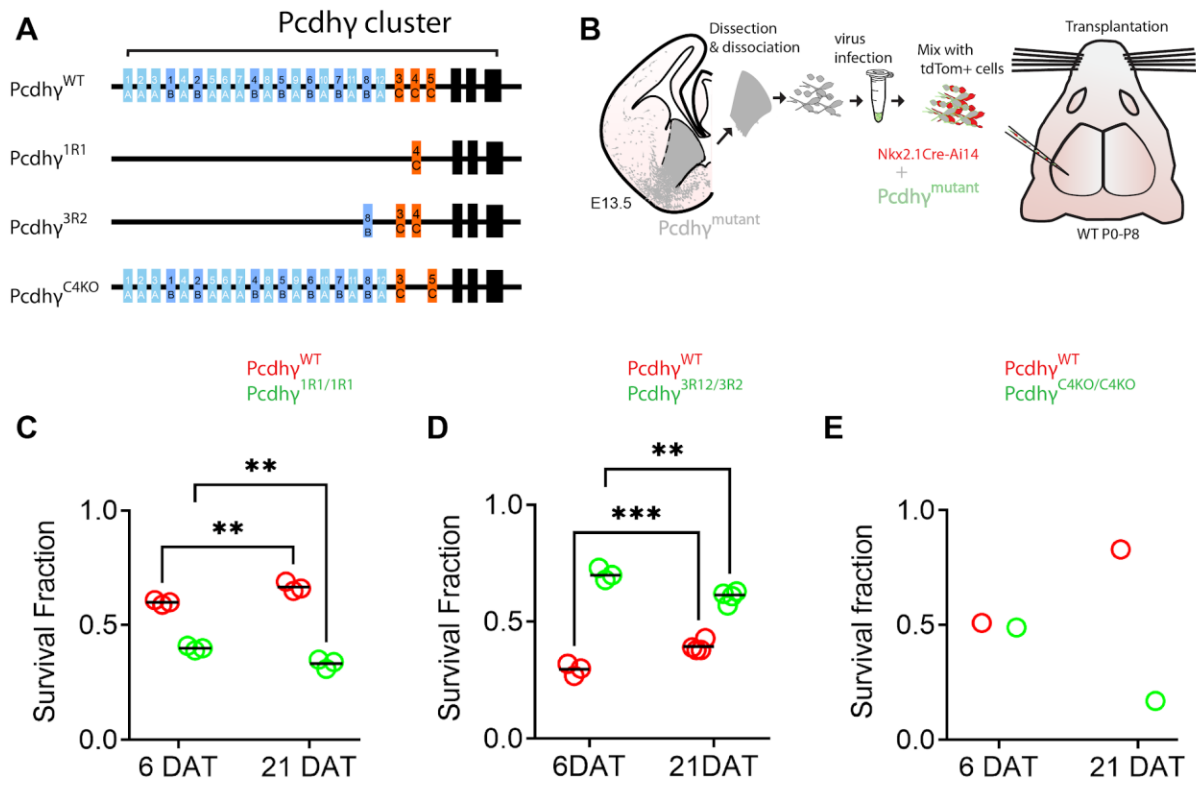


**Figure 14.1** - With the exception of *Pcdhy*c4, all other *Pcdhy* isoforms, including *Pcdhy*c5 are largely not required for cIN survival.

**Figure 14.1** - (A) Diagram of the *Pcdhy* WT and mutant alleles *Pcdhy*<sup>1R1</sup>, *Pcdhy*<sup>3R2</sup>, and *Pcdhy*<sup>C4KO</sup>. (B) Schematic of the MGE dissection, cell dissociation, lentiviral infection of MGE cIN precursors carrying the different mutations (*Pcdhy*<sup>1R1</sup>, *Pcdhy*<sup>3R2</sup>, or *Pcdhy*<sup>C4KO</sup>) and transplantation into P0-P8 WT hosts.. Infected cells from either *Pcdhy*<sup>1R1</sup>, *Pcdhy*<sup>3R2</sup>, or *Pcdhy*<sup>C4KO</sup> mutant embryos were mixed with MGE cIN precursors from *Nkx2.1*<sup>Cre</sup>-Ai14 embryos carrying WT *Pcdhy*, and the mixture was transplanted into WT neonate host. (C-E) Quantifications of the GFP (*Pcdhy* mutant, green dots) and tdTomato (*Pcdhy* WT, red dots) positive cells from mice co-transplanted with either *Pcdhy*<sup>1R1</sup> and *Pcdhy*<sup>WT</sup>(C), *Pcdhy*<sup>3R2</sup> and *Pcdhy*<sup>WT</sup>(D) or *Pcdhy*<sup>C4KO</sup> and *Pcdhy*<sup>WT</sup>(E). Each dot represents the average proportion of GFP or TdTomato positive cells from the total number of cells (GFP plus tdTomato) per brain section. ANOVA , \*\*p= 0.0044, ns = not significant; For C n=3; for D n=3 & 4; for E n=1; 10 brain sections were analyzed per mouse from each transplantation cohort.

To validate the above results, we crossed the  $Pcdhy^{1R1}$  and  $Pcdhy^{C4KO}$  mice to the MGE/POA reporter mouse line to enable a genetically encoded label for the cINs (**Figure 15A and Figure 16A**). Since mice that are homozygous for the  $Pcdhy^{C4KO}$  allele develop normally (no apparent weight, size, or brain abnormalities) and are born in normal Mendelian ratios, but die soon after birth, we utilized the co-transplantation method described above to study cINs survival postnatally in the above mutant mice (**Figure 15B and Figure 16B**).

As control, cINs expressing GFP were derived from micro dissected MGEs from  $Gad67$ -GFP embryos. cINs lacking  $Pcdhyc4$  were derived from equivalent dissections of  $Nkx2.1^{Cre}$ - $Ai14$ - $Pcdhy^{C4KO/C4KO}$  embryos expressing the tdTomato protein in MGE-derived cells. MGE cells from the two genotypes were dissociated, mixed in similar proportions, and grafted into the cortex of WT neonate mice. The proportion of GFP or tdTomato labeled cells was analyzed at 6 and 21 DAT. At 6 DAT the tdTomato positive  $Pcdhy^{C4KO/C4KO}$  mutant cells averaged 54.1% out of all the transplant-derived cells analyzed in each of the brain sections (**Figure 15C-D**). By 21 DAT, tdTomato  $Pcdhy^{C4KO/C4KO}$  mutant cell population dropped to 31% (**Figure 15C-D**). These results suggests that both the GFP  $Pcdhy$  WT and tdTomato  $Pcdhy^{C4KO/C4KO}$  mutant cells undergo cell death between 6 and 21 DAT, but the  $Pcdhyc4$  KO cells died at much higher rates, validating our preliminary results using viral labeled cells.

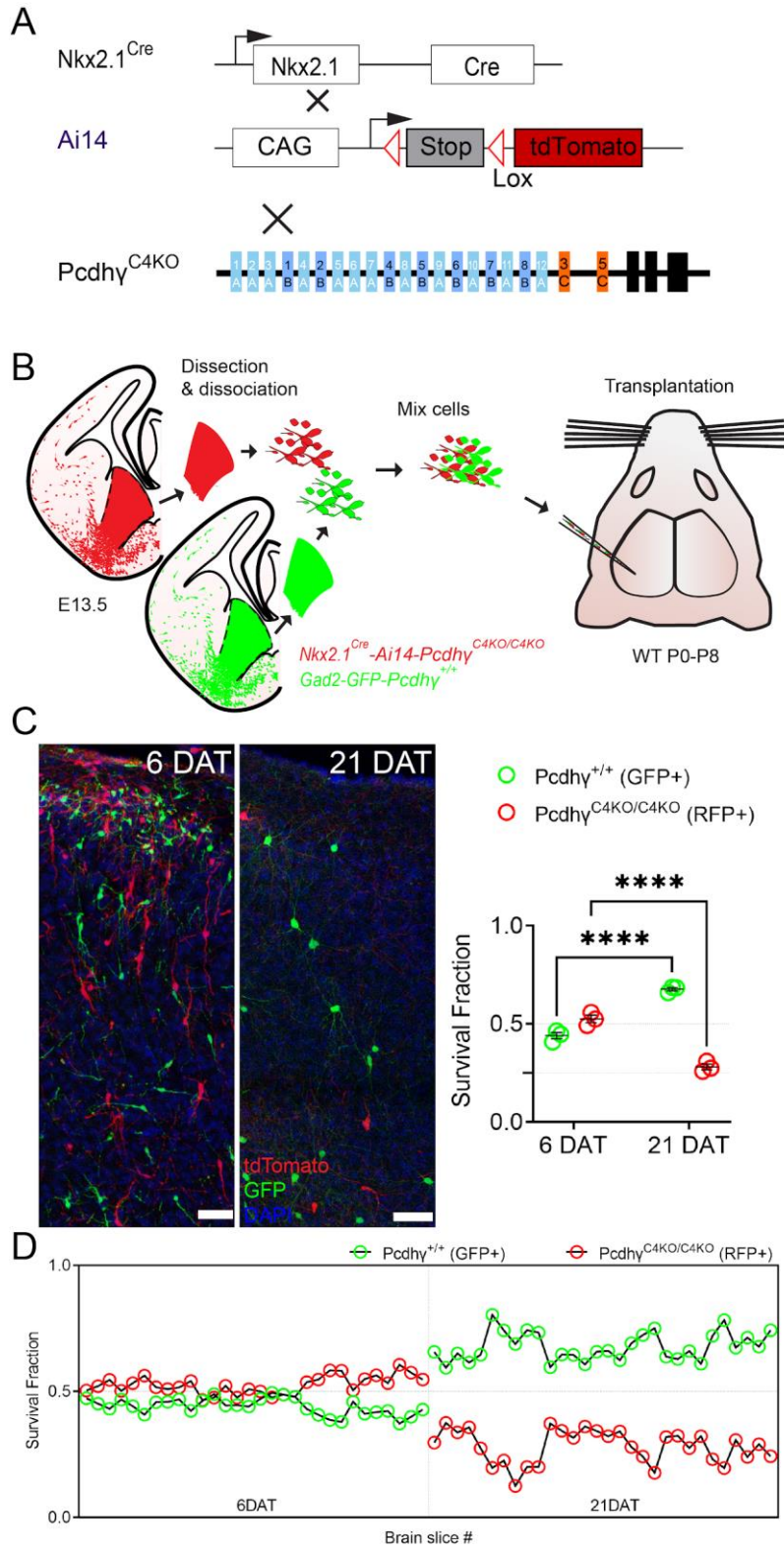


**Figure 15.1** - Genetic labeling of MGE-derived cIN confirms that the loss of Pcdhyc4 increased cIN cell death.

**Figure 15.1** - (A) Diagram of mouse crosses to obtain  $Pcdhy^{C4KO}$  homozygous MGE cells labeled with MGE-specific genetic reporter.  $Nkx2.1^{Cre}$  mice, which carry the conditional Ai14 allele to fluorescently label MGE-derived cINs, were crossed  $Pcdhy^{C4KO}$  mice that carry a constitutive deletion of the  $Pcdhyc4$  isoform. (B) The MGEs of  $Pcdhy^{C4KO}$  homozygous mutant embryos were dissected, dissociated, and mixed with equal numbers of MGE cells from control  $Gad67$ -GFP embryos at E13.5. The mixture of GFP+ ( $Pcdhy$ -WT) and tdTomato+ ( $Pcdhy^{C4KO/C4KO}$ ) cells was grafted into the cortex of WT neonate mice. (C) Left - Confocal images acquired from the cortex of 6 and 21 DAT mice. The transplanted cells were labeled with GFP ( $Pcdhy^{WT}$ ) or tdTomato ( $Pcdhy^{C4KO/C4KO}$ ). Right - Quantifications (shown as survival fraction) of surviving GFP or tdTomato labeled MGE-derived cINs at 6 and 21 DAT. Both the GFP and tdTomato labeled cells undergo PCD between 6 and 21DAT. At 6 DAT the proportion of GFP and tdTomato cells was similar, but by 21DAT the proportion of tdTomato ( $Pcdhy^{C4KO/C4KO}$ ) cells dropped significantly compared to the control cells (GFP). (D) Survival fraction quantification from (C) is shown by the brain section (each circle) at 6 and 21 DAT. Scale bar = 50  $\mu$ m, ANOVA,  $**p = 0.0001$ ,  $n = 3$  mice per time point and 10 brain sections per mouse from one transplant cohort.



We next asked if cINs expressing Pcdhyc4 but lacking all other Pcdhy isoforms survive to levels comparable to cINs carrying the entire Pcdhy gene cluster as suggested by our viral labeling experiment. To this end, control MGEs were obtained from Gad67-GFP mice and cells lacking all Pcdhy isoforms, except C4 from *Nkx2.1<sup>Cre</sup>-Ai14-Pcdhy<sup>1R1/1R1</sup>* embryos. The MGE at E13.5 were dissected, the cells dissociated, mixed in similar proportions, and grafted into the cortex WT neonate mice (**Figure 16B**). The survival of the GFP and tdTomato labeled cells was analyzed at 4, 6, 13 and 21 DAT. Quantification of the GFP or tdTomato shows similar proportions of GFP or tdTomato positive cells at 4 DAT. The proportion of GFP and tdTomato positive cells remained constant up to 6 DAT, but showed a small but significant decrease (~10%) in the Pcdhy<sup>1R1/1R1</sup> mutant cells from 6 to 21 DAT (n=3), consistent with our earlier results using the viral-labeled approach method (**Figure 16C-D**). The reduction in the number of cINs carrying the Pcdhy<sup>1R1/1R1</sup> allele may be explained by the reported reduced levels of Pcdhyc4 in the Pcdhy<sup>1R1/1R1</sup> mice (Garrett et al. 2019). However, we cannot rule out the possibility that the lack of expression of the other 21 Pcdhy isoforms contributed to this reduction.

Together with the above observations using the viral-labeling of MGE-derived cIN and the genetic labeling of mutant mice carrying combinations of PCDHy isoforms deletions (**Figures 14-16**) indicate that cIN survival is regulated primarily by a single PCDHy protein, the c4 isoform.

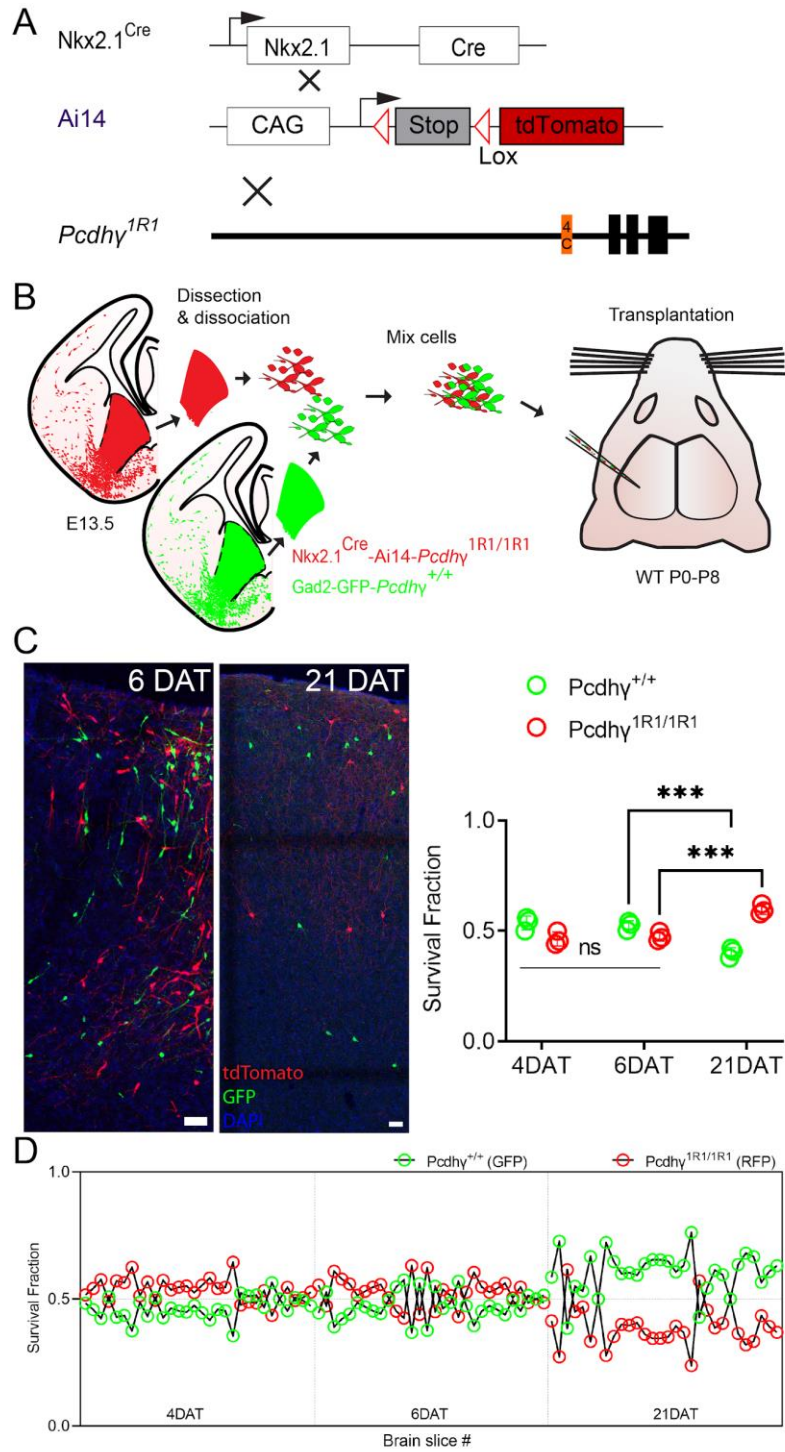


**Figure 16.1** - Elimination of all *Pcdhy*, except for *Pcdhy*c4, results in survival of the majority of cINs.

**Figure 16.1** - (A) Diagram of mouse crosses to obtain  $Pcdhy^{1R1}$  homozygous MGE cells labeled with MGE-specific genetic reporter.  $Nkx2.1^{Cre}$  mice, which carry the conditional Ai14 allele to fluorescently label MGE-derived cINs, were crossed  $Pcdhy^{1R1}$  mice that express  $Pcdhyc4$  but carry a constitute deletion of 21 out of the 22  $Pcdhy$  isoforms. (B) The MGEs of  $Pcdhy^{1R1}$  homozygous mutant embryos were dissected, dissociated, and mixed with equal numbers of MGE cells from control  $Gad67$ -GFP embryos at E13.5. The mixture of GFP+ ( $Pcdhy^{WT}$ ) and tdTomato+ ( $Pcdhy^{1R11/R1}$ ) was grafted into the cortex of WT neonate mice. (C) Left -Confocal images acquired at 6 and 21 DAT of the GFP or tdTomato labeled transplanted cells in the cortex. Right - Quantifications (shown as survival fraction) of GFP or tdTomato-labeled MGE-derived cells at 4, 6, 13, and 21 DAT. Both the GFP and tdTomato-labeled cells undergo PCD between 6 and 21DAT. The proportion of GFP and tdTomato cells was similar between 4 and 6 DAT. A small but significant decrease in the fraction of tdTomato+ cells (red circles) was observed between 6 and 21 DAT. (D) Quantifications of (C) shown for each of the analyzed brain sections (represented by a circle) at 4 and 21 DAT. Scale bar = 50  $\mu$ m, ANOVA, \*\* $p = 0.0001$ ,  $n = 3$  mice per time point and 10 brain sections per mouse from one transplant cohort.

## **PART V - Pcdhyc4 plays a key role in cIN survival**

### **Expression of Pcdhyc4 rescues cINs that lack the entire Pcdhy gene cluster.**

In Part IV of my thesis work, I investigated how different Pcdhy isoforms affect the survival of cINs. The work suggests that Pcdhy C-type isoforms, and particularly Pcdhyc4, play a key role in the regulation of cIN survival. To further test this hypothesis, I cloned lentiviral constructs encoding Pcdhyc4 or Pcdhyc5 and introduced them into cIN precursors cells lacking all Pcdhy. Since cINs lacking the function of all Pcdhy are nearly eliminated when co-transplanted with WT cINs expressing Pcdhy (see **Figure 9A, D and E.**), I reasoned that a rescue effect would be most evident in *Nkx2.1<sup>Cre</sup>-Ai14-Pcdhy<sup>fcon3/fcon3</sup>* cells.

In order to clone the Pcdhy expressing constructs, I used the pLenti-CAG-empty-ires-EGFP, a lentiviral vector that drives the expression of the enhanced green fluorescent protein (EGFP) under the strong CAG promoter. The “ires” sequence was removed to create the control vector expressing GFP (pLenti-CAG-EGFP) (**Figure 17A**). The Pcdhyc4 and Pcdhyc5 coding regions were cloned into the control plasmid, downstream of the CAG promoter and upstream of the EGFP sequence (**Figure 17A-C**). In the pLenti-CAG-Pcdhyc5-EGFP construct, the Pcdhyc5 coding sequence is connected to the GFP sequence via a two amino acid linker and under a single open reading frame. Similarly, in the pLenti-CAG-Pcdhyc4-EGFP construct, the Pcdhyc4 is connected to the GFP coding sequence via a two amino acid linker. Therefore, from either of the above constructs, PCDHYC4 or PCDHYC5 proteins that are fused to GFP can be produced (**Figure 17C**).

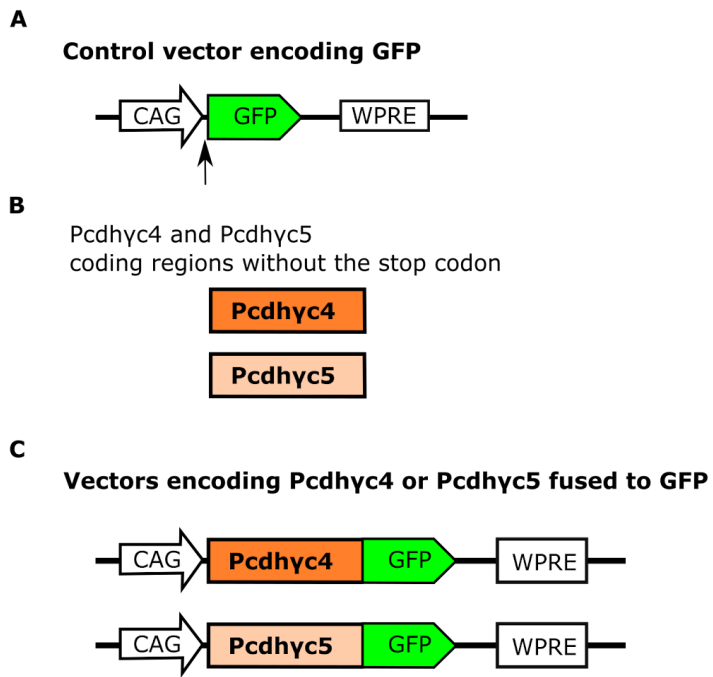


**Figure 17.1** - Lentiviral constructs expressing Pcdhyc4 and Pcdhyc5.

**Figure 17.1** - (A) Diagram of the control lentiviral construct used to label cINs with GFP in **Figures 14.1, 18.1, and 19.1**. Note that the strong CAG promoter drives the expression of GFP. (B) Schematic showing coding regions for *Pcdhyc4* and *Pcdhyc5*. The *Pcdhyc4* and *Pcdhyc5* protein coding region was cloned into the control vector in (A), and positioned downstream of the CAG promoter but upstream of the enhanced GFP coding sequence. (C) Diagrams depicting each of the cloned lentiviral constructs for the expression of *Pcdhyc4* or *Pcdhyc5*. The stop codon was removed from the coding sequence of *Pcdhyc4* or *Pcdhyc5*, but each of the *Pcdhyc4* or *Pcdhyc5* coding region was cloned in-frame with the GFP coding sequence, such that the pLenti-CAG-Pcdhyc4-GFP or the pLenti-CAG-Pcdhyc5-GFP generated a PCDHYC5 or PCDHYC5 protein that is fused to GFP.

The control pLenti-CAG-EGFP, the pLenti-CAG-Pcdhyc4-EGFP and a pLenti-CAG-Pcdhyc5-P2A-GFP (not shown) were validated in vitro for expression and toxicity in cultured neurons. The pLenti-CAG-Pcdhyc5-EGFP was not validated. The MGEs of Nkx2.1Cre-Ai14 embryos at E13.5 were dissociated and cultured with dorsal cortex cells of an equivalent age (**Figure18A**). The cultured cells were infected with lentivirus expressing GFP, Pcdhyc5-P2A-GFP or Pcdhyc4-GFP, fixed at 3, 5, 7, 9, and 11 days after infection and stained against GFP and tdTomato (**Figure18A**). All cells infected with the control virus expressed GFP at all time points, with no apparent dimming in the expression of GFP at the later time points (**Figure 18B**). Cells infected with Pcdhyc5-P2A-GFP expressing virus also expressed GFP but at lower levels compared to the control infected cells. Lower expression levels are likely due to the increased size of the Pcdhy construct and lower viral titer. Similarly, cells infected with the Pcdhyc4-GFP expressing construct expressed GFP at a lower level. Pcdhyc4 fused to GFP could be detected at the cell surface, including the soma, perisomatic regions and processes, and to some extent within the cell body. This is consistent with the normal localization of Pcdhyc4, a cell-surface adhesion protein. Expression of either PCDHYC5-P2A-GFP or PCDHYC4-GFP did not appear to be toxic to the cells as similar proportions of GFP and RFP positive cells were observed across the different time points analyzed (data not shown).

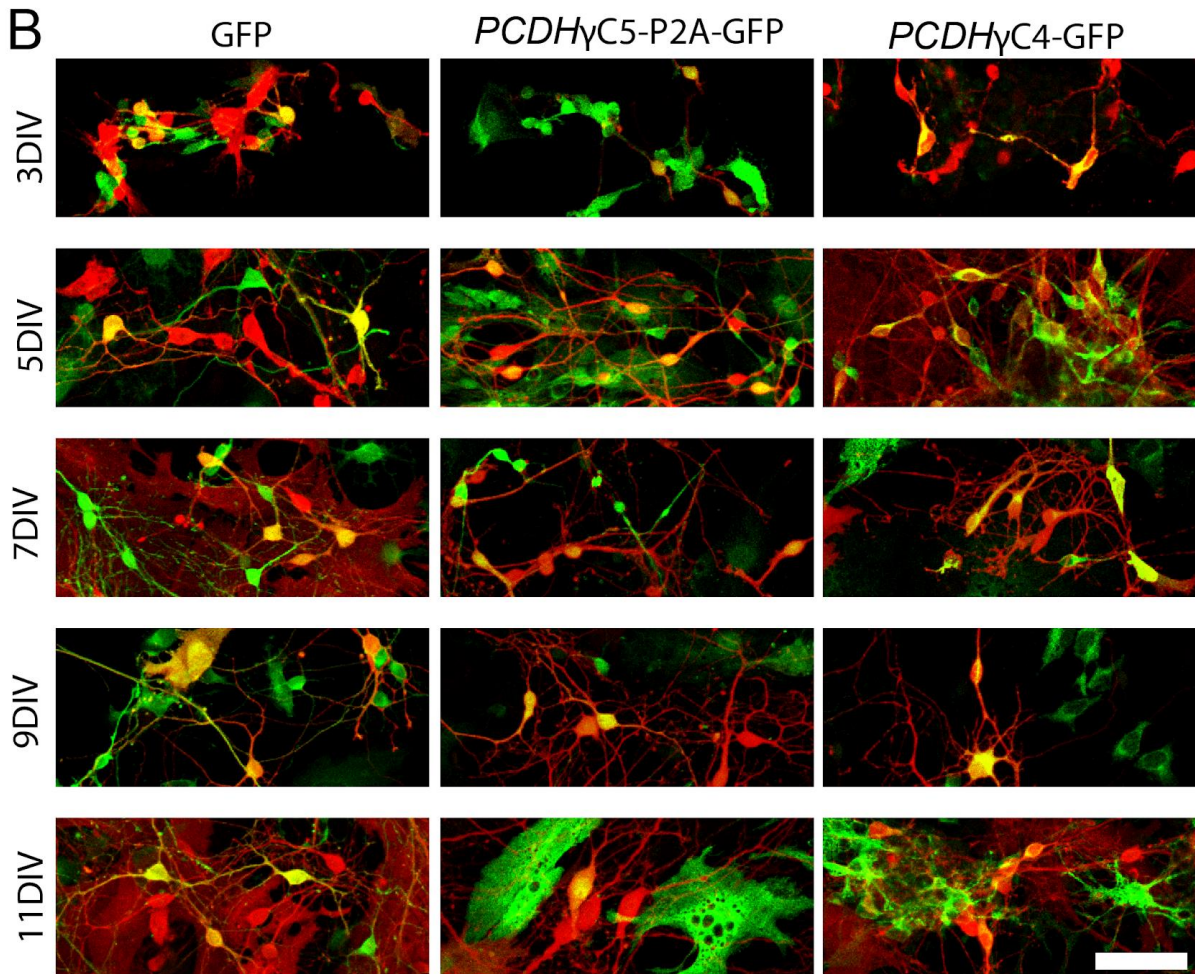
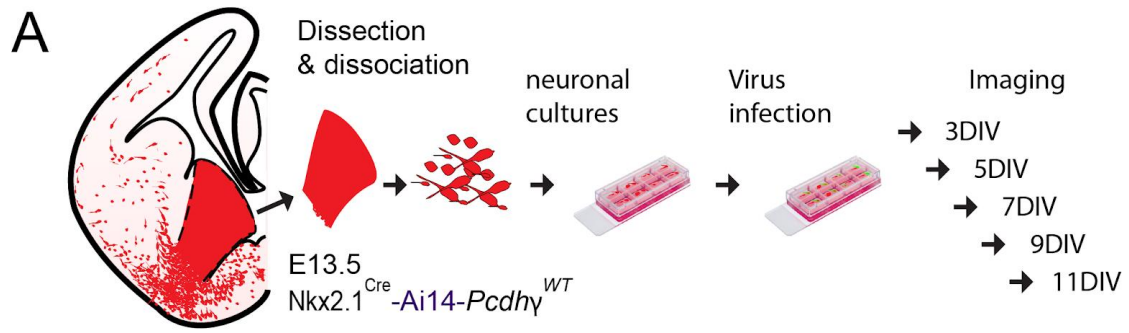


**Figure 18.1** - In vitro validation of lentiviral constructs expressing Pcdhy.



**Figure 18.1** - (A) Schematic representation of the in vitro culture assay, infection, and imaging of cINs expressing GFP, PCDHyC5-P2A or PCDHyC4-GFP. cIN precursors from E13.5 MGE of Nkx2.1 Cre-Ai14 embryos were dissociated, cultured, and infected with lentivirus. The infected cells were identified via expression of tdTomato and GFP and imaged at 3, 5, 7, 9, and 11 days in vitro (DIV). (B) Representative images of the infected cINs at 3DIV, 5DIV, 7DIV, 9DIV, and 11DIV. The cINs are labeled with tdTomato, and the infected cells express GFP. GFP can be readily detected at all time points in the infected cells expressing either GFP, PCDHyC5-P2A, or PCDHyC4-GFP.

We next tested the effect of each of the above viral constructs on the survival of transplanted cINs. Dissociated MGE cells from E13.5 of Nkx2.1 Cre-Ai14-Pcdhy<sup>fcon3/fcon3</sup> embryos were infected in suspension with lentivirus expressing either GFP, Pcdhyc4, or Pcdhyc5 (**Figure19 and Figure20**). Importantly, each construct was tested independently and in separate experiments (explained in more detail below). The cell-virus mixture from each viral construct was pelleted and excess viral particles were washed before transplantation. The infected cells were grafted into the cortex of WT mice. Since each mouse was transplanted with the same mixture of virally infected cells, the effect of expressing one of the above constructs on cINs could be determined by quantifying the number of infected cells to the non-infected cells over time. The infected cells were identified by expression of GFP and tdTomato (yellow cells), while non-infected cells expressed only tdTomato (red cells) and were used as controls. To measure the effect on cIN survival, we quantified the fraction of the infected cells (yellow cells) and non-infected cells (red cells) at 6 and 21 DAT, before and after the period of PCD. We first infected MGE cIN precursor cells carrying WT Pcdhy with lentivirus expressing GFP and transplanted them into the cortex WT mice (**Figure19 A-B**). In this control experiment, we tested whether lentiviral infection or the expression of GFP alone could affect survival. At 6 DAT, the fraction of infected cells was approximately 50% and remained constant between 6 and 21 DAT, suggesting that infection with lentivirus and expression of GFP had no impact on survival (**Figure 19 C-D**).

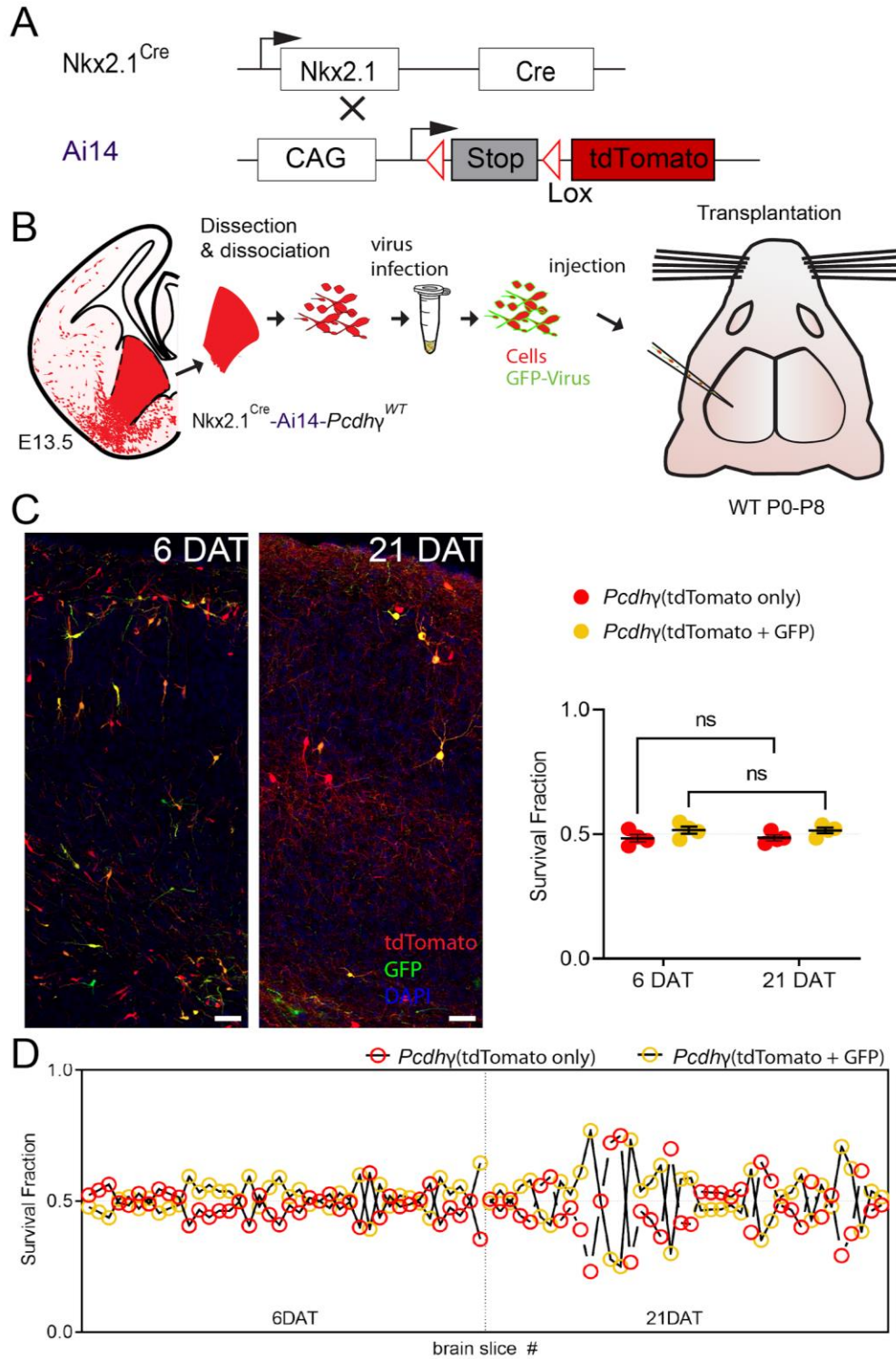


**Figure 19.1** - Infection with lentivirus and expression of GFP does not affect the survival of cINs.

**Figure 19.1 - (A)** Diagram of mouse crosses to obtain  $Pcdhy^{WT}$  MGE cells labeled with MGE-specific genetic reporter. **(B)** Schematic of lentiviral infection and transplantation of MGE cIN precursors. The MGEs of  $Nkx2.1^{Cre}$ -Ai14 embryos that carry  $Pcdhy^{WT}$  were dissected, dissociated, and infected in suspension with lentivirus expressing GFP. The infected cells were grafted into the cortex of WT recipient mice P0-P8. **(C)** Confocal acquired images of the transplanted cINs in the cortex at 6 and 21 DAT. Notice that all transplanted cells are labeled with tdTomato (red), while cells expressing virally-driven GFP are labeled in green. Quantifications of the tdTomato+ only or tdTomato+GFP+ (double labeled, yellow) cells are shown as the fraction of cells from the total tdTomato+ cells at 6 and 21 DAT. **(D)** Quantifications from **(C)** are shown to the right (each dot) at 6 and 21 DAT. Note that the survival fraction is not affected by the viral injection or the expression of GFP. Scale bar = 50  $\mu$ m, ANOVA, ns = not significant, n = 3-4 mice per time point and 10 brain sections per mouse from one transplant cohort.

We next tested whether the expression of Pcdhyc4 effected the survival of cINs lacking the function of the entire Pcdhy gene cluster (using the Pcdhy<sup>fcon3/fcon3</sup> mice). MGE precursor cells from E13.5 Nkx2.1 Cre-Ai14-Pcdhy<sup>fcon3/fcon3</sup> embryos were infected with the Pcdhyc4 expressing lentivirus (**Figure 20 A-B**). As above, the infected cells were identified via GFP expression. At 6 DAT roughly 35% of the tdTomato cells expressed GFP, while the remaining population expressed tdTomato. Importantly, both the GFP positive and GFP negative populations undergo cell death between 6 and 21 DAT. As described in our earlier results, transplanted Pcdhy mutant cINs are nearly eliminated during the period of PCD. However, Pcdhy mutant cINs that expressed the lentiviral-driven Pcdhyc4 isoform were rescued from cell death. Indeed, the fraction of tdTomato cells that also expressed GFP changed from 35% to 70% between 6 and 21 DAT, while the GFP negative population decreased from 65% to 30% during the same period of time (**Figure 20 C-D**). These results indicate that the introduction of Pcdhyc4 to cINs lacking Pcdhy function, is sufficient to prevents mutant cells from undergoing apoptosis during the period of PCD.

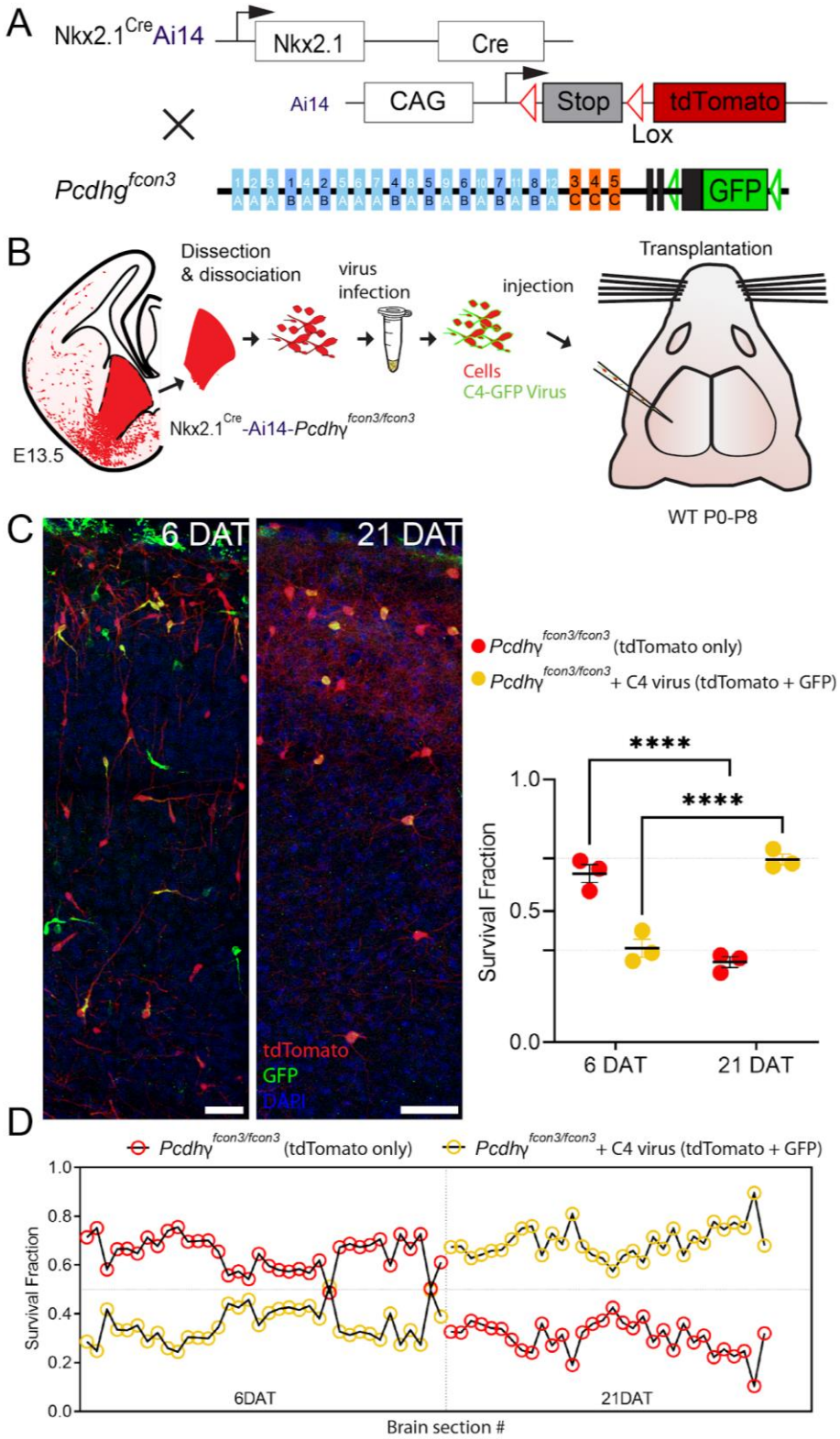


**Figure 20.1** - Lentiviral expression of Pcdhyc4rescues cINs lacking the function of all Pcdhy isoforms.

**Figure 20.1 - (A)** Diagram of mouse crosses to obtain *Pcdhy* mutant MGE cells labeled with MGE-specific genetic reporter. *Nkx2.1<sup>Cre</sup>* that also carries the conditional *Ai14* allele to fluorescently label MGE-derived cINs were crossed to *Pcdhy<sup>fcon3/fcon3</sup>* mice to remove the function of all 22 genes in the *Pcdhy* gene cluster. (B) Schematic of the lentiviral infection and transplantation of MGE cIN precursors. The MGEs of *Nkx2.1<sup>Cre</sup>-Ai14-Pcdhy<sup>fcon3/fcon3</sup>* embryos were dissected, dissociated, and infected in suspension with lentivirus expressing PCDHyC4-GFP. The infected cells were grafted into the cortex of WT recipient mice P0-P8. (C) Confocal acquired images of the transplanted cINs in the cortex at 6 and 21 DAT. Notice the expression of GFP can be found near the cell surface including the cell processes, reflecting the actual location of *Pcdhy* since GFP is fused to PCDHyC4. Quantifications of the tdTomato+ only or tdTomato+GFP+ (yellow cells) cells are shown as the fraction of cells from the total tdTomato+ cells at 6 and 21 DAT. The fraction of the yellow cells increases from 6 to 21DAT, while the fraction of the tdTomato+ but negative for GFP decreases at equivalent time points. (D) Quantifications from (C) are shown by the brain section (each dot) at 6 and 21 DAT. Scale bar = 50  $\mu$ m, ANOVA, \*\*\*\*p = 0.0001 ns, n = 3 mice per time point and 10 brain sections per mouse from one transplant cohort.

The above results, while preliminary, are consistent with Part 4 of my thesis indicating that the Pcdhyc4 isoform encoded in the Pcdhy gene cluster, plays a key role in the regulation of PCD among cINs. Key questions remain unanswered, including whether cell death can be prevented in all cINs that express the Pcdhyc4 isoforms, and if not, what fraction of those cells that express Pcdhyc4 survive, and why a fraction of Pcdhyc4-expressing cINs still undergo apoptosis. It will be interesting to test whether the expression of Pcdhyc4 in cINs carrying a full set of Pcdhy affects their survival. It will also be of interest to study if lentiviral-mediated expression Pcdhyc3 or Pcdhyc5 isoforms modify cIN survival during the normal period of cell death.

## **Part VI - Future directions**

The above experiments suggest that of the 58 clustered Pcdh isoforms, expression of Pcdhyc4 is key to survival and Pcdhyc4 alone might entirely account for the regulation of cIN survival in the cortex. Nevertheless, several questions remain unanswered. For example, it would be necessary to determine if expression of Pcdhyc4 can rescue cINs that undergo normal PCD. This would be answered by forcing the expression Pcdhyc4 in WT cINs that carry a full set of Pcdhy (including Pcdhyc4). Preliminary experiments suggest that this is not the case (data not shown). However, this observation requires additional experiments in which either all or a high proportion of the transplanted cINs are forced to express the Pcdhyc4 isoform. It would also be interesting to determine if all cINs expressing the Pcdhyc4 survive? This could be primarily determined by quantifying all the transplanted cells in the cortex of host mice at a baseline time point and then after the period of cell death. It would also be interesting to force the expression of Pcdhyc3 or Pcdhyc5 and determine whether these affect cIN survival. The above data from straight mutant mice already suggest that Pcdhyc3 and Pcdhyc5 do not play a significant role for the survival of cINs. Lastly, given recent observations () that correlated activity is key to the



regulation of PCD, it would be interesting to determine whether cINs that lack *Pcdhyc4* have aberrant or de-correlated activity among themselves or with host pyramidal cells.

## CHAPTER 4: DISCUSSION

The findings above indicate that *Pcdhy* genes play a critical role in regulating cIN survival during the endogenous period of cIN PCD in the neocortex. Specifically, the *Pcdhyc3*, *Pcdhyc4* and *Pcdhyc5* isoforms within the *Pcdhy* gene cluster are essential for the selection of those cINs that survive past the period of PCD and become part of the adult cortical circuit. *Pcdhy* genes do not affect the production or migration of cINs and appear to be dispensable for the survival of cINs beyond the normal period of cell death. Together with previous work in the spinal cord and retina, these results suggest that *Pcdhyc3*, *Pcdhyc4*, and *Pcdhyc5* isoforms are key to the regulation of PCD in the CNS. In contrast, deletions of the *Pcdhy $\alpha$*  and *Pcdhy $\beta$*  gene clusters did not alter cell death during this period.

Our initial approach involved the removal of *Pcdhy* function from all GABAergic cINs via the *Gad2-Cre-Ai14-Pcdhy<sup>fcon3/fcon3</sup>* mouse line. These mice displayed a dramatic reduction of cINs of all subtypes, including a significant decrease in the number of VIP+ cells, which are derived from the CGE. A similar observation has been recently reported by Carriere et al (2020). In these mice, *Pcdhy* function was also removed from most other GABAergic neurons throughout the nervous system, as well as from a small fraction of astrocytes (Taniguchi et al. 2011). Since the removal of *Pcdhy* function in all *Gad2-Cre* expressing cells could affect the survival of cINs indirectly, we used *Nkx2.1-Cre-Ai14* mice to more specifically remove *Pcdhy* function from MGE/POA derived cINs. As in the *Gad2-Cre-Ai14-Pcdhy<sup>fcon3/fcon3</sup>* mice, a sharp decrease in cINs was observed, but now only MGE-derived PV, SST, and a subpopulation of RLN cIN were affected. Importantly, *Nkx2.1* is also expressed in the POA, and a small fraction

of cINs in the neocortex (~10%) are derived from Nkx2.1 expressing cells in the POA. We were not able to distinguish cINs derived from the POA. However, the number of VIP cells was not affected in these mice, suggesting that the reduction in the number of MGE-derived cINs does not affect the survival of those derived from the CGE. Consistent with recent observations (Carriere et al., 2020), the number of un-recombined PV and SST (PV+/tdTomato- and SST+/tdTomato-) cINs in *Nkx2.1-Cre-Ai14-Pcdhy<sup>fon3/fon3</sup>* mice, increased compared to WT mice (**Supplement Figure 7**). These cells, which are likely derived from the dorsal Nkx6.2+/Nkx2.1-MGE domain (Hu, Vogt, Sandberg, et al. 2017; Fogarty et al. 2007; Sousa et al. 2009; Hu, Vogt, Lindtner, et al. 2017) may increase their survival in compensation for the loss of Nkx2.1-derived cINs lacking Pcdh- $\gamma$  function. However, we cannot exclude that the increased number of un-recombined PV and SST cells in *Nkx2.1-Cre-Ai14-Pcdhy<sup>fon3/fon3</sup>* mice resulted from increased production or migration of cIN derived from regions of low, or no, expression of Nkx2.1. Further experiments will be required to understand the origin of these un-recombined PV+/Ai14- and SST+/Ai14- cINs and whether the observed increase in their numbers is due to compensatory survival mechanisms.

Consistent with the results above, Pcdhy loss of function in SST-expressing cINs via the *Sst-Cre-Ai14-Pcdhy<sup>fon3/fon3</sup>* mouse line resulted in a similar reduction of SST+ cINs in the cortex of the mutant mice. However, removal of Pcdhy function from PV+ cINs using the PV-Cre line did not lead to changes in the number of PV+ cINs in the cortex. Importantly, the PV-Cre transgene becomes activated specifically in PV cINs starting at around ~P16. This is a time after the period of PCD for cINs. These findings therefore suggested that Pcdhy function is not required for cIN survival after the period of normal cell death.

PCDHys are not required for the normal production of young Nkx2.1 derived cINs in the MGE, or for their migration into the mouse cerebral cortex. The extent of proliferation as

measured by quantification of cells expressing the mitotic marker Phospho-histone H3 (pHH3) in the ventricular and subventricular zone in the MGE was essentially the same in mice that carried WT or lacked the function of *Pcdhy*, and the number of migrating MGE derived cINs into the cortex was also indistinguishable between control and mutant mice. We did not directly address whether interference with *Pcdha* and *Pcdhβ* isoforms affected the birth and migration of cINs, but we infer these two clusters also have no, or minimal effects on cIN production and migration because the final numbers of MGE derived cINs were not significantly affected after the loss of either *Pcdha* or *Pcdhβ*. However, the aggregate loss of *Pcdhs* in multiple clusters might in principle be required for phenotypes to be manifested (Ing-Esteves et al. 2018). Our findings, therefore, cannot exclude the possibility that simultaneous elimination of the *Pcdha* and *Pcdhβ* isoforms might have an effect on cIN production, migration, or apoptosis. However, the elimination of *Pcdhy* gene cluster alone increases cell death among cINs, establishing that removal of a limited number of isoforms is sufficient to reveal the cell-death phenotype, and suggesting *Pcdh* diversity might not be essential for cIN survival.

Importantly, the increase in PCD observed following the loss of *Pcdhy* function was fully rescued when the pre-apoptotic gene *Bax* was also eliminated. Not only was the increased *Pcdhy* dependent cell death eliminated in *Bax* mutant animals, but these animals had a ~ 40% increase in the numbers of surviving cINs compared to WT controls, identical to the effect of the *Bax* mutation in wild type animals. This observation is consistent with previous observation showing that ~40% of cINs are eliminated during the period of PCD (Southwell et al. 2012; Wong et al. 2018). Moreover, the increased death of cINs after removal of *Pcdhy* function occurs precisely during the normal period of PCD. These observations indicate that *Pcdhy* isoforms are required specifically to regulate cIN numbers during the critical window of PCD for cIN. This is consistent with previous studies in the retina and spinal cord that have pointed to *Pcdhys* as key mediators of PCD (Lefebvre et al. 2008; W. V. Chen et al. 2012).

Together, the observations above suggested that while the *Pcdha* and *Pcdhβ* genes do not regulate cIN survival, those isoforms encoded in the *Pcdhy* gene cluster are key to the survival of cINs during the normal period of cell death. Whether all 22 *Pcdhy* isoforms are required for cIN survival and how *Pcdhy* regulate survival remained largely unanswered. Previous studies have indicated that the C-type isoforms in the *Pcdhy* gene cluster (*Pcdhyc3*, *Pcdhyc4* and *Pcdhyc5*) are required for the postnatal survival of mice and regulate survival of cells in the retina and spinal cord ((Lefebvre et al. 2008; W. V. Chen et al. 2012)). A more recent study suggests that the *Pcdhyc4* isoform is the key mediator in the regulation of neuronal cell death in the spinal cord (Garrett et al. 2019). How the *Pcdhyc4* isoform in the *Pcdhy* gene cluster mediates cell death remains a fundamental question for future research. Interestingly, the *Pcdhyc4* isoform appears to be unique in that it is the only *Pcdh* isoform that does not bind in a homophilic manner (Garrett et al. 2019) and it is not translocated to the membrane unless it is associated with other PCDHs (Thu et al. 2014). The mechanism by which the *Pcdhyc4* isoform regulates cell-cell interactions among young cINs, leading to the adjustment of local circuit neuron numbers, remains unclear.

Heterochronic transplantation of cIN precursors from the MGE into the cortex of WT mice allowed us to test for the survival of *Pcdhy* WT and mutant cINs simultaneously and in the same microenvironment. The co-transplantation assay also allowed us test whether *Pcdhy* regulate survival in a non-cell autonomous manner, whether cINs of the same age that carry different sets of *Pcdhy* interact to regulate survival, and whether survival of *Pcdhy* mutant cells occurred in accordance with the age of the cells. As previously reported (Southwell et al. 2012), cINs die following their own time-course of maturation. Consistent with this, the transplanted cells (extracted from the MGE at E13.5) died with a delay of 7-13 days compared to the endogenous host cINs when transplanted into P1-P7 WT mice. In these co-transplants, cINs labeled with GFP or tdTomato but carrying WT *Pcdhy* undergo an approximately 40% reduction

in density between 6 and 21DAT, reflecting the timing and proportion of normal cell death endogenous cINs undergo in WT mice. This is consistent with the notion that the cellular age of cINs determines the timing of PCD (Southwell et al. 2012) and that cIN cell death is largely regulated at the cell or population level, a process that is largely independent of trophic support (Southwell et al. 2012). Interestingly, the role of Pcdhy function was clearly evident in the co-transplants of WT and mutant cINs in that the survival of the mutant cells was extremely low compared to that of WT cells. The dramatic decrease in the survival of Pcdhy-mutant cINs occurs precisely during the period of PCD for the transplanted population. The survival of transplanted WT cINs as well as that of Pcdhy mutant cINs was constant over a wide range of densities, as evidenced by the fact that while the density of transplanted cINs decreases as a function of the distance from the transplantation site, the proportion of dying cells of both phenotypes was similar at different distances from the site of transplantation. These observations argue against local trophic support availability such as neurotrophins or activity; support mediated by neurotrophins, or local activity could be expected to exist in excess within areas of low density of transplanted cells.

Interestingly, the survival of WT cINs was also reduced when co-transplanted with Pcdhy deficient MGE-cells although this difference did not reach statistical significance with the numbers of cases studied\*. If true, these findings would be consistent with the notion that cell-cell interactions among young cIN after their migration, is an essential step in determining their final numbers. However, we cannot exclude that the increase in the elimination of WT cells may result from a non-specific (e.g., toxic) effect of the increased cell death among Pcdhy mutant cells. If the latter occurs, the process is specific to the population of Nkx2.1<sup>+</sup> MGE-derived cINs because there was no effect on cell death of WT CGE-derived VIP cINs (**Figure 3E**, **Supplement Figure 4**) or on non-Nkx2.1-derived SST or PV cells (**Supplement Figure 7**).

Interactions mediated by Pcdhys, may directly or indirectly regulate survival of cINs of the same age and origin.

In the spinal cord, only a small subset of Pcdhy isoforms appears to be required for neuronal survival. Based on our qPCR data on cINs (see part 1), we hypothesized that cINs in the neocortex might also not require all Pcdhy isoforms for survival. Particularly, the Pcdhyc5 showed a pronounced increase in expression during the peak of cell death, suggesting Pcdhyc5 might be key to cIN survival. However, unlike the spinal cord where cell death takes place prenatally (Wang et al. 2002; Prasad et al. 2008), cIN PCD occurs mostly postnatally. Since mice lacking Pcdhy C-type isoforms (*Pcdhyc3*, *Pcdhyc4*, and *Pcdhyc5*) die soon after birth, we could not study the extent of cIN cell death directly in these mutant animals. We, therefore, took advantage of transplantation and co-transplantation to compare the survival of cells lacking these three isoforms. The loss of cINs lacking *Pcdhyc3*, *c4* & *c5* isoforms was identical to that when the function of the entire Pcdhy cluster is lost. This further suggests that these Pcdhy C-isoforms (*Pcdhyc3*, *Pcdhyc4*, and *Pcdhyc5*) are the key to the regulation of cIN death. The co-transplantation assay, implemented in the present study, provides strong evidence that Pcdhys in cIN are key to their selection by PCD. PCDHy proteins could be mediating initial cell-cell interactions that are important for the survival of cINs. Two non-exclusive possibilities exist: (1) PCDHy mediate cell-cell interaction among young cIN to adjust their population size, and levels of inhibition, according to the numbers that reached the cortex; (2) PCDHy mediate interactions with locally produced excitatory pyramidal neurons to adjust final numbers according to local levels of excitation. For the latter, MGE derived cINs could interact with pyramidal neurons via PCDHyC-type isoforms. However, alternative # 2 is unlikely to explain how PCDHys adjust cIN numbers since the conditional removal of Pcdhy in pyramidal cells show no effect on the survival of cINs (Carriere et al., 2020). However, we cannot exclude that initial connectivity with excitatory pyramidal neurons may indeed require the proper

expression of *Pcdhy* among cINs through non-homophilic interactions. Interestingly, both in the cortex and the spinal cord, two different neural structures, PCDHyC-type isoforms appear to be the key regulators of survival of local circuit cINs.

A recent study has shown that coordinated activity of synaptically connected assemblies of cINs is essential for their survival (Duan et al. 2020). Pyramidal cells receive information from these assemblies via GABA<sub>A</sub>γ<sub>2</sub>-signaling and through the de-synchronization of their activity regulate cIN program cell death. *Pcdhys* could be important in bringing together cINs of a common origin and at similar stages of maturations for the formation of initial cINs functional assemblies. The formation of these assemblies of synchronously firing cINs and the subsequent selection by pyramidal driven de-synchronization could explain both cell/population autonomous (Southwell et al. 2012), and non-cell autonomous (Wong et al. 2018) mechanism of cIN PCD. Interestingly, the *Pcdh* isoform γC5 binds to the GABA<sub>A</sub>γ subunit of the GABA receptor (Li et al. 2012), but the role of γC5-GABA<sub>A</sub>γ interaction on neuronal survival remains unknown. The transplantation assay provides a powerful tool to further study how *Pcdhys*, cell-cell interactions, and cellular age contribute to cIN selection. It will be interesting, for example, to determine if heterochronically transplanted cINs form functional assemblies and whether these assemblies are affected by the removal of different *Pcdhys*.

We started addressing some of the above possibilities by transplanting cINs lacking various combinations of the *Pcdhy* genes. We took advantage of a series of mutant animals lacking specific subsets of *Pcdhy* isoforms that recently became available. Using the CRISPR/Cas9 genome editing tool, a group from the Jackson Laboratory and University of Iowa developed a large cohort of new mouse lines with mutations or deletions in one or several clustered *Pchd* genes (Garrett et al. 2019). We obtained three newly generated mouse lines: the *Pcdhy*<sup>1R1</sup>, *Pcdhy*<sup>C4KO</sup> and *Pcdhy*<sup>3R2</sup> (**Figure 14A**). *Pcdhy*<sup>1R1</sup> mice express *Pcdhyc4* but have a

constitutive deletion of all the remaining Pcdhy isoforms (21 out of 22 isoforms). Conversely, the Pcdhy<sup>C4KO</sup> mice have a constitutive deletion of Pcdhyc4 but express the remaining 21 Pcdhy isoforms. The Pcdhy<sup>3R2</sup> mice express Pcdhyc3 and Pcdhyc4 but lacks Pcdhyc5 and all of the Pcdhy A- and Pcdhy B- type isoforms, with the exception of B8. Importantly these new mouse lines harbor constitutive deletions of Pcdhy isoforms and some of the deletions such as that of Pcdhyc4 result in neonatal lethality, transplantation was necessary not only to bypass the neonate lethality but also isolate the MGE cINs from potential non-cell autonomous effects that may result by interaction from other cells with Pcdhy deletions. I initially used GFP virally labeled cells lacking Pcdhyc4, Pcdhyc5, or solely expressing Pcdhyc4 to test how different *Pcdhy* C-type isoforms affected cIN cell death. This preliminary data suggest that Pcdhyc5 is not required for cIN survival. Similarly, cINs lacking all Pcdhy isoforms, except for Pcdhyc4, show a small significant decrease in survival that could attributed to decreased levels of Pcdhyc4 in these mutant cells, suggesting that most Pcdhy isoforms, including Pcdhyc3 and Pcdhyc5 dot not play a significant role in the regulation of cell death. Surprisingly, however, the sole loss of Pcdhyc4 leads to a pronounced decrease in the survival of transplanted MGE derived cINs in cortex. I extended these initial observations by crossing the above *Pcdhy*<sup>1R1</sup> and *Pcdhy*<sup>C4KO</sup> mice to reporter mice to specifically label MGE derived cINs, and used transplantation to compare the survival of cINs. These experiments also indicate that the lack of Pcdhyc4 is sufficient to induce a significant increase in cIN cell death. Consistent with the above experiments, most transplanted MGE-cells that solely expressed Pcdhyc4 survived normally. These observations validated the above findings, further indicating that Pcdhy diversity is not required for survival and suggesting Pcdhyc4 is a key regulation or cell death in cINs in the cortex.

To complement the findings above, I force the expression of Pcdhyc4 in cINs lacking the entire set of Pcdhy genes. Since most cINs that lack function of all Pcdhy isoforms are eliminated when transplanted in the cortex of WT mice, we reasoned that the expression of



Pcdhyc4 in these mutant cells would prevent them from undergoing cell death. Indeed, expression of Pcdhyc4, resulted in increased survival of the mutant cells when compared to cells that did not express Pcdhyc4. Together, our findings indicate that a single Pcdhy isoform, Pcdhyc4, may be solely responsible for the regulation of cIN cell death in the cortex.

Nevertheless, several key questions remain for future research including how Pcdhyc4 regulates survival of cIN, what types of cell-cell interactions is Pcdhyc4 mediating, how expression of Pcdhyc4 affects survival of cINs that do not express Pcdhyc4. Other important questions include whether all cINs that express Pcdhyc4 survive, and how the expression of Pcdhyc4 relates to the correlated neuronal activity found during the peak of cIN cell death.

Together this work along with previous work from the Alvarez-Buylla laboratory suggest that the final number of cIN in the cerebral cortex is determined at least in part through a cell or population intrinsic mechanism that could involve cell-cell interactions. Furthermore, others have shown that the perturbation of activity in ENs or cIN at the peak of PCD (P7-P9) results in increased or decreased numbers of cINs (Wong et al. 2018; Duan et al. 2020; Wong et al. 2022), suggesting that PCD is in part regulated through activity-dependent mechanisms. It remains undetermined what role, if any, Pcdhyc4 plays in the regulation of activity during the peak of PCD. Given the key role Pcdhyc4 plays in the survival of cIN and the fact that Pcdhyc4 is a cell-adhesion molecule that is involved in strictly homophilic cell-cell recognition (Thu et al. 2014), initial cell-cell interactions within the cIN population could be mediated through Pcdhyc4. In this regard, it would be interesting to determine whether network activity is perturbed (decreased or increased) in cINs lacking Pcdhyc4. In addition, loss of vesicular GABA release from cINs leads to their increased participation in network activity and concomitantly to increased cIN survival (Duan et al. 2020). Hence it would also be interesting to remove the function of vesicular GABA release and of Pcdhy in cINs and determine their survival during PCD. Lastly, it would be interesting to determine the expression of C-type Pcdhy isoforms in

individual cells in the cortex during the period of PCD to determine the expression dynamics of these isoforms during PCD.

During the evolution of multiple mammalian species including humans, the cerebral cortex has greatly expanded in size and in the number of excitatory and inhibitory neurons it contains. Interestingly, the proportion of cINs to ENs is also increased in the human cerebral cortex, compared to that of mice (Fang et al. 2022). The significance of increased cIN numbers (in some brain regions proportionally to ENs) is unclear, but it could be argued that more evolved brains demand increased numbers of cINs for fine tuning cerebral circuitries with higher order functions. Regardless, appropriate numbers of cINs are considered essential in the modulation of cortical function. The embryonic origin of cINs, far from the cerebral cortex, raises basic questions about how their numbers are ultimately controlled in development and during evolution. Coordinated increased production of cINs in the MGE and CGE is an essential step to satisfy the demand of an expanded cortex (Hansen et al. 2013). In addition, MGE and CGE derived cINs in larger brains require increased and protracted production of young cINs that in turn require longer and more protracted migratory periods (Paredes et al. 2022; Paredes et al. 2016). Moreover, recent work from the Nowakowski Laboratory (UCSF) suggests that RGCs in the developing human cerebral cortex could represent a new origin for cINs and provide an additional source of cINs for the expanded human cerebral cortex (Delgado et al. 2022). Independent of their origin, the young cINs arrive at the cortex in excess of their final number. This is ultimately adjusted by a period of PCD once the young cINs have migrated into the cortical plate and have begun to make synaptic connections in mice. Here we have identified the *Pcdhyc4* isoforms in the *Pcdhy* gene cluster as an essential molecular component in the regulation of PCD among cINs in mice. The fact that a cell surface adhesion protein plays a key role in this regulation suggests that interactions with other cells, possibly other cINs of the same age (Southwell et al. 2012), or possibly excitatory pyramidal cells (Wong et al. 2018), is part of

the logic to adjust the final number of these essential GABAergic cells for proper brain function. An understanding of the cell-cell interactions that use Pcdhyc4 to regulate cIN cell death should give fundamental insights into how the cerebral cortex forms and evolves. Lastly, it would be interesting to determine if the principles of cIN cell adjustment to proportionally match the number ENs apply to the human cerebral cortex, and in particular whether Pcdhyc4 plays a role in regulating the adjustment of neuron numbers. Recent work already suggests that the *PCDHGC4* gene plays a critical role in normal brain development as mutations in this gene are associated with neurodevelopmental syndrome with progressive microcephaly, seizures, and joint anomalies (Iqbal et al. 2021).

## APPENDIX I - METHODS

### *Animals.*

All protocols and procedures followed the University of California, San Francisco (UCSF) guidelines and were approved by the UCSF Institutional Animal Care Committee. Whenever possible, the number of males and females was matched for each experimental condition. The following breeders were purchased from the Jackson Laboratory: Ai6, Ai14, Gad1-GFP, Gad2-ires-Cre (*Gad2<sup>Cre</sup>*), *BAC-Nkx2.1-Cre* (*Nkx2.1<sup>Cre</sup>*), SST-ires-Cre (*SST<sup>Cre</sup>*), PV-ires-Cre-pA (*PV<sup>Cre</sup>*), R26-CreERT2, *Vgat<sup>fl/fl</sup>*, *Bax<sup>-/-</sup>*, *Bax<sup>fl/fl</sup>* and WT C57BL/6J. *Pcdh-γ-fcon3* (FCON3) mice were obtained from Joshua Sanes at Harvard University. *Pcdhα<sup>acon/acon</sup>*, *Pcdhβ<sup>del/del</sup>*, *Pcdhy<sup>tako/tako</sup>*, and *Pcdhy<sup>tcko/tcko</sup>* mice were obtained from Tom Maniatis at Columbia University. *Pcdhy<sup>1R1/1R1</sup>* (1R1), *Pcdhy<sup>C4KO/C4KO</sup>* (C4KO) and *Pcdhy<sup>3R2/3R2</sup>* (3R2) mice obtained from Joshua Weiner at the University of Iowa.

*Pcdhy* loss of function mice were obtained by crossing *Pcdhy<sup>fcon3/fcon3</sup>* mice with *Gad2<sup>Cre</sup>-Ai14-Pcdhy<sup>fcon3/+</sup>* mice, *Nkx2.1<sup>Cre</sup>-Ai14-Pcdhy<sup>fcon3/+</sup>*, *PV<sup>Cre</sup>-Ai14-Pcdhy<sup>fcon3/+</sup>* or *Sst<sup>Cre</sup>-Ai14-Pcdhy<sup>fcon3/+</sup>*. *Pcdhya1-A3* isoform knockout mice were obtained from crosses of *Pcdhy<sup>tako/tako</sup>* mice to

*Nkx2.1<sup>Cre</sup>-Ai14-Pcdhy<sup>tako/+</sup>* mice. *Pcdha* loss function mice were obtained by crossing *Pcdha<sup>acon/acon</sup>* mice with *Nkx2.1<sup>Cre</sup>-Ai14-Pcdha<sup>acon/+</sup>* mice. *Pcdhβ* loss function mice were obtained by crossing *Pcdhβ<sup>del/del</sup>* mice with *Nkx2.1<sup>Cre</sup>-Ai14-Pcdhβ<sup>del/+</sup>* mice. *Pcdhy<sup>1R1/1R1</sup>* (1R1) and *Pcdhy<sup>C4KO/C4KO</sup>* (C4KO) mice were crossed to *Nkx2.1<sup>Cre</sup>-Ai14* breeders to label the *Nkx2.1* progenitor cells.

For cell transplantation experiments, GFP-expressing tissue in embryos was produced by crossing WT C57BL/6J to heterozygous mice expressing green fluorescent protein-expressing (GFP) driven by *Gad1* or by crossing *Nkx2.1<sup>Cre</sup>;Ai6* breeder to WT C57BL/6J mice. In general, tdTomato-expressing tissue in embryos was obtained by crossing the various mutant alleles to the *Nkx2.1<sup>Cre</sup>-Ai14* line. *Pcdh-γ<sup>fcon3/fcon3</sup>* mutant embryonic tissue was obtained from embryos produced by crossing *Nkx2.1<sup>Cre</sup>-Ai14-Pcdhy<sup>fcon3/+</sup>* mice with *Pcdhy<sup>fcon3/fcon3</sup>* mice. *Pcdhy<sup>tako/tako</sup>* mutant embryonic tissue was obtained from embryos produced by crossing *Nkx2.1<sup>Cre</sup>-Ai14-Pcdhy<sup>tako/+</sup>* mice to homozygote *Pcdhy<sup>tako/tako</sup>* mice. *Pcdhy<sup>tcko/tcko</sup>* mutant tissue was obtained from embryos produced by crossing *Nkx2.1<sup>Cre</sup>-Ai14-Pcdhy<sup>tcko/+</sup>* mice to heterozygote *Pcdhy<sup>tcko/+</sup>* mice. *Pcdhy<sup>1R1/1R1</sup>* mutant tissue was obtained from embryos produced by crossing *Nkx2.1<sup>Cre</sup>-Ai14-Pcdhy<sup>1R1/1R1</sup>* breeders. *Pcdhy<sup>C4KO/C4KO</sup>* mutant tissue was obtained from embryos produced by crossing *Nkx2.1<sup>Cre</sup>-Ai14-Pcdhy<sup>C4KO/+</sup>* breeders. *Gad1-GFP*, *Nkx2.1<sup>Cre</sup>*, *Ai6* and *Nkx2.1<sup>Cre</sup>-Ai14* offspring were genotyped under an epifluorescence microscope (Leica), and PCR genotyping was used to screen for *Pcdha<sup>acon/acon</sup>*, *Pcdhy<sup>fcon3/fcon3</sup>*, *Pcdhy<sup>tako/tako</sup>*, *Pcdhy<sup>tcko/tcko</sup>*, *Pcdhy<sup>1R1/1R1</sup>*, *Pcdhy<sup>C4KO/C4KO</sup>* and *Pcdhy<sup>C4KO/C4KO</sup>* alleles in tdTomato positive embryos or reporter negative embryos. All cell transplantation experiments were performed using wild type C57Bl/6 recipient mice P0 to P8. All mice were housed under identical conditions.

*Plasmids:* The following plasmids were used in this work: pLenti-CAG-ires-EGFP, pLenti-CAG-EGFP, pLenti-CAG-P2A-EGFP, pLenti-CAG-Pcdyc5-P2A-EGFP, pLenti-CAG-Pcdyc4-

EGFP. pLenti-CAG-dEctoPcdyc4-EGFP, pLenti-CAG-dCytoPcdyc4-EGFP, pLenti-CAG-Pcdyc3-EGFP, and pLenti-CAG-Pcdyc5-EGFP.

*Timed pregnant mice:* In experiments requiring timed pregnant mice, the day when the sperm plug was observed was considered E0.5. Males were paired with two or more female mice the night before and checked for plugs early the following day. MGE cells for transplantation were acquired from the MGEs of E12.5 to E15.5 embryos.

*Transplantation:*

Generally ~200,000 cells are obtained from each MGE of an E13.5 embryo. A successful transplantation experiment required cells obtained from a minimum of two embryos. Generally, experiments that involve the co-transplantation of cells that carry different fluorophores and different *Pcdhy* alleles, three embryos of each genotype and fluorophore provided the minimum number of cells for one experiment of two timepoints. We utilized at least four embryos of each genotype for experiments with two or more timepoints or in which a larger number of cells were injected. Many of the *Pcdhy* mutations were neonatal lethal and produced a cell death phenotype. For these *Pcdhy* alleles, starting with a large number of cells ensures enough cells will survive for downstream analysis. Therefore, in these scenarios at least 6 embryos of each genotype were utilized. For co-transplantation experiments, the concentration of cells of each genotype or fluorophore was determined using a hemocytometer; the GFP or tdTomato labeled cells were then mixed in the desired proportions. To prepare the cells for transplantation, the cells suspension was concentrated by spinning in a table centrifuge for five minutes at 800g(rcf). The supernatant was removed, and the resulting pellet was resuspended and mixed well in a final volume of 1-6 $\mu$ L of Leibovitz L-15 medium (L15). This concentrated cell suspension was loaded into beveled glass micropipettes (~60-100  $\mu$ m diameter, Wiretrol 5  $\mu$ L, Drummond Scientific Company) prefilled with mineral oil and mounted on a microinjector. The viability and

concentration of the cells in the glass micropipette was determined by using 100nl of cells diluted 200X in 10µL of L15 medium and 10µL trypan blue. The number of cells was then determined using a hemocytometer. The desired number of cells was injected into neonate mice P0 to P8. Importantly, if the cell pellet is too diluted (e.g. less than 1 million cells in 6ul) the concentration of cells within the micropipette might differ. For example, cells might aggregate and form clusters of various densities within the micropipette. Additionally, oftentimes the cells closer to the micropitter tip show a higher density. Lastly, mice that are injected first could have more cells than mice injected last due to decreased cell viability over the entire injection period. In order to increase reproducibility and consistency between mice, it is best to start with a highly concentrated cell pellet (e.g. 6 million cells). Prior to the injection of cells, the recipient mice (C57Bl/6) were anesthetized by hypothermia (~3-5 minutes) and positioned in a clay head mold that stabilizes the skull (Merkle, Mirzadeh, and Alvarez-Buylla 2007). Micropipettes were positioned at an angle of 0 or 30 degrees from vertical in a stereotactic injection apparatus. After the injections were completed, the transplanted mice were placed on a warm surface to recover from hypothermia. The mice were then labeled with a clipped toe and returned to their mothers until they were perfused or weaned (P21). Transplantation of cells involving the *Pcdhy*<sup>tako/tako</sup>, *Pcdhy*<sup>tcko/tcko</sup> and *Pcdhy*<sup>C4KO/C4KO</sup> alleles was performed utilizing cells from MGEs that had been cryopreserved.

*Tissue dissection and cell dissociation.* For quantitative PCR analysis, tdTomato and GFP cells were dissociated from the P30 mouse cortex as described in (Saxena et al. 2012). Briefly, the brains were dissected and collected in ice-cold L15 medium, and sectioned at 1mm interval using a stainless steel brain matrix (Tedpella). The cortex was dissected using a surgical scaffold under a dissecting microscope and subsequently cut into chunks of ~ 1mm. The cortex tissue was subsequently dissociated as described in (Saxena et al. 2012). GFP or tdTomato

positive cells were FACS-sorted at the UCSF FACS-sorting facility using a 100 $\mu$ m nozzle and collected for downstream analysis. Cells for transplantation obtained from MGEs dissected from E13.5 embryos as previously described (Southwell et al. 2012). Dissections were performed in ice-cold L15 medium. The MGEs were kept in L15 medium at 4°C. After collecting and genotyping the embryos, MGE with the same genotype were pulled together and mechanically dissociated using a P1000 pipette into a single cell suspension by repeated pipetting in L15 medium containing DNase I (180 $\mu$ g/ml). For experiments involving cells from cryopreserved MGEs, cryovials of interest were removed from -80°C, thawed at 37°C for 5 minutes and the content of each tube was resuspended in a 15mL falcon tube containing room temperature L15 medium. The MGE tissue naturally sinks to the bottom of the tube. The L15/DMSO supernatant was removed and replaced with fresh room temperature L15 medium to wash residual DMSO. The MGE tissue was next transferred to a 1.5mL Eppendorf tube with a P1000 pipette, and resuspended in 500 $\mu$ l of L15 medium containing DNase. The MGEs were dissociated as above.

*Cryopreservation of MGE in toto.* Dissected MGEs from each embryo were collected in 500  $\mu$ L L15 medium and kept on ice until cryopreserved. MGEs were resuspended in 10% DMSO in L15 medium and cryopreserved as previously described (Rodríguez-Martínez, Martínez-Losa, and Alvarez-Dolado 2017). Vials were cooled to -80°C at a rate of -1°C/minute in a Nalgene™ Mr. Frosty Freezing Container and transferred the next day to liquid nitrogen for long term storage. Importantly, tissue for genotyping was collected from each embryo and labeled with a code name matching the codename of each cryotube used for the cryopreservation.

*Injection coordinates in neonates.* The mouse head grows continuously in neonates, requiring injection coordinates to be determined at every other day intervals (e.g. P2, P4, P6, P8). The initial injections were done using lambda as a zero reference point. Lambda can be readily

identified in P0 to P3 pups. However, after P4, the skin color increases, and hair growth can be observed by P8. Towards the end of my PhD, I changed the zero-reference point to increase the reproducibility between mice for the target coordinates in each experiment. The eye corner can be a more reliable starting point if one can consistently identify the same landmark in both eyes and from mouse to mouse. The eye corner can then be used at the zero reference point for the antero-posterior coordinate. The midline was used at the zero reference point for the medial-lateral coordinates. In order to establish the midline zero point, the distance between the two eye corners was measured and divided by half. When determined appropriately, the zero reference point taken at the midline is very reproducible and useful for very targeted injection such as the injection of cells into the wedge region of the lateral ventricles. The eye corner zero reference point used for the antero-posterior coordinate is less reproducible since the length of the brain can vary from mouse to mouse or if the head is not positioned in the same way from mouse to mouse. For instance, if the head is tilted slightly downwards or upwards, it can affect the actual target coordinates.

*Cell counting.* For cell density counts in the visual and barrel cortex, cells were directly counted using a Zeiss Axiover-200 inverted microscope (Zeiss) and an AxioCam MRm camera (Zeiss), using Stereo Investigator (MBF). tdTomato+ cells were counted at every sixth section (i.e., 300  $\mu$ m apart) along the rostral-caudal axis of visual and barrel cortex. Total cell counts were extrapolated by Stereo Investigator. Cell densities were determined by dividing the total number of tdTomato+ cells by the volume of the region of interest in the visual or barrel cortex, identified by landmarks, for each animal. To measure PV, SST, RLN and VIP-positive cell densities in the visual cortex, cells were counted from confocal-acquired images, also at every sixth section. Cleaved caspase-3-positive (CC3+) cells were counted from images acquired on a Zeiss Axiover-200 inverted microscope (Zeiss) and a AxioCam MRm camera (Zeiss) using NeuroLucida (MBF). Cleaved caspase-3-positive (CC3+) cells were counted in the cortex at



every sixth section along the rostral-caudal axis for each animal. CC3+ cells in the olfactory bulb, hippocampus, and piriform cortex were not counted. For layer distribution analysis of tdTomato+ cells and for analysis of tdTomato negative (non-recombined) PV and SST positive cells, cells were counted from confocal-acquired images and using Fiji software cell counter function.

For cell counts from transplanted animals, GFP positive cells and tdTomato-positive cells were counted in all layers of the neocortex. Cells that did not display neuronal morphology were excluded from all quantifications. The vast majority of cells transplanted from the E13.5 MGE exhibited neuronal morphologies in the recipient brain. Images of transplanted cells were acquired on a SP8 confocal, or a Zeiss Axiovert-200 inverted microscope (Zeiss) with an AxioCam MRm camera (Zeiss) with a 10X magnification. Only the region of the cortex containing GFP, or tdTomato-positive cells was imaged. GFP and tdTomato-positive cells were counted using NeuroLucida (MBF). For quantification of the absolute numbers of transplanted cells in the neocortex of host recipients, cells from every second coronal section were counted. The raw cell counts were then multiplied by the inverse of the section sampling frequency (2) to obtain an estimate of total cell number (Figure ##). In some experiments the absolute number of grafted cells varied between transplants; hence we report findings as the fraction of GFP+ or tdTomato+ cells that survive from the total transplant-derived cell number in that animal (GFP + tdTomato-positive). We determined for these experiments the number of transplant-derived cells of the different genotypes before and, in different animals, after the period of cell death. For some experiments, we also quantified the number of transplant-derived cells during the period of cell death. In data presented as the fraction of transplant-derived cells, GFP positive and tdTomato-positive cells were counted from coronal sections along the rostral-caudal axis in at least 10 sections per animal, and only in sections containing more than 10 cells. To determine the fraction of GFP+ or tdTomato+ cells in each experiment, the number of GFP or tdTomato-positive cells was divided by the total cell number (GFP + tdTomato) in that section.

This fraction does not reflect the absolute number of cells, but their relative contribution to the overall population of transplant-derived cells at different DAT. For experiments involving the expression of lentiviral driven GFP or *Pcdhy* in transplanted cINs, at least 10 images per mouse were acquired in the confocal at 20X magnification. In these experiments, survival was determined by comparing the fraction of infected (GFP+) cells to the fraction of noninfected cells (GFP-) from the total number of transplanted cells (tdTomato+ ) in each brain section.

*Viral vector subcloning.* All lentiviral plasmids were cloned from the backbone construct pLenti-CAG-ires-EGFP (addgene plasmid #122953). A kozak sequence was added at the start of the coding region for all genes cloned. Plasmids were cloned using the Gibson Cloning Kit (NEB). The pLenti-CAG-EGFP construct was cloned by removing the ires sequence in between the BstXI and BamHI restriction sites from the backbone construct. The pLenti-CAG-P2A-EGFP plasmid was cloned by removing the ires-GFP sequence in between the restriction sites BamHI and BstXI and replacing it with a P2A-GFP gBlock sequence. The P2A sequence contains a GSG linker in the 5' and is flanked by AgeI restriction sites. An EcoRI restriction enzyme site was added adjacent to the 5' AgeI site for cloning purposes. To clone the pLenti-CAG-Pcdhyc5-P2A-EGFP plasmid, the pLenti-CAG-P2A-EGFP backbone was linearized at the EcoRI restriction site, and a PCR amplified mouse *Pcdhyc5* coding sequence lacking the stop codon was cloned upstream of and in-frame with the P2A-GFP sequence. This construct was used to express two separate proteins PCDHYC5 and GFP from one single transcript. To clone the pLenti-CAG-Pcdhyc4-EGFP (fusion construct), the pLenti-CAG-ires-EGFP plasmid was digested with BamHI and BstXI to remove the ires sequence. A PCR generated *Pcdhyc4* coding sequence lacking the stop codon and containing a two amino acid (Ser, Arg) linker was cloned upstream of and in-frame with the GFP coding sequence. This construct was used to express Pcdhyc4 fused to GFP. The pLenti-CAG-dEctoPcdhyc4-EGFP was cloned from the pLenti-CAG-Pcdgc4-EGFP backbone by digesting out the sequence in between AgeI and

XcmI sites and replacing it with the gBlock gC4deltaecto. This construct was used to express Pcdhyc4 lacking the extracellular domain, but retaining the transmembrane and cytoplasmic domain which is fused to GFP. The pLenti-CAG-dCytoPcdgc4-EGFP was cloned from the pLenti-CAG-Pcdgc4-EGFP backbone by digesting out the sequence in between BsmBI and BsrGI and replacing it with gBlock gC4deltacyto. This construct was used to express Pcdhyc4 lacking the cytoplasmic domain, but retaining the extracellular and transmembrane domain which is fused to GFP. The pLenti-CAG-Pcdyc5-EGFP construct (Pcdgc5 fused to GFP sequence) was cloned from the pLenti-CAG-dEctoPcdgc4-EGFP plasmid backbone by digesting with BamHI and AgeI to remove a 594pb sequence and replacing it with the IDT gene block mPcdhyc5 Ex1-2gblock. This construct was used to express PCDHYC5 fused to GFP. Similarly, the pLenti-CAG-Pcdhyc3-EGFP construct was cloned from the pLenti-CAG-dEctoPcdyc4-EGFP plasmid backbone by digesting with BamHI and AgeI to remove a 594pb sequence and replacing it with the IDT gene block mPcdhyc3 Ex1-2gblock. This construct was used to express PCDHYC3 fused to GFP.

*Gene blocks.* The following gBlocks used in the above cloning were ordered from IDT: P2A-GFP, gC4deltaecto, gC4deltacyto, and mPcdhyc5 Ex1-2gblock as double stranded DNA sequences.

*Viruses.* The AAV-syn-GCaMP7f virus was purchased from addgene. All lentivirus used in this study were made in the laboratory or from the UCSF lentiviral core. Briefly viruses were produced in Lenti-X 293T cells (TakaraBio). Cells were grown to  $\geq 90\%$  confluency in maintenance media (DMEM/F-12, 15 mM HEPES, 2.5 mM GlutaMAX, 1% Pen/Strep, 10% FBS) in 15cm plates coated with Poly-D-lysine (Sigma-Aldrich P7405) at final concentration of 0.1mg per mL. Once cells reached the desired confluency, media was changed to DMEM/F-12 + 2% FBS. Cells were transfected using *TransIT*<sup>®</sup>-293 Transfection Reagent (Mirusbio) and

Opti-MEM (Thermofisher). After 6 to 12 hours post-transfection, the media was changed to lentivirus production media (DMEM/F-12, 15 mM HEPES, 2.5 mM GlutaMAX, 1% Pen/Strep, 2% FBS) and 60 $\mu$ L of ViralBoost Reagent was added (ALSTEM) per 15cm plate. Virus supernatant was collected 48 hour post-transfection, filtered through a 45 $\mu$ m filter, and precipitated with Lentivirus Precipitation Solution (ALSTEM) overnight following manufacturer's instructions. The viral pellet from two 15cm plates was concentrated in a final volume of 100 $\mu$ l for Pcdh constructs and 200 $\mu$ l for the control construct.

*Viral infection of MGE precursor cells.* Following the dissociation of the MGEs, cells were concentrated by spinning in a table centrifuge for five minutes at 800g. Cells were subsequently infected with 2-5  $\mu$ L Adeno-associated virus (AVV) in a 50 $\mu$ L cell suspension in L15 or with 20-150 $\mu$ L of lentivirus to an equal cell suspension volume. For lentiviral infection, the cell pellet was subsequently resuspended in an equal volume of Lentivirus and L15 medium. The cell-virus mix was incubated at 22-32C at 1000rpm (190rcf) for 3hours, while mixing every 30 minutes. For AVV virus infection, the cell pellet was subsequently resuspended in 50 $\mu$ l of L15 medium and 2-5 $\mu$ l of virus and incubated at room temperature for 2 hours while mixing every 30 minutes.

*Immunostaining.* P21 and older mice were fixed by transcardiac perfusion with 10mL of ice-cold PBS followed by 10mL of 4% formaldehyde/PBS solution; 5ml of either solution was used for P15 and younger mice. Brains were incubated overnight (12-24hrs) for postfixation at 4°C, then rinsed with PBS and cryoprotected in 30% sucrose/PBS solution for 48 hours at 4°C. Unless otherwise stated, immunohistochemistry was performed on 50  $\mu$ m floating sections in Tris Buffered Saline (TBS) solution containing 10% normal donkey serum, 0.5% Triton X-100 for all procedures on postnatal mice. Immunohistochemistry from embryonic tissue was performed on 20  $\mu$ m cryostat sections. All washing steps were done in 0.1% Triton X-100 TBS for all

procedures. Sections were incubated overnight at 4°C with selected antibodies, followed by incubation at 4°C overnight in donkey secondary antibodies (Jackson ImmunoResearch Laboratories). Brain sections that had been transplanted with lentivirus infected MGE cells were incubated two nights in primary antibodies and overnight with secondary antibodies to enhance the viral expressed reporter GFP. For cell counting and *post hoc* examination of marker expression, sections were stained using chicken anti-GFP (1:2500, Aves Labs, GFP-1020, RRID:AB\_10000240), rabbit anti-RFP (Rockland), rat anti-tdTomato (Kerafast), mouse anti-Reelin (1:500 MBL, D223–3, RRID:AB\_843523), rabbit anti-PV (1:1000, Swant PV27, RRID:AB\_2631173), mouse anti-parvalbumin (anti-PV, 1:500, Sigma-Aldrich, P3088, RRID:AB\_477329), rat anti-somatostatin (SST, 1:500, Santa Cruz Biotechnology, sc-7819, RRID:AB\_2302603), anti-cleaved caspase 3 (1:400, Cell Signaling Technology, 9661L, RRID:AB\_2341188), rabbit anti-phosphohistone-H3 (1:500; EDM millipore, RRID:AB\_310177), rabbit anti-Nkx2.1 (1:250, Life Technologies, RRID:AB\_793532).

*Neuron Morphology analysis.* Recipient brains were co-transplanted with Gad1-GFP (WT *Pcdhy*) and *Nkx2.1<sup>Cre</sup>-Aj14-Pcdhy<sup>fcon3/fcon3</sup>* (mutant *Pcdhy*) MGE cIN precursors. Transplanted cells were identified in sections (50 µm) stained for GFP and tdTomato and analyzed at 6, 8, 10 and 12 days after transplantation (DAT). Neuron morphology was reconstructed from confocal image (20X objective-4X zoom) stacks taken at 1 µm intervals, using Neurolucida software (MBF). Sections with a relatively low density of GFP+ (WT) and TdTomato+ (Mutant) transplant-derived neurons (in order to clearly image individual cells) were selected and (145.31µm<sup>2</sup>) fields tiled to cover all the visible processes. All GFP+ (WT) and TdTomato+ (Mutant) positive neurons in these tiles were reconstructed. Reconstructions of WT or mutant cells at 36 days post transplantation were carried out from confocal image (63X) stacks taken at 0.5 µm intervals in brain sections (200 µm) stained against tdTomato and PV or SST. Neuron morphometric analysis was done using Neurolucida Explorer.

*RT-PCR.* Total RNA was prepared from dissected cortex using Trizol (Invitrogen) and reverse-transcribed by Quantiscript Reverse Transcriptase (Qiagen), using a mix of oligo-dT and random primers, according to the manufacturer's protocol.

*Slice electrophysiology.* As in (Larimer et al. 2016, 2017; Priya et al. 2019), host animals were anesthetized and decapitated at 8, 9, 10, 11, or 12 days after transplant. The brain was removed into ice-cold dissection buffer containing (in mM): 234 sucrose, 2.5 KCl, 10 MgSO<sub>4</sub>, 1.25 NaH<sub>2</sub>PO<sub>4</sub>, 24 NaHCO<sub>3</sub>, 11 dextrose, 0.5 CaCl<sub>2</sub>, bubbled with 95% O<sub>2</sub> / 5% CO<sub>2</sub> to a pH of 7.4. Coronal slices of visual cortex (200 μm thick) were cut via vibratome (Precisionary Instruments) and transferred to artificial cerebrospinal fluid (ACSF) containing (in mM): 124 NaCl, 3 KCl, 2 MgSO<sub>4</sub>, 1.23 NaH<sub>2</sub>PO<sub>4</sub>, 26 NaHCO<sub>3</sub>, 10 dextrose, 2 CaCl<sub>2</sub> (bubbled with 95% O<sub>2</sub> / 5% CO<sub>2</sub>), incubated at 33°C for 30 min, then stored at room temperature. Fluorescently identified transplant-derived MGE-lineage cINs (tdTomato+ ; *Pcdh-γ<sup>fc3/fc3</sup>* or GFP; WT) were viewed using IR-DIC video microscopy. Whole-cell current-clamp recordings were made with a Multiclamp 700B (Molecular Devices) using an internal solution that contained (in mM): 140 K-gluconate, 2 MgCl<sub>2</sub>, 10 HEPES, 0.2 EGTA, 4 MgATP, 0.3 NaGTP, 10 phosphocreatine (pH 7.3, 290 mosm). Data were low-pass filtered at 2.6 kHz and digitized at 10 kHz by a 16 bit analog-to-digital converter (National Instruments). Data acquisition and analysis were done with custom software written in Matlab (<https://www.mathworks.com/matlabcentral/fileexchange/21903-mphys>). A Mann-Whitney (nonparametric) test, followed by multiple comparisons correction using the Benjamini-Hochberg stepdown method for control of false discovery rate (0.05 familywise) was used for the determination of statistical significance for all comparisons of physiological properties.

*Statistical Analysis.* The person carrying quantifications was blinded to the genotype, except for data shown in **Supplement Figure 3**, and **Supplement Figure 6 and 7**. With the exception of

slice electrophysiology data, all results were plotted and tested for statistical significance using Prism 8. All samples were tested for normality using the Shapiro-Wilk normality test. Unpaired comparisons were analyzed using the two-tailed unpaired Student's *t* test for normally distributed, and Mann-Whitney test for not normally distributed samples. For multiple comparisons analysis of one variable, either a one-way ANOVA with post hoc Tukey's test was used to compare the mean of each column with the mean of every other column, or a Dunnett test was used to compare the mean of each column to the mean of the control group for normally distributed samples. For samples with non-Gaussian distributions, a nonparametric Kruskal-Wallis test was performed followed by a post-hoc Dunn's test. Two-way ANOVA with post hoc Sidak's test was used for multiple comparisons with more than one variable. Outliers were identified using ROUT method with alpha set to 0.05.

## Reference list

- Agmon, Ariel, Greg Hollrigel, and Diane K. O'Dowd. 1996. "Functional GABAergic Synaptic Connection in Neonatal Mouse Barrel Cortex." *The Journal of Neuroscience: The Official Journal of the Society for Neuroscience* 16 (15): 4684.
- Alcántara, S., J. Frisén, J. A. del Río, E. Soriano, M. Barbacid, and I. Silos-Santiago. 1997. "TrkB Signaling Is Required for Postnatal Survival of CNS Neurons and Protects Hippocampal and Motor Neurons from Axotomy-Induced Cell Death." *The Journal of Neuroscience: The Official Journal of the Society for Neuroscience* 17 (10): 3623–33.
- Alifragis, Pavlos, Anastasia Liapi, and John G. Parnavelas. 2004. "Lhx6 Regulates the Migration of Cortical Interneurons from the Ventral Telencephalon but Does Not Specify Their GABA Phenotype." *The Journal of Neuroscience: The Official Journal of the Society for Neuroscience* 24 (24): 5643–48.
- Allene, Cattani, Ackman, and Bonifazi. n.d. "Sequential Generation of Two Distinct Synapse-Driven Network Patterns in Developing Neocortex." *Journal of Atomic and Molecular Physics*. <https://www.jneurosci.org/content/28/48/12851.short>.
- Alzu'bi, A., S. Lindsay, J. Kerwin, S. J. Looi, F. Khalil, and G. J. Clowry. 2017. "Distinct Cortical and Sub-Cortical Neurogenic Domains for GABAergic Interneuron Precursor Transcription Factors NKX2.1, OLIG2 and COUP-TFII in Early Fetal Human Telencephalon." *Brain Structure & Function* 222 (5). <https://doi.org/10.1007/s00429-016-1343-5>.
- Anastasiades, Paul G., and Simon J. B. Butt. 2011. "Decoding the Transcriptional Basis for GABAergic Interneuron Diversity in the Mouse Neocortex." *The European Journal of Neuroscience* 34 (10): 1542–52.
- Anderson, S. 1999. "Differential Origins of Neocortical Projection and Local Circuit Neurons: Role of Dlx Genes in Neocortical Interneuronogenesis." *Cerebral Cortex*. <https://doi.org/10.1093/cercor/9.6.646>.
- Anderson, S. A., D. D. Eisenstat, L. Shi, and J. L. Rubenstein. 1997. "Interneuron Migration from



- Basal Forebrain to Neocortex: Dependence on Dlx Genes." *Science* 278 (5337): 474–76.
- Baquet, Z. C., J. A. Gorski, and K. R. Jones. 2004. "Early Striatal Dendrite Deficits Followed by Neuron Loss with Advanced Age in the Absence of Anterograde Cortical Brain-Derived Neurotrophic Factor." *The Journal of Neuroscience: The Official Journal of the Society for Neuroscience* 24 (17). <https://doi.org/10.1523/JNEUROSCI.3920-03.2004>.
- Batista-Brito, Renata, and Gord Fishell. 2009. "The Developmental Integration of Cortical Interneurons into a Functional Network." *Current Topics in Developmental Biology* 87: 81.
- Ben-Ari, Y., E. Cherubini, R. Corradetti, and J. L. Gaiarsa. 1989. "Giant Synaptic Potentials in Immature Rat CA3 Hippocampal Neurons." *The Journal of Physiology* 416 (1): 303–25.
- Ben-Ari, Yehezkel, Ilgam Khalilov, Alfonso Represa, and Henri Gozlan. 2004. "Interneurons Set the Tune of Developing Networks." *Trends in Neurosciences* 27 (7): 422–27.
- Blanquie, Oriane, Werner Kilb, Anne Sinning, and Heiko J. Luhmann. 2017. "Homeostatic Interplay between Electrical Activity and Neuronal Apoptosis in the Developing Neocortex." *Neuroscience* 358 (September): 190–200.
- Borrell, Víctor, and Magdalena Götz. 2014. "Role of Radial Glial Cells in Cerebral Cortex Folding." *Current Opinion in Neurobiology* 27 (August): 39–46.
- Butt, S. J., M. Fuccillo, S. Nery, S. Noctor, A. Kriegstein, J. G. Corbin, and G. Fishell. 2005. "The Temporal and Spatial Origins of Cortical Interneurons Predict Their Physiological Subtype." *Neuron* 48 (4). <https://doi.org/10.1016/j.neuron.2005.09.034>.
- Cai, Jun, Qiang Zhu, Kang Zheng, Hong Li, Yingchuan Qi, Qilin Cao, and Mengsheng Qiu. 2010. "Co-Localization of Nkx6.2 and Nkx2.2 Homeodomain Proteins in Differentiated Myelinating Oligodendrocytes." *Glia* 58 (4): 458–68.
- Canzio, Daniele, Chiamaka L. Nwakeze, Adan Horta, Sandy M. Rajkumar, Eliot L. Coffey, Erin E. Duffy, Rachel Duffié, et al. 2019. "Antisense lncRNA Transcription Mediates DNA Demethylation to Drive Stochastic Protocadherin  $\alpha$  Promoter Choice." *Cell* 177 (3): 639–53.e15.

- Chao, Hsiao-Tuan, Hongmei Chen, Rodney C. Samaco, Mingshan Xue, Maria Chahrour, Jong Yoo, Jeffrey L. Neul, et al. 2010. "Dysfunction in GABA Signalling Mediates Autism-like Stereotypies and Rett Syndrome Phenotypes." *Nature* 468 (7321): 263–69.
- Chen, Vivian S., James P. Morrison, Myra F. Southwell, Julie F. Foley, Brad Bolon, and Susan A. Elmore. 2017. "Histology Atlas of the Developing Prenatal and Postnatal Mouse Central Nervous System, with Emphasis on Prenatal Days E7.5 to E18.5." *Toxicologic Pathology* 45 (6): 705–44.
- Chen, Weisheng V., Francisco J. Alvarez, Julie L. Lefebvre, Brad Friedman, Chiamaka Nwakeze, Eric Geiman, Courtney Smith, et al. 2012. "FUNCTIONAL SIGNIFICANCE OF ISOFORM DIVERSIFICATION IN THE PROTOCADHERIN GAMMA GENE CLUSTER." *Neuron* 75 (3): 402.
- Chen, Weisheng V., Chiamaka L. Nwakeze, Christine A. Denny, Sean O'Keefe, Michael A. Rieger, George Mountoufaris, Amy Kirner, et al. 2017. "Pcdhac2 Is Required for Axonal Tiling and Assembly of Serotonergic Circuitries in Mice." *Science* 356 (6336): 406–11.
- Connors, B. W., L. S. Benardo, and D. A. Prince. 1983. "Coupling between Neurons of the Developing Rat Neocortex." *The Journal of Neuroscience: The Official Journal of the Society for Neuroscience* 3 (4): 773–82.
- Corbin, Joshua G., Michael Rutlin, Nicholas Gaiano, and Gord Fishell. 2003. "Combinatorial Function of the Homeodomain Proteins Nkx2.1 and Gsh2 in Ventral Telencephalic Patterning." *Development* 130 (20): 4895–4906.
- Deacon, T. W., P. Pakzaban, and O. Isacson. 1994. "The Lateral Ganglionic Eminence Is the Origin of Cells Committed to Striatal Phenotypes: Neural Transplantation and Developmental Evidence." *Brain Research* 668 (1-2): 211–19.
- Delgado, R. N., D. E. Allen, M. G. Keefe, Mancía Leon Wr, R. S. Ziffra, E. E. Crouch, A. Alvarez-Buylla, and T. J. Nowakowski. 2022. "Individual Human Cortical Progenitors Can Produce Excitatory and Inhibitory Neurons." *Nature* 601 (7893).

<https://doi.org/10.1038/s41586-021-04230-7>.

- Delgado, R. N., B. Mansky, S. H. Ahanger, C. Lu, R. E. Andersen, Y. Dou, A. Alvarez-Buylla, and D. A. Lim. 2020. "Maintenance of Neural Stem Cell Positional Identity by Mixed-Lineage Leukemia 1." *Science* 368 (6486). <https://doi.org/10.1126/science.aba5960>.
- Dietmar Schreiner, Joshua A. Weiner. 2010. "Combinatorial Homophilic Interaction between  $\gamma$ -Protocadherin Multimers Greatly Expands the Molecular Diversity of Cell Adhesion." *Proceedings of the National Academy of Sciences of the United States of America* 107 (33): 14893.
- Duan, Zhe Ran S., Alicia Che, Philip Chu, Laura Modol, Yannick Bollmann, Rachel Babij, Robert N. Fetcho, et al. 2020. "GABAergic Restriction of Network Dynamics Regulates Interneuron Survival in the Developing Cortex." *Neuron* 105 (1): 75–92.e5.
- Dupont, Erwan, Ileana L. Hanganu, Werner Kilb, Silke Hirsch, and Heiko J. Luhmann. 2006. "Rapid Developmental Switch in the Mechanisms Driving Early Cortical Columnar Networks." *Nature* 439 (7072): 79–83.
- Egorov, Alexei V., and Andreas Draguhn. 2013. "Development of Coherent Neuronal Activity Patterns in Mammalian Cortical Networks: Common Principles and Local Heterogeneity." *Mechanisms of Development* 130 (6-8): 412–23.
- Enomoto, H., R. O. Heuckeroth, J. P. Golden, E. M. Johnson, and J. Milbrandt. 2000. "Development of Cranial Parasympathetic Ganglia Requires Sequential Actions of GDNF and Neurturin." *Development* 127 (22): 4877–89.
- Esumi, Shigeyuki, Naoki Kakazu, Yusuke Taguchi, Teruyoshi Hirayama, Ayako Sasaki, Takahiro Hirabayashi, Tsuyoshi Koide, Takashi Kitsukawa, Shun Hamada, and Takeshi Yagi. 2005. "Monoallelic yet Combinatorial Expression of Variable Exons of the Protocadherin- $\alpha$  Gene Cluster in Single Neurons." *Nature Genetics* 37 (2): 171–76.
- Fang, Rongxin, Chenglong Xia, Jennie L. Close, Meng Zhang, Jiang He, Zhengkai Huang, Aaron R. Halpern, et al. 2022. "Conservation and Divergence of Cortical Cell Organization

- in Human and Mouse Revealed by MERFISH.” *Science* 377 (6601): 56–62.
- Fietz, Simone A., Iva Kelava, Johannes Vogt, Michaela Wilsch-Bräuninger, Denise Stenzel, Jennifer L. Fish, Denis Corbeil, et al. 2010. “OSVZ Progenitors of Human and Ferret Neocortex Are Epithelial-like and Expand by Integrin Signaling.” *Nature Neuroscience* 13 (6): 690–99.
- Flames, Nuria, Ramón Pla, Diego M. Gelman, John L. R. Rubenstein, Luis Puelles, and Oscar Marín. 2007. “Delineation of Multiple Subpallial Progenitor Domains by the Combinatorial Expression of Transcriptional Codes.” *The Journal of Neuroscience: The Official Journal of the Society for Neuroscience* 27 (36): 9682–95.
- Fogarty, Matthew, Matthew Grist, Diego Gelman, Oscar Marín, Vassilis Pachnis, and Nicoletta Kessaris. 2007. “Spatial Genetic Patterning of the Embryonic Neuroepithelium Generates GABAergic Interneuron Diversity in the Adult Cortex.” *The Journal of Neuroscience: The Official Journal of the Society for Neuroscience* 27 (41): 10935–46.
- Frank, Marcus, Matthias Ebert, Weisong Shan, Greg R. Phillips, Kirsten Arndt, David R. Colman, and Rolf Kemler. 2005. “Differential Expression of Individual Gamma-Protocadherins during Mouse Brain Development.” *Molecular and Cellular Neurosciences* 29 (4): 603–16.
- Garrett, Andrew M., Peter J. Bosch, David M. Steffen, Leah C. Fuller, Charles G. Marcucci, Alexis A. Koch, Preeti Bais, Joshua A. Weiner, and Robert W. Burgess. 2019. “CRISPR/Cas9 Interrogation of the Mouse Pcdhg Gene Cluster Reveals a Crucial Isoform-Specific Role for Pcdhgc4.” *PLoS Genetics* 15 (12): e1008554.
- Gelman, Diego M., Oscar Marín, and John L. R. Rubenstein. 2012. “The Generation of Cortical Interneurons.” *Jasper’s Basic Mechanisms of the Epilepsies*.  
<https://doi.org/10.1093/med/9780199746545.003.0061>.
- Gelman, Diego M., Francisco J. Martini, Sandrina Nóbrega-Pereira, Alessandra Pierani, Nicoletta Kessaris, and Oscar Marín. 2009. “The Embryonic Preoptic Area Is a Novel

- Source of Cortical GABAergic Interneurons." *The Journal of Neuroscience: The Official Journal of the Society for Neuroscience* 29 (29): 9380–89.
- Hamburger, V., and J. W. Yip. 1984. "Reduction of Experimentally Induced Neuronal Death in Spinal Ganglia of the Chick Embryo by Nerve Growth Factor." *The Journal of Neuroscience: The Official Journal of the Society for Neuroscience* 4 (3): 767–74.
- Hansen, David V., Jan H. Lui, Pierre Flandin, Kazuaki Yoshikawa, John L. Rubenstein, Arturo Alvarez-Buylla, and Arnold R. Kriegstein. 2013. "Non-Epithelial Stem Cells and Cortical Interneuron Production in the Human Ganglionic Eminences." *Nature Neuroscience* 16 (11): 1576–87.
- Hansen, David V., Jan H. Lui, Philip R. L. Parker, and Arnold R. Kriegstein. 2010. "Neurogenic Radial Glia in the Outer Subventricular Zone of Human Neocortex." *Nature* 464 (7288): 554–61.
- Hasegawa, Sonoko, Makiko Kumagai, Mitsue Hagihara, Hiroshi Nishimaru, Keizo Hirano, Ryosuke Kaneko, Atsushi Okayama, et al. 2016. "Distinct and Cooperative Functions for the Protocadherin- $\alpha$ , - $\beta$  and - $\gamma$  Clusters in Neuronal Survival and Axon Targeting." *Frontiers in Molecular Neuroscience*. <https://doi.org/10.3389/fnmol.2016.00155>.
- Haubensak, Wulf, Alessio Attardo, Winfried Denk, and Wieland B. Huttner. 2004. "Neurons Arise in the Basal Neuroepithelium of the Early Mammalian Telencephalon: A Major Site of Neurogenesis." *Proceedings of the National Academy of Sciences of the United States of America* 101 (9): 3196–3201.
- Heiko J Luhmann, Rustem Khazipov. 2018. "Neuronal Activity Patterns in the Developing Barrel Cortex." *Neuroscience* 368 (January): 256–67.
- Hendry, S. H., H. D. Schwark, E. G. Jones, and J. Yan. 1987. "Numbers and Proportions of GABA-Immunoreactive Neurons in Different Areas of Monkey Cerebral Cortex." *The Journal of Neuroscience: The Official Journal of the Society for Neuroscience* 7 (5): 1503–19.

- Hernández-Miranda, Luis R., John G. Parnavelas, and Francesca Chiara. 2010. "Molecules and Mechanisms Involved in the Generation and Migration of Cortical Interneurons." *ASN Neuro* 2 (2): e00031.
- Hippenmeyer, Simon, Eline Vrieseling, Markus Sigrist, Thomas Portmann, Celia Laengle, David R. Ladle, and Silvia Arber. 2005. "A Developmental Switch in the Response of DRG Neurons to ETS Transcription Factor Signaling." *PLoS Biology* 3 (5): e159.
- Hirano, Keizo, Ryosuke Kaneko, Takeshi Izawa, Masahumi Kawaguchi, Takashi Kitsukawa, and Takeshi Yagi. 2012. "Single-Neuron Diversity Generated by Protocadherin- $\beta$  Cluster in Mouse Central and Peripheral Nervous Systems." *Frontiers in Molecular Neuroscience* 5 (August): 90.
- Hirata, Tsutomu, Peijun Li, Guillermo M. Lanuza, Laura A. Cocas, Molly M. Huntsman, and Joshua G. Corbin. 2009. "Identification of Distinct Telencephalic Progenitor Pools for Neuronal Diversity in the Amygdala." *Nature Neuroscience* 12 (2): 141–49.
- Hofer, M., S. R. Pagliusi, A. Hohn, J. Leibrock, and Y. A. Barde. 1990. "Regional Distribution of Brain-Derived Neurotrophic Factor mRNA in the Adult Mouse Brain." *The EMBO Journal* 9 (8): 2459–64.
- Huang, E. J., and L. F. Reichardt. 2001. "Neurotrophins: Roles in Neuronal Development and Function." *Annual Review of Neuroscience* 24: 677–736.
- Hu, Jia Sheng, Daniel Vogt, Susan Lindtner, Magnus Sandberg, Shanni N. Silberberg, and John L. R. Rubenstein. 2017. "Coup-TF1 and Coup-TF2 Control Subtype and Laminar Identity of MGE-Derived Neocortical Interneurons." *Development* 144 (15): 2837–51.
- Hu, Jia Sheng, Daniel Vogt, Magnus Sandberg, and John L. Rubenstein. 2017. "Cortical Interneuron Development: A Tale of Time and Space." *Development* 144 (21): 3867–78.
- Ing-Esteves, Samantha, Dimitar Kostadinov, Julie Marocha, Anson D. Sing, Kezia S. Joseph, Mallory A. Laboulaye, Joshua R. Sanes, and Julie L. Lefebvre. 2018. "Combinatorial Effects of Alpha- and Gamma-Protocadherins on Neuronal Survival and Dendritic Self-Avoidance."

- The Journal of Neuroscience: The Official Journal of the Society for Neuroscience* 38 (11): 2713–29.
- Kanatani, Shigeaki, Masato Yozu, Hidenori Tabata, and Kazunori Nakajima. 2008. “COUP-TFII Is Preferentially Expressed in the Caudal Ganglionic Eminence and Is Involved in the Caudal Migratory Stream.” *The Journal of Neuroscience: The Official Journal of the Society for Neuroscience* 28 (50): 13582–91.
- Katarova, Z., G. Sekerková, S. Prodan, E. Mugnaini, and G. Szabó. 2000. “Domain-Restricted Expression of Two Glutamic Acid Decarboxylase Genes in Midgestation Mouse Embryos.” *The Journal of Comparative Neurology* 424 (4): 607–27.
- Khazipov, Rustem, and Heiko J. Luhmann. 2006. “Early Patterns of Electrical Activity in the Developing Cerebral Cortex of Humans and Rodents.” *Trends in Neurosciences* 29 (7): 414–18.
- Kohmura, Naohiro, Kouji Senzaki, Shun Hamada, Nobuyuki Kai, Rie Yasuda, Masahiko Watanabe, Hiroki Ishii, Masahiro Yasuda, Masayoshi Mishina, and Takeshi Yagi. 1998. “Diversity Revealed by a Novel Family of Cadherins Expressed in Neurons at a Synaptic Complex.” *Neuron*. [https://doi.org/10.1016/s0896-6273\(00\)80495-x](https://doi.org/10.1016/s0896-6273(00)80495-x).
- Larimer, Phillip, Julien Spatazza, Juan Sebastian Espinosa, Yunshuo Tang, Megumi Kaneko, Andrea R. Hasenstaub, Michael P. Stryker, and Arturo Alvarez-Buylla. 2016. “Caudal Ganglionic Eminence Precursor Transplants Disperse and Integrate as Lineage-Specific Interneurons but Do Not Induce Cortical Plasticity.” *Cell Reports*. <https://doi.org/10.1016/j.celrep.2016.06.071>.
- Larimer, Phillip, Julien Spatazza, Michael P. Stryker, Arturo Alvarez-Buylla, and Andrea R. Hasenstaub. 2017. “Development and Long-Term Integration of MGE-Lineage Cortical Interneurons in the Heterochronic Environment.” *Journal of Neurophysiology*. <https://doi.org/10.1152/jn.00096.2017>.
- Lavdas, Alexandros A., Maria Grigoriou, Vassilis Pachnis, and John G. Parnavelas. 1999. “The

- Medial Ganglionic Eminence Gives Rise to a Population of Early Neurons in the Developing Cerebral Cortex." *The Journal of Neuroscience*. <https://doi.org/10.1523/jneurosci.19-18-07881.1999>.
- Lee, Soohyun, Jens Hjerling-Leffler, Edward Zagha, Gord Fishell, and Bernardo Rudy. 2010. "The Largest Group of Superficial Neocortical GABAergic Interneurons Expresses Ionotropic Serotonin Receptors." *The Journal of Neuroscience: The Official Journal of the Society for Neuroscience* 30 (50): 16796–808.
- Lefebvre, Julie L., Yifeng Zhang, Markus Meister, Xiaozhong Wang, and Joshua R. Sanes. 2008. "Gamma-Protocadherins Regulate Neuronal Survival but Are Dispensable for Circuit Formation in Retina." *Development* 135 (24): 4141–51.
- Letinic, K., R. Zoncu, and P. Rakic. 2002. "Origin of GABAergic Neurons in the Human Neocortex." *Nature* 417 (6889). <https://doi.org/10.1038/nature00779>.
- Lewis, David A., Takanori Hashimoto, and David W. Volk. 2005. "Cortical Inhibitory Neurons and Schizophrenia." *Nature Reviews. Neuroscience* 6 (4): 312–24.
- Li, Yanfang, Haiyan Xiao, Tzu-Ting Chiou, Hongbing Jin, Bevan Bonhomme, Celia P. Miralles, Noelia Pinal, et al. 2012. "Molecular and Functional Interaction between Protocadherin- $\gamma$ C5 and GABAA Receptors." *The Journal of Neuroscience: The Official Journal of the Society for Neuroscience* 32 (34): 11780–97.
- Lois, Carlos, and Arturo Alvarez-Buylla. 1994. "Long-Distance Neuronal Migration in the Adult Mammalian Brain." *Science*. <https://doi.org/10.1126/science.8178174>.
- Luhmann, Heiko J., Anne Sinning, Jenq-Wei Yang, Vicente Reyes-Puerta, Maik C. Stüttgen, Sergei Kirischuk, and Werner Kilb. 2016. "Spontaneous Neuronal Activity in Developing Neocortical Networks: From Single Cells to Large-Scale Interactions." *Frontiers in Neural Circuits* 10 (May): 40.
- Lui, Jan H., David V. Hansen, and Arnold R. Kriegstein. 2011. "Development and Evolution of the Human Neocortex." *Cell* 146 (1): 18–36.



- Luskin, Maria B. 1993. "Restricted Proliferation and Migration of Postnatally Generated Neurons Derived from the Forebrain Subventricular Zone." *Neuron*. [https://doi.org/10.1016/0896-6273\(93\)90281-u](https://doi.org/10.1016/0896-6273(93)90281-u).
- Manuel, Martine N., Da Mi, John O. Mason, and David J. Price. 2015. "Regulation of Cerebral Cortical Neurogenesis by the Pax6 Transcription Factor." *Frontiers in Cellular Neuroscience* 9 (March): 70.
- Marín, Oscar. 2012. "Interneuron Dysfunction in Psychiatric Disorders." *Nature Reviews. Neuroscience* 13 (2): 107–20.
- Marín, Oscar, and John L. R. Rubenstein. 2003. "Cell Migration in the Forebrain." *Annual Review of Neuroscience* 26 (February): 441–83.
- Marín, Oscar, Stewart A. Anderson, and John L. R. Rubenstein. 2000. "Origin and Molecular Specification of Striatal Interneurons." *The Journal of Neuroscience: The Official Journal of the Society for Neuroscience* 20 (16): 6063–76.
- Markram, Henry, Maria Toledo-Rodriguez, Yun Wang, Anirudh Gupta, Gilad Silberberg, and Caizhi Wu. 2004. "Interneurons of the Neocortical Inhibitory System." *Nature Reviews. Neuroscience* 5 (10): 793–807.
- Ma, Tong, Qiangqiang Zhang, Yuqun Cai, Yan You, John L. R. Rubenstein, and Zhengang Yang. 2012. "A Subpopulation of Dorsal Lateral/caudal Ganglionic Eminence-Derived Neocortical Interneurons Expresses the Transcription Factor Sp8." *Cerebral Cortex* 22 (9): 2120–30.
- Ma, T., C. Wang, L. Wang, X. Zhou, M. Tian, Q. Zhang, Y. Zhang, et al. 2013. "Subcortical Origins of Human and Monkey Neocortical Interneurons." *Nature Neuroscience* 16 (11). <https://doi.org/10.1038/nn.3536>.
- Merkle, Florian T., Zaman Mirzadeh, and Arturo Alvarez-Buylla. 2007. "Mosaic Organization of Neural Stem Cells in the Adult Brain." *Science* 317 (5836): 381–84.
- Miyoshi, Goichi, Simon J. B. Butt, Hirohide Takebayashi, and Gord Fishell. 2007.

“Physiologically Distinct Temporal Cohorts of Cortical Interneurons Arise from Telencephalic Olig2-Expressing Precursors.” *The Journal of Neuroscience: The Official Journal of the Society for Neuroscience* 27 (29): 7786.

Miyoshi, Goichi, Jens Hjerling-Leffler, Theofanis Karayannis, Vitor H. Sousa, Simon J. B. Butt, James Battiste, Jane E. Johnson, Robert P. Machold, and Gord Fishell. 2010. “Genetic Fate Mapping Reveals That the Caudal Ganglionic Eminence Produces a Large and Diverse Population of Superficial Cortical Interneurons.” *The Journal of Neuroscience: The Official Journal of the Society for Neuroscience* 30 (5): 1582.

Mousavi, Kambiz, and Bernard J. Jasmin. 2006. “BDNF Is Expressed in Skeletal Muscle Satellite Cells and Inhibits Myogenic Differentiation.” *The Journal of Neuroscience: The Official Journal of the Society for Neuroscience* 26 (21): 5739–49.

Nery, Susana, Gord Fishell, and Joshua G. Corbin. 2002. “The Caudal Ganglionic Eminence Is a Source of Distinct Cortical and Subcortical Cell Populations.” *Nature Neuroscience* 5 (12): 1279–87.

Nikoletopoulou, Vassiliki, Heiko Lickert, José Maria Frade, Chantal Rencurel, Patrizia Giallonardo, Lixin Zhang, Miriam Bibel, and Yves-Alain Barde. 2010. “Neurotrophin Receptors TrkA and TrkC Cause Neuronal Death Whereas TrkB Does Not.” *Nature* 467 (7311): 59–63.

Nóbrega-Pereira, Sandrina, Diego Gelman, Giorgia Bartolini, Ramón Pla, Alessandra Pierani, and Oscar Marín. 2010. “Origin and Molecular Specification of Globus Pallidus Neurons.” *The Journal of Neuroscience: The Official Journal of the Society for Neuroscience* 30 (8): 2824–34.

Nóbrega-Pereira, Sandrina, Nicoletta Kessarlis, Tonggong Du, Shioko Kimura, Stewart A. Anderson, and Oscar Marín. 2008. “Postmitotic Nkx2-1 Controls the Migration of Telencephalic Interneurons by Direct Repression of Guidance Receptors.” *Neuron* 59 (5): 733–45.

- Noctor, S. C., A. C. Flint, T. A. Weissman, R. S. Dammerman, and A. R. Kriegstein. 2001. "Neurons Derived from Radial Glial Cells Establish Radial Units in Neocortex." *Nature* 409 (6821): 714–20.
- Noctor, Stephen C., Verónica Martínez-Cerdeño, Lidija Ivic, and Arnold R. Kriegstein. 2004. "Cortical Neurons Arise in Symmetric and Asymmetric Division Zones and Migrate through Specific Phases." *Nature Neuroscience* 7 (2): 136–44.
- Oakley, R. A., F. B. Lefcort, D. O. Clary, L. F. Reichardt, D. Prevette, R. W. Oppenheim, and E. Frank. 1997. "Neurotrophin-3 Promotes the Differentiation of Muscle Spindle Afferents in the Absence of Peripheral Targets." *The Journal of Neuroscience: The Official Journal of the Society for Neuroscience* 17 (11): 4262–74.
- Paredes, Mercedes F., David James, Sara Gil-Perotin, Hosung Kim, Jennifer A. Cotter, Carissa Ng, Kadellyn Sandoval, et al. 2016. "Extensive Migration of Young Neurons into the Infant Human Frontal Lobe." *Science* 354 (6308). <https://doi.org/10.1126/science.aaf7073>.
- Paredes, M. F., C. Mora, Q. Flores-Ramirez, A. Cebrian-Silla, A. Del Dosso, P. Larimer, J. Chen, et al. 2022. "Nests of Dividing Neuroblasts Sustain Interneuron Production for the Developing Human Brain." *Science* 375 (6579). <https://doi.org/10.1126/science.abk2346>.
- Parnavelas, John G. 2000. "The Origin and Migration of Cortical Neurones: New Vistas." *Trends in Neurosciences*. [https://doi.org/10.1016/s0166-2236\(00\)01553-8](https://doi.org/10.1016/s0166-2236(00)01553-8).
- Pei, Zhenglei, Bei Wang, Gang Chen, Motoshi Nagao, Masato Nakafuku, and Kenneth Campbell. 2011. "Homeobox Genes Gsx1 and Gsx2 Differentially Regulate Telencephalic Progenitor Maturation." *Proceedings of the National Academy of Sciences of the United States of America* 108 (4): 1675–80.
- Petanjek, Z., B. Berger, and M. Esclapez. 2009. "Origins of Cortical GABAergic Neurons in the Cynomolgus Monkey." *Cerebral Cortex* 19 (2). <https://doi.org/10.1093/cercor/bhn078>.
- Pollen, Alex A., Tomasz J. Nowakowski, Jiadong Chen, Hanna Retallack, Carmen Sandoval-Espinosa, Cory R. Nicholas, Joe Shuga, et al. 2015. "Molecular Identity of Human Outer

- Radial Glia during Cortical Development.” *Cell* 163 (1): 55–67.
- Prasad, Tuhina, Xiaozhong Wang, Paul A. Gray, and Joshua A. Weiner. 2008. “A Differential Developmental Pattern of Spinal Interneuron Apoptosis during Synaptogenesis: Insights from Genetic Analyses of the Protocadherin- $\gamma$  Gene Cluster.” *Development* 135 (24): 4153–64.
- Priya, Rashi, Benjamin Rakela, Megumi Kaneko, Julien Spatazza, Philip Larimer, Mahmood S. Hoseini, Andrea R. Hasenstaub, Arturo Alvarez-Buylla, and Michael P. Stryker. 2019. “Vesicular GABA Transporter Is Necessary for Transplant-Induced Critical Period Plasticity in Mouse Visual Cortex.” *The Journal of Neuroscience*.  
<https://doi.org/10.1523/jneurosci.1253-18.2019>.
- Rauskolb, Stefanie, Marta Zagrebelsky, Anita Dreznjak, Rubén Deogracias, Tomoya Matsumoto, Stefan Wiese, Beat Erne, et al. 2010. “Global Deprivation of Brain-Derived Neurotrophic Factor in the CNS Reveals an Area-Specific Requirement for Dendritic Growth.” *The Journal of Neuroscience: The Official Journal of the Society for Neuroscience* 30 (5): 1739–49.
- Reillo, Isabel, Camino de Juan Romero, Miguel Ángel García-Cabezas, and Víctor Borrell. 2011. “A Role for Intermediate Radial Glia in the Tangential Expansion of the Mammalian Cerebral Cortex.” *Cerebral Cortex* 21 (7): 1674–94.
- Rodríguez-Martínez, Daniel, María Magdalena Martínez-Losa, and Manuel Alvarez-Dolado. 2017. “Cryopreservation of GABAergic Neuronal Precursors for Cell-Based Therapy.” *PLoS One* 12 (1): e0170776.
- Rossignol, E. 2011. “Genetics and Function of Neocortical GABAergic Interneurons in Neurodevelopmental Disorders.” *Neural Plasticity* 2011 (August): 649325.
- Rubenstein, J. L. R., and M. M. Merzenich. 2003. “Model of Autism: Increased Ratio of Excitation/inhibition in Key Neural Systems.” *Genes, Brain, and Behavior* 2 (5): 255–67.
- Rudy, Bernardo, Gordon Fishell, Soohyun Lee, and Jens Hjerling-Leffler. 2011. “Three Groups

- of Interneurons Account for Nearly 100% of Neocortical GABAergic Neurons.”  
*Developmental Neurobiology* 71 (1): 45–61.
- Sandberg, Magnus, Pierre Flandin, Shanni Silberberg, Linda Su-Feher, James D. Price, Jia Sheng Hu, Carol Kim, Axel Visel, Alex S. Nord, and John L. R. Rubenstein. 2016.  
“Transcriptional Networks Controlled by NKX2-1 in the Development of Forebrain GABAergic Neurons.” *Neuron* 91 (6): 1260.
- Saxena, Alka, Akiko Wagatsuma, Yukihiro Noro, Takenobu Kuji, Atsuko Asaka-Oba, Akira Watahiki, Cecile Gurnot, Michela Fagiolini, Takao K. Hensch, and Piero Carninci. 2012.  
“Trehalose-Enhanced Isolation of Neuronal Sub-Types from Adult Mouse Brain.”  
*BioTechniques* 52 (6): 381.
- Seress, L., M. Frotscher, and C. E. Ribak. 1989. “Local Circuit Neurons in Both the Dentate Gyrus and Ammon’s Horn Establish Synaptic Connections with Principal Neurons in Five Day Old Rats: A Morphological Basis for Inhibition in Early Development.” *Experimental Brain Research*. <https://doi.org/10.1007/bf00230680>.
- Sherwood, Chet C., Mary Ann Raghanti, Cheryl D. Stimpson, Muhammad A. Spocter, Monica Uddin, Amy M. Boddy, Derek E. Wildman, et al. 2010. “Inhibitory Interneurons of the Human Prefrontal Cortex Display Conserved Evolution of the Phenotype and Related Genes.” *Proceedings. Biological Sciences / The Royal Society* 277 (1684): 1011–20.
- Shimamura, K., D. J. Hartigan, S. Martinez, L. Puelles, and J. L. Rubenstein. 1995.  
“Longitudinal Organization of the Anterior Neural Plate and Neural Tube.” *Development* 121 (12): 3923–33.
- Silos-Santiago, I., A. M. Fagan, M. Garber, B. Fritsch, and M. Barbacid. 1997. “Severe Sensory Deficits but Normal CNS Development in Newborn Mice Lacking TrkB and TrkC Tyrosine Protein Kinase Receptors.” *The European Journal of Neuroscience* 9 (10): 2045–56.
- Smart, I. H. M. 2002. “Unique Morphological Features of the Proliferative Zones and Postmitotic Compartments of the Neural Epithelium Giving Rise to Striate and Extrastriate Cortex in the

- Monkey.” *Cerebral Cortex*. <https://doi.org/10.1093/cercor/12.1.37>.
- Sousa, Vitor H., Goichi Miyoshi, Jens Hjerling-Leffler, Theofanis Karayannis, and Gord Fishell. 2009. “Characterization of Nkx6-2-Derived Neocortical Interneuron Lineages.” *Cerebral Cortex* 19 Suppl 1 (July): i1–10.
- Southwell, Derek G., Robert C. Froemke, Arturo Alvarez-Buylla, Michael P. Stryker, and Sunil P. Gandhi. 2010. “Cortical Plasticity Induced by Inhibitory Neuron Transplantation.” *Science* 327 (5969): 1145–48.
- Southwell, Derek G., Cory R. Nicholas, Allan I. Basbaum, Michael P. Stryker, Arnold R. Kriegstein, John L. Rubenstein, and Arturo Alvarez-Buylla. 2014. “Interneurons from Embryonic Development to Cell-Based Therapy.” *Science* 344 (6180): 1240622.
- Southwell, Derek G., Mercedes F. Paredes, Rui P. Galvao, Daniel L. Jones, Robert C. Froemke, Joy Y. Sebe, Clara Alfaro-Cervello, et al. 2012. “Intrinsically Determined Cell Death of Developing Cortical Interneurons.” *Nature* 491 (7422): 109–13.
- Sussel, L., O. Marin, S. Kimura, and J. L. Rubenstein. 1999. “Loss of Nkx2.1 Homeobox Gene Function Results in a Ventral to Dorsal Molecular Respecification within the Basal Telencephalon: Evidence for a Transformation of the Pallidum into the Striatum.” *Development* 126 (15): 3359–70.
- Su, Zihao, Ziwu Wang, Susan Lindtner, Lin Yang, Zicong Shang, Yu Tian, Rongliang Guo, et al. 2022. “Dlx1/2-Dependent Expression of Meis2 Promotes Neuronal Fate Determination in the Mammalian Striatum.” *Development* 149 (4). <https://doi.org/10.1242/dev.200035>.
- Tamamaki, N., K. E. Fujimori, and R. Takauji. 1997. “Origin and Route of Tangentially Migrating Neurons in the Developing Neocortical Intermediate Zone.” *The Journal of Neuroscience: The Official Journal of the Society for Neuroscience* 17 (21): 8313–23.
- Tamamaki, Nobuaki, Yuchio Yanagawa, Ryohei Tomioka, Jun-Ichi Miyazaki, Kunihiro Obata, and Takeshi Kaneko. 2003. “Green Fluorescent Protein Expression and Colocalization with Calretinin, Parvalbumin, and Somatostatin in the GAD67-GFP Knock-in Mouse.” *The*

*Journal of Comparative Neurology* 467 (1): 60–79.

Tanaka, Daisuke, Yohei Nakaya, Yuchio Yanagawa, Kunihiko Obata, and Fujio Murakami.

2003. “Multimodal Tangential Migration of Neocortical GABAergic Neurons Independent of GPI-Anchored Proteins.” *Development* 130 (23): 5803–13.

Tang, Yunshuo, Michael P. Stryker, Arturo Alvarez-Buylla, and Juan Sebastian Espinosa. 2014.

“Cortical Plasticity Induced by Transplantation of Embryonic Somatostatin or Parvalbumin Interneurons.” *Proceedings of the National Academy of Sciences of the United States of America* 111 (51): 18339–44.

Taniguchi, Hiroki, Miao He, Priscilla Wu, Sangyong Kim, Raehum Paik, Ken Sugino, Duda

Kvitsiani, et al. 2011. “A Resource of Cre Driver Lines for Genetic Targeting of GABAergic Neurons in Cerebral Cortex.” *Neuron* 71 (6): 995–1013.

Tan, Xin, and Song-Hai Shi. 2013. “Neocortical Neurogenesis and Neuronal Migration.” *Wiley*

*Interdisciplinary Reviews. Developmental Biology* 2 (4): 443–59.

Tasic, Bosiljka, Christoph E. Nabholz, Kristin K. Baldwin, Youngwook Kim, Erroll H. Rueckert,

Scott A. Ribich, Paula Cramer, Qiang Wu, Richard Axel, and Tom Maniatis. 2002.

“Promoter Choice Determines Splice Site Selection in Protocadherin Alpha and Gamma Pre-mRNA Splicing.” *Molecular Cell* 10 (1): 21–33.

Thu, Chan Aye, Weisheng V. Chen, Rotem Rubinstein, Maxime Chevee, Holly N. Wolcott, Klara

O. Felsovalyi, Juan Carlos Tapia, Lawrence Shapiro, Barry Honig, and Tom Maniatis. 2014.

“Generation of Single Cell Identity by Homophilic Interactions between Combinations of  $\alpha$ ,  $\beta$  and  $\gamma$  Protocadherins.” *Cell* 158 (5): 1045.

Tyzio, R., A. Represa, I. Jorquera, Y. Ben-Ari, H. Gozlan, and L. Aniksztejn. 1999. “The

Establishment of GABAergic and Glutamatergic Synapses on CA1 Pyramidal Neurons Is Sequential and Correlates with the Development of the Apical Dendrite.” *The Journal of Neuroscience: The Official Journal of the Society for Neuroscience* 19 (23): 10372–82.

Valcanis, Helen, and Seong-Seng Tan. 2003. “Layer Specification of Transplanted Interneurons

- in Developing Mouse Neocortex.” *The Journal of Neuroscience: The Official Journal of the Society for Neuroscience* 23 (12): 5113.
- Verret, Laure, Edward O. Mann, Gao B. Hang, Albert M. I. Barth, Inma Cobos, Kaitlyn Ho, Nino Devidze, et al. 2012. “Inhibitory Interneuron Deficit Links Altered Network Activity and Cognitive Dysfunction in Alzheimer Model.” *Cell* 149 (3): 708–21.
- Wang, Xiaozhong, Hong Su, and Allan Bradley. 2002. “Molecular Mechanisms Governing Pcdh-Gamma Gene Expression: Evidence for a Multiple Promoter and Cis-Alternative Splicing Model.” *Genes & Development* 16 (15): 1890–1905.
- Wang, Xiaozhong, Joshua A. Weiner, Sabine Levi, Ann Marie Craig, Allan Bradley, and Joshua R. Sanes. 2002. “Gamma Protocadherins Are Required for Survival of Spinal Interneurons.” *Neuron* 36 (5): 843–54.
- Wichterle, H., D. H. Turnbull, S. Nery, G. Fishell, and A. Alvarez-Buylla. 2001. “In Utero Fate Mapping Reveals Distinct Migratory Pathways and Fates of Neurons Born in the Mammalian Basal Forebrain.” *Development* 128 (19): 3759–71.
- Wichterle, Hynek, Jose Manuel Garcia-Verdugo, Daniel G. Herrera, and Arturo Alvarez-Buylla. 1999. “Young Neurons from Medial Ganglionic Eminence Disperse in Adult and Embryonic Brain.” *Nature Neuroscience*. <https://doi.org/10.1038/8131>.
- Wonders, Carl P., and Stewart A. Anderson. 2006. “The Origin and Specification of Cortical Interneurons.” *Nature Reviews. Neuroscience* 7 (9): 687–96.
- Wonders, Carl P., Jelle Welagen, Lauren Taylor, Ihunanya C. Mbata, Jenny Z. Xiang, and Stewart A. Anderson. 2008. “A Spatial Bias for the Origins of Interneuron Subgroups within the Medial Ganglionic Eminence.” *Developmental Biology* 314 (1): 127.
- Wong, Fong Kuan, Kinga Bercsenyi, Varun Sreenivasan, Adrián Portalés, Marian Fernández-Otero, and Oscar Marín. 2018. “Pyramidal Cell Regulation of Interneuron Survival Sculpted Cortical Networks.” *Nature* 557 (7707): 668–73.
- Wu, Q., and T. Maniatis. 1999. “A Striking Organization of a Large Family of Human Neural



Cadherin-like Cell Adhesion Genes.” *Cell* 97 (6): 779–90.

Xu, Qing, Melissa Tam, and Stewart A. Anderson. 2008. “Fate Mapping Nkx2.1-Lineage Cells in the Mouse Telencephalon.” *The Journal of Comparative Neurology* 506 (1): 16–29.

Yang, Jian-Ming, Jing Zhang, Yan-Qin Yu, Shumin Duan, and Xiao-Ming Li. 2012. “Postnatal Development of 2 Microcircuits Involving Fast-Spiking Interneurons in the Mouse Prefrontal Cortex.” *Cerebral Cortex* 24 (1): 98–109.

Yuste, R., D. A. Nelson, W. W. Rubin, and L. C. Katz. 1995. “Neuronal Domains in Developing Neocortex: Mechanisms of Coactivation.” *Neuron* 14 (1): 7–17.

Zhao, Yangu, Oscar Marín, Edit Hermesz, Aaron Powell, Nuria Flames, Miklós Palkovits, John L. R. Rubenstein, and Heiner Westphal. 2003. “The LIM-Homeobox Gene *Lhx8* Is Required for the Development of Many Cholinergic Neurons in the Mouse Forebrain.” *Proceedings of the National Academy of Sciences*. <https://doi.org/10.1073/pnas.1537759100>.

## Publishing Agreement

It is the policy of the University to encourage open access and broad distribution of all theses, dissertations, and manuscripts. The Graduate Division will facilitate the distribution of UCSF theses, dissertations, and manuscripts to the UCSF Library for open access and distribution. UCSF will make such theses, dissertations, and manuscripts accessible to the public and will take reasonable steps to preserve these works in perpetuity.

I hereby grant the non-exclusive, perpetual right to The Regents of the University of California to reproduce, publicly display, distribute, preserve, and publish copies of my thesis, dissertation, or manuscript in any form or media, now existing or later derived, including access online for teaching, research, and public service purposes.

DocuSigned by:  
  
7DBBB91070414FC... Author Signature

8/27/2022  
Date